Modulation of Ash Iron Solubility in Volcanic Eruption Plumes

Dissertation zur Erlangung des Doktorgrades an der Fakultät für Mathematik, Informatik und Naturwissenschaften
Fachberiech Geowissenschaften der Universität Hamburg

vorgelegt von

Gholamali Hoshyaripour

Hamburg

2013

-Korrigierte Fassung-

Tag der Disputation: 19. Dezember 2013

Folgende Gutachter empfehlen die Annahme der Dissertation
Prof. Dr. Matthias Hort
und Dr. Bärbel Langmann

Prof. Dr. Christian Betzler
Leiter des Fachbereichs Geowissenschaften

When you go through a hard period,
When everything seems to oppose you,
When you feel you cannot even bear one more minute, ...
Never give up!
Because it is the time and place that the course will divert!

- Rumi

Abstract

Volcanic ash has been recently identified as a potential fertilizer for the surface ocean. However, the processes that allow conversion of insoluble iron into soluble iron compounds in ash are so far poorly understood. This study investigates the volcanic plume controls on ash iron solubility. A conceptual box model is developed to simulate the high, mid and low temperature chemical, physical and thermodynamic processes in eruption plumes in order to better constrain volcanic ash iron mobilization. The research takes into account the interaction of different species in a solid-liquid-gas system generated from three volcanic settings (convergent plate, divergent plate and hot spot).

Among other volatiles, volcanic eruptions inject significant amounts of sulfur into the atmosphere mainly in the form of SO_2 and H_2S. The ratio of these species (H_2S/SO_2), which is usually used as the mirror for the oxidation state of the source magma, varies significantly according to the type of activity, tectonic setting etc. We consider the hot core (T>600°C) as a box model in which 1000°C magmatic gas and 25°C ambient air are mixed and show that it functions as a hot oxidizing reactor for S species. Processes inside the hot core usually decrease the H_2S content of the system but it can either increase or decrease SO_2 depending on the initial oxidation state. Thus, the SO_2 injected into the atmosphere is not essentially generated directly from the magma but it can be produced in the hot core as the result of H_2S oxidation. Besides, volcanic cloud compositions do not necessarily mirror the source conditions. Considering three types of tectonic settings (convergent plate, divergent plate and hot spot) we propose that H_2S emission is more likely under reduced conditions in divergent plate and hot spot volcanic settings.

When adding ash to the hot core model we find that the hot core of a volcanic plume does not produce soluble iron directly but significantly controls the Fe mineralogy and oxidation state at the ash surface. We find that the final iron mineralogy at the ash surface (i.e. the ash's oxidation front) is likely to be independent of temperature and oxygen fugacity and is closely correlated to the ratio of H_2 and H_2S content of the magmatic gas to the amount of entrained oxygen (X_{mix}). If $\log X_{mix}$ reaches -3.5 in the hot core, most of the iron will be oxidized to Fe^{3+} which is its less soluble form. Considering typical volcanic plume compositions (i.e., convergent plate, divergent plate and hot spot) with different oxidation states, we conclude that reduced conditions in divergent plate and hot spot volcanoes seem more favorable for iron fertilization because $\log X_{mix}$ does not fall below -3.5 and >80% of the total iron remains in ferrous form.

As all material eventually leaves the hot core we simulate the sulfuric acid and water condensation as well as gas-ash/aerosol interactions in 0°C<T<600°C. The simulation is

based on a series of coupled mass balance equations for different species in the eruption column. The terms incorporated into these equations are parameterized based on the physiochemical interactions of gas, liquid and solid species. Some of the major processes considered in this study are: gas scavenging by liquid water and dissolution of ash in the liquid phase. Results show that sulfuric acid condenses at about 150°C followed by water condensation at about 50°C which also dissociates sulfuric acid and produces H^+ ions in the liquid phase. The aqueous phase scavenges the surrounding gas species (SO_2, HCl, HF) and concurrently dissolves the ash surface constituents. Since HCl is in the range of 4 orders of magnitudes more soluble than SO_2, its dissolution mainly controls the pH of the liquid. Hence, high HCl concentrations in the gas phase (the typical condition at convergent plate volcanoes) results in lower pH in the aqueous phase (pH<0.5) and consequently, an increase in the ash dissolution rate. On the other hand, reduced iron carrying minerals (e.g., fayalite) show a much higher dissolution rate in comparison with oxidized species (e.g., hematite). Thus, the presence of the reduced iron species in the mineral assemblage (the typical condition at divergent plate and hot spot volcanoes) seems to be more favorable for the soluble iron production.

We conclude that bio-available iron production is weakly correlated with the tectonic setting and is instead controlled by the halide content of the eruption plume and the oxidation state of the iron at the ash mineral assemblage.

Zusammenfassung

Der Einfluss vulkanischer Eruptionen auf das Klima ist vielfältig. Allgemein akzeptiert ist u.a. die Tatsache, dass Aerosole, die sich bei Vulkaneruptionen in der Stratosphäre bilden, zu einer Abkühlung auf der Erdoberfläche führen. Relativ neu dagegen ist der Zusammenhang zwischen dem Eintrag vulkanischer Asche, der Bildung von Biomasse im oberflächennahen Ozean und damit verbunden eine Bindung von CO_2 aus der Atmosphäre. Entscheidend an diesem Prozess ist das Vorhandensein von bioverfügbarem Eisen (also Fe^{2+}) auf der Oberfläche vulkanischer Asche. Allerdings sind die Prozesse, welche zur Umwandlung von unlöslichen Eisen in den verschiedenen Mineralphasen und vulkanischem Glas in lösliche Fe-Verbindungen führen bisher schlecht verstanden. In dieser These untersuche ich Prozesses in vulkanischen Eruptionswolken, welche die Eisenlöslichkeit beeinflussen. Hierzu wurde ein sogenanntes Boxmodel entwickelt, welches es erlaubt chemische, physikalische und thermodynamische Prozesse in den Hoch-, Mittel- und Niedrigtemperaturbereichen einer Eruptionssäule zu untersuchen. Hierbei werden u.a. die Wechselwirkungen verschiedener Spezies im fest-flüssig-gasförmigen System berücksichtig.

Neben vielen verschiedenen Volatilen tragen Eruptionen u.a. signifikante Mengen an Schwefel in Form von SO_2 and H_2S in die Atmosphäre ein. Das Verhältnis dieser beiden Spezies (H_2S/SO_2), welches üblicherweise als Indikator für den Oxidationszustand genommen wird, ändert sich signifikant mit dem Magmentyp und z.B. der tektonischen Provinz. Zuerst betrachten ich den heißen inneren Kern einer Eruptionswolke, wobei die initial 1.000°C heiße Wolke durch Einmischung von 25°C heißer Umgebungsluft auf 600°C abkühlt. Prozesse im heißen inneren Kern verringern den H_2S Gehalt des Systems, der SO_2 Gehalt kann entweder abnehmen oder ansteigen, je nachdem wie der initiale Oxidationszustand des Magmas war. SO_2 im heißen Kern der Eruptionssäule wird nicht notwendigerweise vollständig aus dem Magma eruptiert, sondern kann auch durch Oxidation von H_2S gebildet werden. Dies bedeutet, dass die Zusammensetzung der vulkanischen Wolke oberhalb des vulkanischen Vents nicht unbedingt die Originalzusammensetzung des Magmas widerspiegelt. Im Hinblick auf die 3 verschiedenen tektonischen Regime (konvergente Ränder, divergente Ränder und Hot spots) kann man vermuten, dass H_2S Emissionen bei eher reduzierten Bedingungen an divergenten Rändern und Hotspots wahrscheinlich sind und dort insbesondere sich die SO_2 Konzentration durch Oxidation von H_2S noch ändert.

Wenn man zusätzlich zu den vulkanischen Gasen auch noch die Asche in der heißen Zone der Eruptionssäule berücksichtigt, so lässt sich zeigen, dass die vulkanischen Gase und

die Umgebungsluft die Eisenmineralogie und den Oxidationszustand der Mineralien an der Oberfläche der Asche kontrollieren. Es deutet sich an, dass die Eisenmineralogie an der Oberfläche der Asche nahezu unabhängig von den genauen Temperatur- und Oxidationsbedingungen ist. Im Gegensatz dazu scheint das Mengenverhältnis von H2 und H_2S zur Menge an eingemischter Umgebungsluft (X_{mix}) ein wesentlicher Faktor für den Oxidationszustand zu sein. Wenn logX_{mix} einen Wert von -3.5 erreicht, ist das meiste Eisen oxidiert und daher liegt es in der nun weniger löslichen Oxidationsstufe vor. Vergleicht man nun die in den verschiedenen tektonischen Regimes erreichten Oxidationsstufen, so erscheinen sowohl Hotspot Vulkane und Vulkanismus an divergierenden Plattenrändern die Düngung mit Eisen durch Eintrag zu begünstigen, weil in 80% der untersuchten Fälle ein logX_{mix} von -3.5 nicht erreicht wird.

Da beim weiteren Transport in höhere Regionen der Eruptionssäule die Eruptionssäule unter 600°C abkühlt, muss untersucht werden, wie sich z.B. die Kondensation von Volatilen (Schwefelsäure, Wasser etc.) sowie die Interaktion im Gas/Asche/Aerosol Gemisch auswirken. Das hierzu entwickelte Boxmodel basiert auf gekoppelten Massenbilanzgleichungen für die verschiedenen Spezies in der Eruptionssäule. Die in den Gleichungen berücksichtigten Terme sind basierend auf den physico-chemischen Wechselwirkungen zwischen Gas, Flüssigkeit und Asche parametrisiert worden. Einige der wesentlichen Prozesse, die in dem Model berücksichtigt wurden, sind das Lösen von Gasen in Wasser und das Auflösen der Asche in der flüssigen Phase. Die Rechungen zeigen, dass Schwefelsäure bei ca. 150°C kondensiert, gefolgt von Wasser bei etwa 50°C. Die Schwefelsäure dissoziiert in Wasser, was zum Anstieg der H^+ Konzentration in der flüssigen Phase führt. Die flüssige Phase löst weiterhin Gase wie SO_2, HCl und HF, was zu einem Anlösen der Ascheoberfläche führt. Da HCl ca. 4 Größenordungen besser löslich in Wasser ist als SO_2, kontrolliert die Lösung von HCl im wesentlichen den pH Wert der Lösung. Daher führen große HCl Konzentrationen (typisch für konvergente Ränder) zu niedrigen pH Werten in der flüssigen Phase (pH<0.5) was zu einer verstärkten Anlösung der Asche führt. Anderseits zeigen Mineralphasen, in denen Eisen nicht aufoxidiert wurde (z.B. Fayalit) eine deutlich größere Lösungsrate in saurer Umgebung im Vergleich zu den aufoxidierten Phasen wie Hämatit. Insgesamt erscheint daher das Vorhandensein von nicht aufoxidiertem Eisen (typisch für divergente Ränder und Hotspot) die Entstehung von löslichem Eisen zu begünstigen.

Zusammenfassend kann man sagen, dass die Entstehung von bioverfügbarem Eisen nur schwach vom tektonischen Regime abhängt. Ein wesentlicher Faktor scheint daher neben der Oxidationsstufe der Mineralphasen in der Asche die Halogenkonzentration in dem eruptierten vulkanischen Gas zu sein.

Acknowledgements

Foremost, I would like to express my sincere gratitude to my advisors Prof. Dr. Matthias Hort and Dr. Bärbel Langmann for the continuous support of my Ph.D research.

My sincere thanks also goes to my advisory panel chair Prof. Dr. Kay Emeis for his encouragement and insightful comments.

I thank P. Delmelle, T. Mather and M. H. Reed for their scientific collaborations in different parts of this research.

I am grateful to my colleagues at Institute of Geophysics, especially Dr. Ali Dehghani for his generous help and support.

Last but not the least, I would like to thank the Cluster of Excellence CliSAP (EXC177), University of Hamburg, for the financial support and also SICSS for providing a unique scientific research environment.

Contents

List of Figures

List of Tables

To my lovely wife, Sarvenaz, without whose love, support, and continued patience it would not have been possible to write this doctoral thesis; and to my parents, who have over the years supported and guided me in my endeavors.

Chapter 1

Introduction

1.1 Motivation

Volcanic eruptions are among the most fascinating yet hazardous natural phenomena. Every year, 50-60 volcanic eruptions are a testimony to the restless power within our dynamic planet and roughly 10 eruptions cause deaths and significant damages [Marti and Ernst, 2005]. Although active or potentially active volcanoes occur in narrow belts that collectively occupy less than 1% of the Earth's total surface area [Tilling, 2005], their hazard and environmental impacts could be incredibly extensive [Marti and Ernst, 2005]. One only has to think of the 1991 eruption of Mount Pinatubo, Philippines, for instance, to get a sense of the awesome power and wide-ranging impacts of volcanic eruptions. The fertile slopes of this volcano were densely populated before the eruption [Pinatubo Volcano Observatory Team, 1991]. The sudden awakening of this sleeping giant in 1991 caused 847 people to lose their lives and forced 1.2 million people to abandon their homes [Banzon-Bautista, 1996]. In general, about 2 million people were affected by the Mt. Pinatubo eruption and the lahars that followed. The economic bill reached more than one billion US dollars with about 140,000 houses totally or partially destroyed, significant portions of public infrastructure affected and tens of thousands of hectares of fertile farmland buried under deep pyroclastic and lahar materials [Gaillard, 2008]. The impacts of this eruption upon the global environment were noteworthy too. While 17 megatons of SO_2 gas was injected into the stratosphere during this eruption causing an extensive sulfate aerosol cloud leading to a global cooling of about 0.5°C during the following two years [Minnis et al., 1993], deposition of the volcanic ash on the surface ocean resulted in a phytoplankton bloom and global atmospheric CO_2-drawdown [Watson, 1997]. Huge explosive volcanic eruptions affecting the entire globe like Mt. Pinatubo may occur once in a few decades [Self, 2006]. However, with many

well-documented major volcanic eruptions in the last three decades (e.g., the eruptions of Mount St. Helens in 1980 in the northwestern United States, El Chichón in 1982 in Mexico, Galungung in 1982 in Indonesia, Hawaii from 1992 to present, Mt. Unzen from 1991 to 1994 in Japan, and Soufriere Hills, Montserrat from 1996 to present), it appears that eruptions arguably have the potential to have all of these impacts and many more upon their surroundings and the overall global environment (including the land [Ayris and Delmelle, 2012a], atmosphere [Mather, 2008], oceans [Duggen et al., 2010] and thus, the climate [Robock, 2000]).

Aside from its devastating nature, volcanism is a spectacular display of the energy and materials fluxes from the Earth's interior to the Earth's surface [Marti and Ernst, 2005]. The energy flux is derived from both the heat and explosive energy released. The matter flux is a mixture of solids and gases which is derived from molten rock called magma as well as from volatile species (H_2O, CO_2, SO_2, HF, HCl etc.) initially dissolved within that magma [Ayris, 2010]. Most of the solid material (so-called Tephra) released during an eruption is volcanic ash, which is defined as particles with diameters less than 2 mm. Volcanic ash is typically composed of silicate glass and minerals and is known to have a very rough surface structure [Delmelle et al., 2005]. Its composition is highly variable extending from basaltic (i.e., rich in alkali metals) to rhyolitic (i.e. silicate rich) [Schmincke, 2004]. It is generated during fragmentation and transport of magma in the conduit and its dispersion in the atmosphere. It may also be derived from the conduit wall rock that has been eroded during an eruption [Heiken and Wohletz, 1992].

Volcanic ash is both good and evil at the same time; the very fine ash (particles smaller than 10 μm) can be inhaled by humans and is known to cause respiratory diseases [Baxter, 1999]. It is also one of the main threats to the aviation [Casadevall, 1991]. The eruption of Eyjafjallajökull in 2010, for instance, lead to a direct loss of at least 1.3 billion Euros to airlines with more than 4 million passengers affected and more than 100,000 canceled flights [Oxford-Economics, 2010]. However, volcanic ash is also known to give rise to very fertile farming grounds leading to highly populated areas near volcanoes. It was estimated that by the twenty-first century more than 500 million people live within the proximity of volcanoes [Peterson, 1986]. This certainly increases the potential of major tragedies during volcanic eruptions [Tilling, 2005]. Furthermore, volcanoes have increasingly moved into the focus of the tourist industry, not the least because many ocean islands are of volcanic origin and make great vacation spots [Schmincke, 2004]. Regardless of being good or evil, all causes are related to volcanic ash and gas being dispersed in the atmosphere and on land and the deposition of ash into the open oceans was for a long time considered to be the final graveyard for volcanic material.

1.2 Volcanic ash and the ocean

The oceans cover 70% of the Earth's surface and most of the world's volcanoes are located close to or in the oceans [Schmincke, 2004]. Most interest in depositing volcanic ash in the oceans has focused on their incorporation into sediment layers for e.g., estimating tephra fluxes [Straub and Schmincke, 1998]. However, recently Duggen et al. [2010] showed that volcanic ash can fertilizes the surface ocean through releasing iron into the surface ocean. But the role of iron in the ocean has already been explored earlier by Martin and Fitzwater [1988] who discovered that iron is one of the limiting nutrients for phytoplankton growth in the surface ocean. Following this initial study and after the 1991 eruption of Mt. Pinatubo, Philippines, Sarmiento [1993] and later, Watson [1997] hypothesized that ash from major volcanic eruptions may release sufficient iron and other nutrients into the surface ocean stimulating the marine primary productivity (MPP) and thereby triggering global atmospheric CO_2-drawdown. To evaluate this hypothesis, Frogner et al. [2001] studied the fertilizing potential of volcanic ash from the Hekla eruption in 2000. Through laboratory experiments, they found that volcanic ash in contact with water initially releases high amounts of iron, silica, and manganese together with sulfate, chloride and fluoride. Other experimental studies confirmed that the ash from volcanic eruptions affects the MPP through rapid iron-release in contact with seawater [Duggen et al., 2007, Jones and Gislason, 2008, Olgun et al., 2011]. Langmann et al. [2010] reported the first direct evidence for natural iron fertilization and a phytoplankton bloom due to volcanic ash deposition. They studied the connection between the eruption of the Kasatochi volcano in August 2008 and a large-scale phytoplankton bloom in the iron-limited oceanic region of the NE Pacific. They demonstrated that for this eruption volcanic ash functioned as a fertilizer for the surface ocean.

Iron within the bulk ash particles is mostly in insoluble form (e.g., as a component of the glass and as primary Fe-bearing silicate and Fe-oxide minerals [Schmincke, 2004]. In the surface ocean, however, volcanic ash is assumed to release iron mostly in the form of sulfate, chloride and fluoride salts on the ash surface, which are soluble, i.e., bio-available, species [Duggen et al., 2010, Frogner et al., 2001]. There are numerous definitions for bio-available iron [see Lindenthal et al., 2013, and the references therein]. In the context of this thesis, bio-available iron refers to soluble iron species. Several physicochemical processes in the volcanic plume and cloud are assumed to contribute to the transformation of insoluble iron into the soluble surficial salts (see Ayris and Delmelle [2012b] for a detailed review). However, such processes are poorly constrained so far.

1.3 Eruption plume and the ash iron

Volcanic eruptions usually occur where a body of molten rock and exsolved volatile species rises buoyantly through the earth's crust, and ultimately reaches the surface at a weak point, or via a volcanic vent [Sparks et al., 1997]. Prior to the explosive magma discharge near the surface, magma is first fragmented which can take place in two different ways [Marti and Ernst, 2005]:
1. If the magma contains significant amounts of dissolved volatiles, the formation and growth of bubbles, both mainly controlled by the decompression, lead to an increase in volume. At some point, the volume fraction of volatiles reaches a critical value (anywhere between 40 and 75 vol%). Then the two phase flow consisting of an interconnected magma phase with interspersed bubbles transforms into a two phase flow with gas being the carrier phase that contains interspersed droplets of magma.
2. If the magma comes into contact with water near the surface, it becomes fragmented by the rapid conversion of water to steam or by rapid quenching (Phreatomagmatic eruption).

Regardless of the process, such events are called explosive eruptions. The style of an explosive eruption (i.e., from the effusion of basaltic magma as lava flows and fire fountaining in Hawaiian eruptions to the generation of high altitude plumes during plinian eruptions) depends on many factors including the composition of the magma, gas content, structure of the volcano and the rate of the magma discharge [Carey, 2005]. In the case that erupted material (i.e., tephra and gas mixture) is able to entrain and heat enough ambient air, it can reduce its density below that of the surrounding atmosphere and a volcanic plume develops and continues to rise. Otherwise, it would collapse as a low fountain and generate pyroclastic flows and surges [Sparks et al., 1997]. In this study we focus on plinian and sup-plinian eruptions, which usually generate volcanic plumes with the height of at least a few kilometers [Sparks et al., 1997] (Fig. 1.1).

As shown in Fig. 1.1, during its journey from the fragmentation level to the high elevations, volcanic ash passes through different environmental conditions (e.g., temperature, pressure and relative humidity). Near the vent, where temperatures are >600°C, hot volcanic processes (e.g., direct gas-ash interaction, sublimation) prevail [Ayris et al., 2013], while at high altitudes temperatures reach the freezing point and the environmental conditions are close to those of the surrounding atmosphere. Ayris and Delmelle [2012b] reviewed the key volcanic and atmospheric contributions that are likely to modulate ash iron solubility. Volcanic controls (high and mid temperature reactions) are assumed to be very important for reactions on the ash surface. These controls are expected to have a marked influence on further (photo-) chemical reactions during transport of the ash

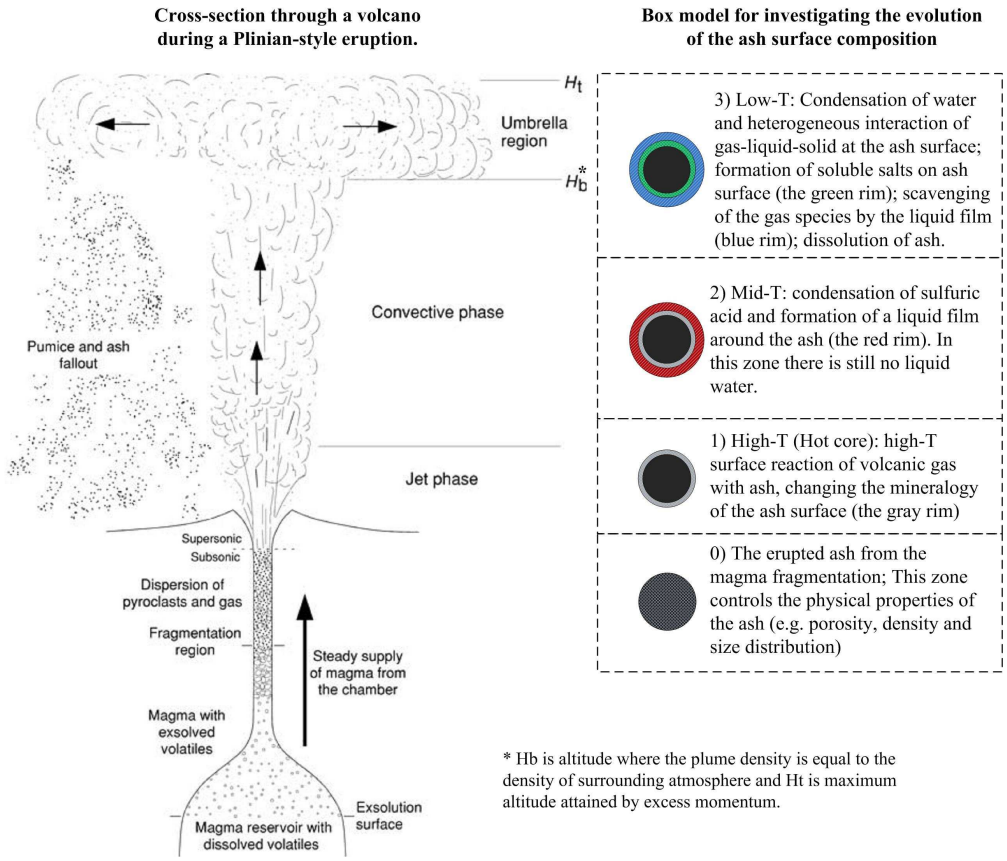

FIGURE 1.1: Mechanism of a plinian eruption and the gas-ash/aerosol interactions. The profile in the left panel is from Carey [2005]. Magma fragmentation generates a mixture of tephra and gas which leaves the vent at a velocity of 50-300 m/s [Mastin, 2007]. The momentum is the main driving force during the first few hundred meters or kilometers (jet phase). Then, the plume starts to entrain and heats the surrounding air, reducing its density and then rises due to convection (convective phase). Finally, when the density of the plume is equal to that of the surrounding atmosphere, it generates the umbrella region and moves horizontally with the wind.

in the atmosphere far away from the vent [Ayris and Delmelle, 2012b]. At high temperatures (T>600°C i.e. in absence of a liquid phase), gas-ash interaction in the eruption plume can lead to volatile scavenging, in particular of SO_2, HCl and HF [Óskarsson, 1980, Rose, 1977]. The reactions between these gases and the ash surface are thought to be partly responsible for the deposition of alkali and alkaline earth sulfate as well as chloride salts on the ash surface [Delmelle et al., 2007]. Frogner et al. [2001] and Duggen et al. [2010] also consider the formation of Fe-bearing salts on the ash surface to be the result of such reactions. The formation of soluble iron at the ash surface has been suggested to be connected with processes such as the transport of iron chlorine ($FeCl_2$) into the fluid phase within the hot core of the plume [Duggen et al., 2010], surface adsorption of halogen gases and condensation of sulfuric and halogen acids on ash particles [Óskarsson, 1980] as well as dissolution and precipitation cycles [Delmelle et al., 2007]. Nevertheless, a precise insight into how insoluble volcanic iron transforms

into soluble and thus, bio-available form has so far been lacking.

1.4 Research questions and objectives

Above, the states of the art of the research on volcanic ash fertilization impact on the surface ocean and the ash iron mobilization in eruption plumes have been discussed. However, there are still several open questions when it comes to understanding the production of bio-available iron during volcanic eruptions. This thesis sought to improve existing knowledge of in-plume ash iron mobilization through the development of a conceptual box model for simulating gas-ash/aerosol interactions in volcanic plumes. The plume is divided into temperature dependent zones: high, mid and low temperature zones (see Fig. 1.1 right panel). Each zone is represented as a box where a range of chemical and thermodynamic interactions among ash, aerosols and gas is simulated numerically. The input into the first box (high-T) is a mixture of magmatic gas and ash which can have various compositions. Olgun et al. [2011] reported that the ash from different volcanic settings (convergent plate, divergent plate and hot spot) release different amounts of Fe in contact with seawater. Interestingly enough, the gas chemistry and rock mineralogy varies strongly with tectonic setting [Gerlach, 2004, Lindsley, 1991]. Therefore, the gas and ash composition inside volcanic plumes from different tectonic settings are distinct. Hence, different scenarios can be defined in order to cover the various gas and ash compositions related to the tectonic settings.

The main scope of this thesis is to find answers to the following questions:

1. How does the high temperature zone control the gas and ash surface compositions?
2. What are the key parameters/processes which control iron mobilization in the plume?
3. How much iron would be finally dissolved in the liquid phase?
4. Which tectonic setting is more favorable for bio-available iron production?

The simulations begin at the vent and continue up to the natural buoyancy level of the plume. Furthermore, aqueous chemistry and microphysics in the volcanic cloud (including ice and rain drops), that could affect the fate of the dissolved iron are beyond the scope of this thesis. It should be noted that this research does not intend to simulate any specific eruption but simply to present a comparative study for identifying the favorable processes and source conditions for ash iron mobilization.

1.5 Thesis outline

This research develops a conceptual temperature dependent box model in order to study the role of the pilinian and sub-pilinian volcanic eruption plumes in iron solubility and speciation. The effect of the high temperature zone (the hot core) on the erupted gas and ash is investigated in chapters 2 and 3, respectively, based on the thermodynamic equilibrium at temperatures >600°C. Further to this, mid and low-T in-plume processes (e.g., sulfuric acid and water condensation, scavenging of the volatiles by liquid phase and ash dissolution) are discussed in chapter 4. The general conclusions of the research and the outlook are given in chapter 5.

Chapter 2

How does the hot core of a volcanic plume control the sulfur speciation in volcanic emission?[1]

2.1 Introduction

Volcanoes are well-known emission sources of sulfur species. During recent years, the impact of volcanic S species on the atmosphere and climate attracted the attention of many researchers [e.g., Bekki, 1995, Delmelle, 2003, Robock, 2000, von Glasow et al., 2009]). S gases, which are predominantly in form of sulfur dioxide (SO_2) and hydrogen sulphide (H_2S) [Aiuppa et al., 2005, Bates et al., 1992], contribute typically 2 to 35 percent of volcanic gas emissions with values of 15-21 Tg/year for SO_2 and 1-37 Tg/year for H_2S [Halmer et al., 2002]. Simultaneous measurements and observations of volcanic SO_2 and H_2S are rare [Halmer et al., 2002, Symonds et al., 1994] due to difficulties in analytically resolving S speciation in high-T gases [Montegrossi et al., 2001, O'Dwyer et al., 2003] as well as detecting H_2S spectroscopically in volcanic clouds [Clarisse et al., 2011, Toda et al., 2004].

The proportion of these two species (H_2S/SO_2 in moles), also known as redox ratio, increases with increasing pressure and with decreasing temperature and oxygen fugacity of the magma [Carroll and Holloway, 1994, Wallace, 2001]. Measurements in hot volcanic gases revealed that this ratio is extremely variable [Aiuppa et al., 2005, 2007a,b, Gerlach, 2004, Symonds et al., 1994]. For instance, in degassing fumaroles, the H_2S/SO_2 ratio

[1]This chapter is the manuscript: Hoshyaripour, G., Hort, M., Langmann, B. (2012) How does the hot core of a volcanic plume control the sulfur speciation in volcanic emission? Geochem. Geophys. Geosyst., 13, Q07004, doi:10.1029/2011GC004020. which is cited in this thesis as [Hoshyaripour et al., 2012]

varies in the range of 0.01-100 [Aiuppa et al., 2005, O'Dwyer et al., 2003]. In general, this ratio is low in high-temperature volcanic gases released at atmospheric pressure [Giggenbach, 1996, Symonds et al., 1994] and is high in low-temperature fumaroles and solfataras, where discharges arise from deep hydrothermal systems [Giggenbach, 1980]. In other words, in the former, SO_2 is the prevalent sulfur species while H_2S dominates in the latter [Aiuppa et al., 2005].

In addition to high temperature S flux and speciation data, advanced measurement and observation techniques resulted in very good insight into sulfur speciation in volcanic clouds [Clarisse et al., 2011, Hunton et al., 2005, Rose et al., 2006]. Hunton et al. [2005] studied the volcanic cloud of the Hekla 2000 eruption via in-situ aircraft observations. They reported 1 ppmv SO_2 concentration in the plume but no H_2S was observed. This outcome was in very good agreement with results of Rose et al. [2006] who also detected 1-1.2 ppmv SO_2 but no H_2S in the 33-34 hour old volcanic cloud of the same eruption. The absence of H_2S in the cooled volcanic plume (i.e., H_2S/SO_2=0) suggests that this species has been depleted via in-plume processes [Hunton et al., 2005, Rose et al., 2006]. However, the oxidation of H_2S under atmospheric conditions may be of the order of 2 to 5 days [Aiuppa et al., 2007a, Rose et al., 2006, Seinfeld and Pandis, 2006]. In addition, since H_2S is only slightly soluble in liquid water, its removal by cloud and rain drops at lower heights is negligible [Textor et al., 2004]. Therefore, quick depletion of H_2S in a few hours old volcanic plume cannot be due to either low-temperature oxidation processes or scavenging by the liquid phase and another alternative sink for this species must exist.

Recently, it has become clear that volcanic vents are not simply passive point sources of gas emission, but that in fact they also act as high-T reactors where mixtures of volcanic and atmospheric gases might react, generating new and previously unexpected reaction products [Gerlach, 2004, Martin et al., 2006, 2009]. Hence, these hot reactors can be considered as a main cause of changes in the sulfur speciation [Africano and Bernard, 2000, Getahun et al., 1996]. Studies over recent decades revealed that in high-temperature (T>500°C) volcanic gases the reaction rates are sufficiently fast to ensure that the system is very close to equilibrium conditions [Gerlach, 2004, Symonds and Reed, 1993]. Considering this assumption, Martin et al. [2009] studied the high-temperature mixture of volcanic and atmospheric gases and concluded that in lack of air (<6% air) H_2S does not re-equilibrate. This is in agreement with the finding of Aiuppa et al. [2007b] who used experimental data coupled with modeling studies on the gas plume of Mount Etna. They reported that the H_2S/SO_2 ratio shows no systematic change with plume aging and suggested that H_2S is kinetically stable during short-range transport and T<600°C. However, in the case of higher temperatures and also more air entrainment, the sink for the H_2S is still unknown.

This study aims to investigate the effect of high-T gas-air mixing on sulfur speciation and redox state with respect to chemical, physical and thermodynamic properties of the hot core of volcanic plumes. Considering the data for hot gas (T>600°C) [Gerlach, 2004, Symonds et al., 1994], a box model is considered to identify the processes which can change the S speciation during the first few minutes in the eruption plume. Section 2.2 describes the modeling concepts, procedures and scenarios. In section 2.3 the effects of different initial conditions and also various processes in the hot core on S speciation are discussed. In addition, the model outputs are evaluated against an observed volcanic cloud. Finally, conclusions are given in section 2.4.

2.2 Methodology

2.2.1 Concepts of mixing

Considering the great diversity in the style of volcanic eruptions (i.e., from effusion of basaltic magma as lava flows and fire fountaining in Hawaiian eruptions to the generation of high-altitude plumes in plinian eruptions), there are different mechanisms for high-T mixing of volcanic and atmospheric gases. In general, what controls the nature of mixing are temperature and eruption dynamics (i.e., turbulence and air entrainment). If the plume is able to entrain and heat enough air, it can reduce its density below that of the surrounding atmosphere and continue to rise. Otherwise, it would collapse as a low fountain and generate pyroclastic flows and surges [Sparks et al., 1997]. This study focuses on the mixing processes in the hot core of subplinian and plinian eruption plumes which usually have high temperature (T>600°C) as well as high air entrainment due to high turbulence at the plume boundaries [Sparks et al., 1997]. For simplification, we can assume that the effect of decompression on temperature is negligible [Ogden et al., 2008]. Thus, the main cause of the cooling is ambient air entrainment.

2.2.2 Modeling procedure and scenarios

To identify the hot core control on the H_2S/SO_2 ratio, a conceptual box model has been considered (Fig. 2.1) which covers the chemical processes in the temperature range 600°C<T<1000°C and thus, can be solved using thermodynamic equilibrium models. Such models have been widely used by several authors in order to simulate the mechanism of hot volcanic gas interaction with wall rock [e.g., Africano et al., 2003, Symonds and Reed, 1993] and also atmospheric gases [e.g., Gerlach, 2004, Martin et al., 2006, 2009]. Here, we use two most cited models SOLVGAS and GASWORKS [Symonds and Reed, 1993] to model the processes in the hot mixture of volcanic and atmospheric

gases. SOLVGAS calculates homogeneous equilibrium (distribution of species) in a gas phase while GASWORKS computes heterogeneous equilibria among gases, solids and liquids during processes of cooling, gas-gas mixing, pressure changes and gas-rock reaction [Symonds and Reed, 1993, Symonds et al., 1987]. More details on these programs have been provided elsewhere [see Symonds and Reed, 1993] and thus, their description is not given here. A significant advantage of these models is the ease with which compositional parameters such as air to magmatic gas ratio (V_A/V_M) can be explored, alongside physical parameters such as temperature and pressure.

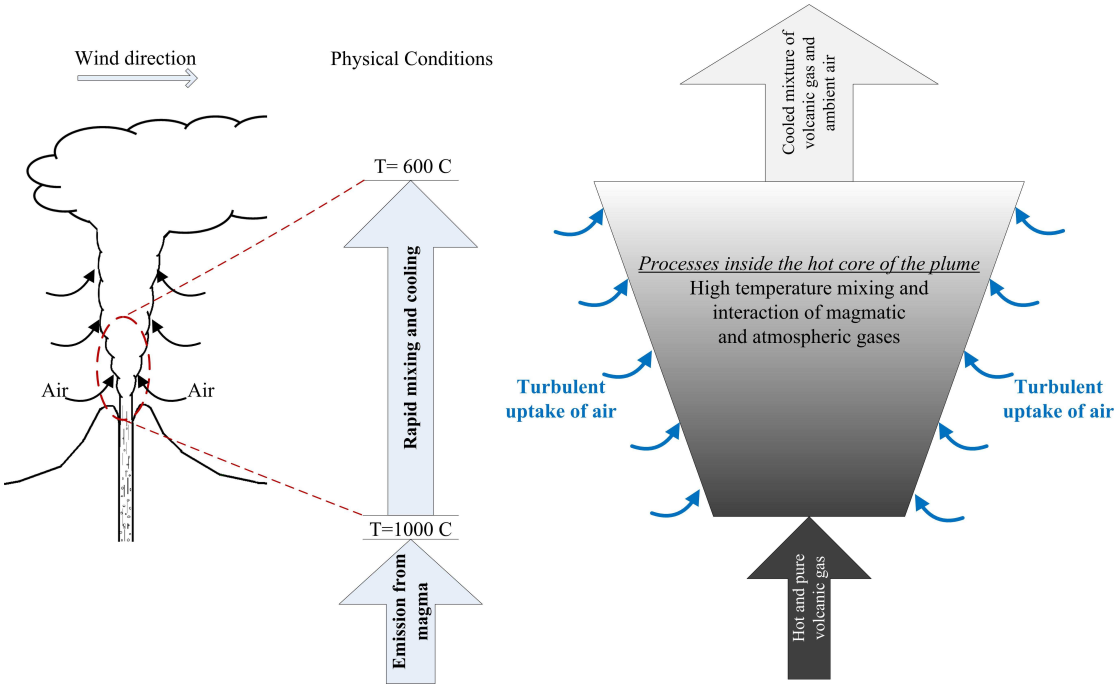

FIGURE 2.1: Considered conceptual box model for the hot core of a volcanic plume

As shown in Fig. 2.1, we need directly sampled uncontaminated high-T volcanic gas data as model input. Such data are generally sparse [Rose et al., 2006, Symonds et al., 1994]. To optimize the model, we use the data of directly sampled high-T volcanic gases from different volcanoes reported by Gerlach [2004] proposing three typical compositions for three different tectonic settings: convergent plate (CP), divergent plate (DP) and hot spot (HS) (Table 2.1). The scope of this research is identifying the sensitivity of sulfur speciation in various volcanoes to cooling and mixing processes in the hot core of volcanic plumes. Based on the compositions given in Table 2.1 and in order to check the sensitivity of the model against the oxygen fugacity (fO_2), we define some modeling scenarios. These scenarios have been calculated using SOLVGAS by introducing the initial composition (Table 2.1) as the starting point. Second, the temperature of the system has been adjusted to 1000°C for having the same initial temperature for all scenarios for comparison reasons (see Table 2.2, main oxidation states). Then, a range

for the oxidation state of the system, which is represented by the logarithm of oxygen fugacity ($\log fO_2$), is considered by varying $\log fO_2$ by ± 1. Thus, 9 high-T volcanic gas compositions are simulated as modeling scenarios (Table 2.2). The pressure is held constant at 1 bar in all calculations. We note that some of the initial conditions like T and fO_2 may seem unusual regarding some volcanic settings. This is done because the conceptual model of this study is not designed to reproduce a specific situation at one volcano but rather to identify the role of different initial conditions and processes in S speciation in different types of volcanoes. The impacts of these assumptions will be discussed in section 2.4.

TABLE 2.1: Average high-T volcanic gas composition in mole %

Volcano type	Convergent plate	Divergent plate	Hot spot
T(°C)	768	1130	1140
log fO_2	-14.41	-9.31	-8.82
Source	Arc Mean	Erta'Ale	Kīlauea
Reference	[Gerlach, 2004]	[Symonds et al., 1994]	[Gerlach, 2004]
H_2O	91.9	75.1	75.7
CO_2	4.6	13.1	3.2
H_2	0.5	1.59	0.95
H_2S	0.67	1.01	0.16
SO_2	1.44	7.84	19.4
HCl	0.76	0.42	0.17
HF	0.061	0.42	0.18
CO	0.03	0.6	0.09

In previous studies on high-T mixtures usually one physical parameter (temperature (T) or (V_A/V_M)) has been considered as variable [Gerlach, 2004, Martin et al., 2006, 2009]. Here, for the first time, we consider mixing and cooling concurrently which means changing T and V_A/V_M simultaneously. GASWORKS has the capability of mixing two gases with different temperature and composition. At each step, we mix the hot volcanic gas (T=1000°C) with 25°C air (78% N_2, 21% O_2, O.1% Ar) by increasing V_A/V_M which makes the system more oxidized and also cools it. Air is mixed with the magmatic gas until a temperature of 600°C is reached which corresponds approximately to V_A/V_M = 1.0. At T<600°C and during the first few hours of the eruption, we assume that the changes in H_2S/SO_2 as well as HCl/SO_2, HCl/HF, H_2SO_4/SO_2 etc are negligible [Aiuppa et al., 2005, 2007b]. Therefore, the predicted ratios in the output of the high-T box model can be compared to the measured ratios in few hours old volcanic clouds [e.g., Hunton et al., 2005, Rose et al., 2006]. To investigate the effect of cooling and mixing on the gas composition separately, we consider two additional procedures for each scenario: cooling without air entrainment from 1000°C to 600°C as well as the mixing of magmatic gas with air at constant temperature (T=1000°C) from V_A/V_M=0 to 1.0.

TABLE 2.2: Modeling scenarios simulated with SOLVGAS in mole %

Volcano type	Convergent plate(CP)			Divergent plate(DP)			Hot spot(HS)		
Redox state	Reduced	Main	Oxidized	Reduced	Main	Oxidized	Reduced	Main	Oxidized
logfO_2	-11.94	-10.94	-9.94	-11.89	-10.89	-9.89	-11.39	-10.39	-9.39
T(°C)	1000	1000	1000	1000	1000	1000	1000	1000	1000
H_2O	88.31	91.05	91.85	76.66	75.78	75.37	82.91	75.94	75.72
CO_2	3.98	4.50	4.65	10.81	13.38	14.08	2.59	3.25	3.34
H_2	4.69	1.44	0.49	4.07	1.12	0.40	2.15	0.64	0.23
H_2S	1.58	0.29	0.01	5.01	0.85	0.05	4.71	0.39	0.02
SO_2	0.26	1.76	2.12	0.94	7.39	9.10	6.67	19.16	20.31
HCl	0.71	0.76	0.77	0.36	0.42	0.44	0.14	0.17	0.17
HF	0.06	0.06	0.06	0.36	0.42	0.44	0.15	0.18	0.18
CO	0.34	0.11	0.04	0.92	0.32	0.12	0.11	0.04	0.02

We note that gas-ash interaction in the eruption plume leads to volatile scavenging, in particular SO_2, HCl and HF [Óskarsson, 1980, Rose, 1977]. Studies showed that during explosive eruptions as much as 33% of the erupted sulfur can be adsorbed on ash as acid aerosol particles and 5% of it can be trapped via gas-ash interaction [Ayris and Delmelle, 2012b, Rose, 1977]. This suggests that scavenging is more important after the formation of liquid acid aerosols in volcanic plumes and is therefore thought to be negligible in a first order approximation and the temperature range of this study (600°C-1000°C) where liquid phase formation is very unlikely. However, this effect will be considered during the evaluation of Hekla 2000 eruption in section 2.3.4.

2.3 Results

2.3.1 Cooling without air entrainment

The effect of cooling from 1000°C to 600°C on major S species in the volcanic gas (H_2S, SO_2, H_2SO_4 and SO_3) is shown in Fig. 2.2. For all volcano types it is obvious that during cooling the system favors less oxidized species (e.g., H_2S) than oxidized species (e.g., SO_2 and SO_3). For instance, with falling temperature, H_2S increases according to reaction 2.1 when it proceeds toward the left:

$$H_2S + 2H_2O \rightleftharpoons SO_2 + 3H_2 \tag{2.1}$$

These cooling trends are controlled by entropy effect, whereby lower temperatures favor fewer moles of gas (left side of reaction 2.1). Giggenbach [1996] proposed that the temperature dependence of the equilibrium constant (K_{eq}) of reaction 2.1 can be expressed as:

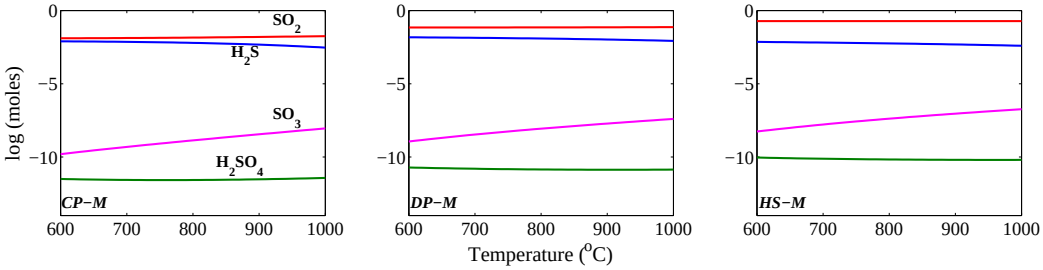

FIGURE 2.2: The effect of cooling from 1000°C to 600°C on major S species; blue: H_2S, red: SO_2, green: H_2SO_4 and pink: SO_3; CP-M: convergent plate in main oxidation state, DP-M: divergent plate in main oxidation state, HS-M: hot spot in main oxidation state

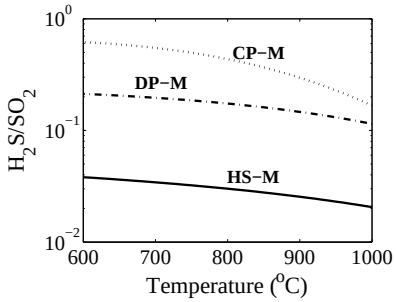

FIGURE 2.3: H_2S/SO_2 ratio during cooling for CP-M, DP-M and HS-M scenarios

$$K_{eq} = \log((f_{SO_2} \cdot f_{H_2}^3)/(f_{H_2S} \cdot f_{H_2O}^2)) = 3.66 - 10744/T \tag{2.2}$$

where f is the fugacity ratio (assumed to be equal to concentrations) and T is temperature in K. Thus, during cooling K_{eq} decreases rapidly and results in a considerable redox ratio increase. Fig. 2.3 displays the H_2S/SO_2 ratio which increases for all types of volcanoes during cooling. These changes are pronounced for the CP-M case in which the redox ratio becomes approximately 3 times larger. In other words, sulfur redox ratio increases more drastically during cooling in the scenario with the lowest oxygen fugacity. The abundance of reduced sulfur species at lower temperature has been reported by many researchers [e.g., Aiuppa et al., 2005, Giggenbach, 1996]. Thus in an air free magmatic gas the lower the temperature, the higher the H_2S content. This effect is notable in CP volcanoes which typically have lower initial temperature (T<1000°C). They can have higher initial H_2S content and thus more potential of H_2S injection into the atmosphere.

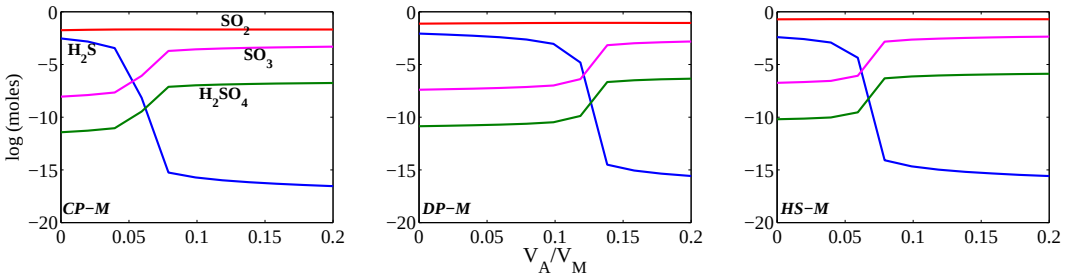

FIGURE 2.4: Major S species concentrations during mixing with air at constant temperature (i.e., increasing V_A/V_M at T=1000°C) for CP-M, DP-M and HS-M scenarios.

2.3.2 Mixing with air at constant temperature

Fig. 2.4 shows the results of the mixing of volcanic gas with air at 1000°C. Since after V_A/V_M =0.2, changes in number of moles are negligible, the x axis is limited to this value. Considering the presence of molecular oxygen (O_2) in the system, reaction 2.1, which consumes the atomic oxygen from H_2O, does not control the H_2S/SO_2 ratio anymore. In this case, according to the reaction 2.3, the complete oxidation H_2S to SO_2 results in depletion of hydrogen sulphide in the system and also increase in SO_2:

$$H_2S + 1.5O_2 \rightleftharpoons SO_2 + H_2O \tag{2.3}$$

which can be further oxidized to SO_3 and H_2SO_4 according to reactions 2.4 and 2.5:

$$2SO_2 + O_2 \rightleftharpoons 2SO_3 \tag{2.4}$$

$$SO_3 + H_2O \rightleftharpoons H_2SO_4 \tag{2.5}$$

These reactions become more important as soon as the H_2S content of the system becomes negligible. This is a transition point in Fig. 2.4 where H_2S drastically decreases and SO_3 and H_2SO_4 significantly increase. It occurs at V_A/V_M being around 0.049, 0.095 and 0.041 for CP-M, DP-M and HS-M, respectively. For comparison, the changes in S redox ratio are shown in Fig. 2.5 where H_2S/SO_2 decreases with increasing V_A/V_M. It is obvious that H_2S content becomes extremely small in the system around the above mentioned values for V_A/V_M. Thus, oxygen is no more consumed by the oxidation of H_2S (in reaction 2.3) and there is more O_2 available for reactions 2.4 and 2.5. Hence, reaction 2.4 and accordingly reaction 2.5 proceed more rapidly which result in a considerable increase in SO_3 and H_2SO_4 and also a small decrease in SO_2. After this transition

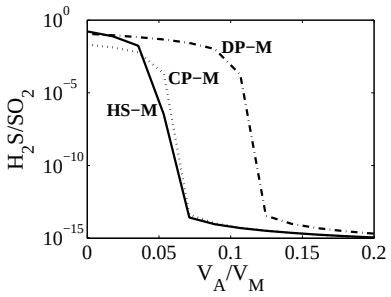

FIGURE 2.5: H_2S/SO_2 ratio during mixing with air at constant temperature (i.e., increasing V_A/V_M at T=1000°C) for CP-M, DP-M and HS-M scenarios.

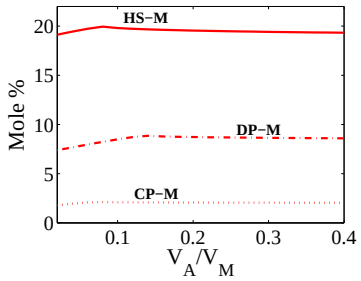

FIGURE 2.6: SO_2 concentration during mixing with air at constant temperature for CP-M, DP-M and HS-M scenarios.

stage, these species become almost stable and do not change significantly. More details about the transition point are discussed in section 2.3.3.

Similar to the cooling (section 2.3.1), changes in the H_2S/SO_2 ratio are more pronounced for the CP scenario which has the lowest fO_2 (see Table 2.2). But the direction of changes is completely reversed. In the mixing procedure, the oxidation reaction 2.3 controls this ratio and considerably decreases it while in the cooling process, where there are no free O_2 molecules, entropy controls the H_2S/SO_2 ratio via reaction 2.1 and increases it. The changes in SO_2 concentration is shown in Fig. 2.6. For example, in DP-M case SO_2 reaches its maximum value at V_A/V_M=0.12 which is the result of reaction 2.3. After this point it starts to decrease due to reaction 2.4 and eventually becomes constant. These trends are similar for other scenarios. For all types of volcanoes, the mixing of magmatic gas with air at 1000°C results in a chain of oxidation reactions 2.3 to 2.5 which depletes H_2S, increases SO_2, SO_3 and H_2SO_4 and thus, decreases the H_2S/SO_2 ratio. This situation happens very fast in CP and HS volcanoes but takes longer for the DP volcanoes. In other words, more air is needed for depletion of reduced gases in DP volcanic gases.

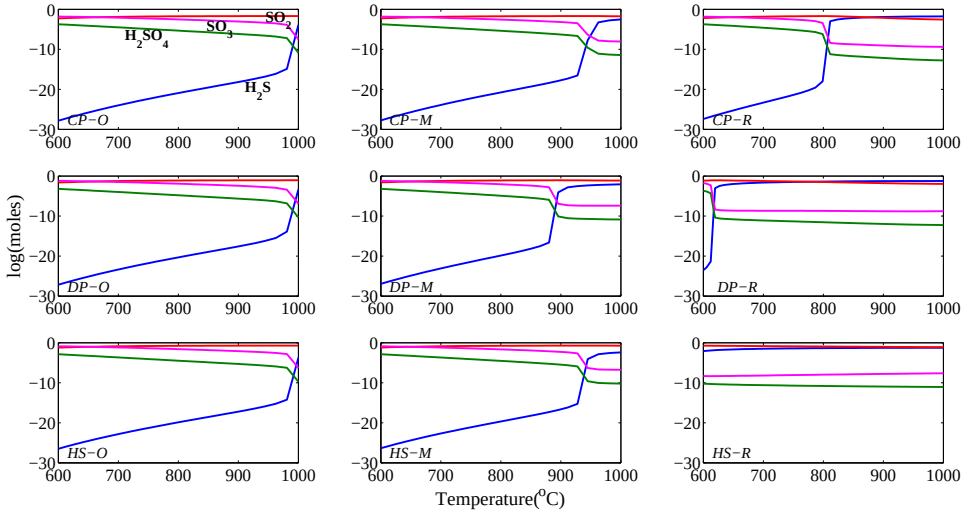

FIGURE 2.7: Major S species during cooling with air entrainment (i.e., mixing of 1000°C magmatic gas with 25°C ambient air which results in simultaneous mixing and cooling) for different oxidation states.

2.3.3 Cooling with air entrainment (cooling and mixing simultaneously)

In order to simulate the mixing of hot volcanic gas with ambient air more realistically which cause the dilution, cooling and thus rising of the volcanic plume, the 1000°C magmatic gas has been mixed with 25°C air which results in simultaneous cooling and mixing. The results for major S species are shown in Fig. 2.7. The general trends for the main scenarios are almost similar to those presented in section 2.3.2 where oxidation of the system at constant T causes a considerable decrease of H_2S and increase of SO_3 and H_2SO_4 via a transition point at around 950°C for CP-M and HS-M and around 900°C for DP-M. But in concurrent mixing and cooling, changes in species concentrations continue after the transition stage without reaching a constant concentration; i.e., SO_3 and H_2SO_4 constantly increase at the expense of SO_2 decrease. The entropy effect can explain these changes. By decreasing temperature, reactions 2.4 and 2.5 proceed towards the right side in order to reduce the moles of gas in the system. If the temperature remains constant (like section 2.3.2) the entropy effect does not play a significant role. Thus, species attain a constant concentration and would not change significantly with adding more air.

By comparing different oxidation states, it is obvious that for all types of volcanoes lower initial fO_2 shifts the transition stage to lower temperatures. While in all oxidized scenarios in Fig. 2.7 the transition occurs very early at T>950°C, in the reduced scenarios it is shifted to 800°C, 620°C and <600°C for CP-R, DP-R and HS-R, respectively. Since

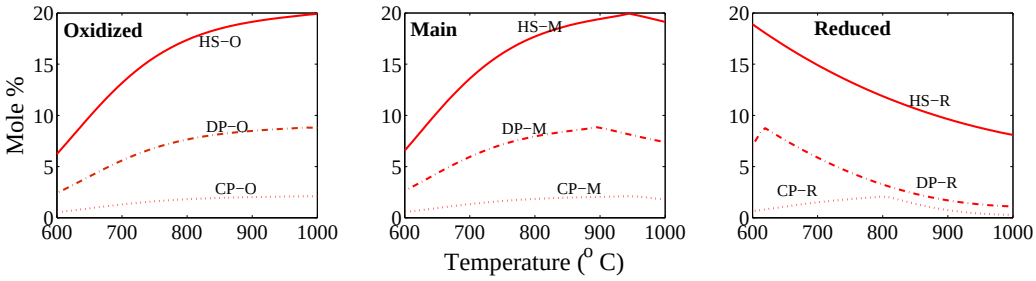

FIGURE 2.8: SO_2 mole concentration as a function of temperature for different volcanoes in different oxidation states during cooling with air entrainment.

after the transition, SO_2 keeps decreasing until 600°C, an early transition can result in a huge decrease in SO_2 concentration in the final plume composition. Fig. 2.8 shows the changes in SO_2 content of the system for different volcanoes and also different oxidation states. There is no significant difference between the main and oxidized scenarios regarding the trends and values. In these cases, 65% to 75% of the initial magmatic SO_2 is oxidized. But the reduced cases which have lower SO_2 at 1000°C show an increase and also the highest values for this compound at 600°C. These effects can be explained by the reactions 2.3 to 2.5. The systems with lower initial oxygen fugacity, which means also higher H_2S concentration or higher H_2S/SO_2 ratio, have more sinks for the entrained O_2 and do not allow the reactions 2.4 and 2.5 to proceed very fast. While there is enough H_2S in the system, its oxidation persistently consumes O_2 via reaction 2.3 which results in production of SO_2 and reduction of the H_2S/SO_2 ratio. An example of changes in S redox state is shown in Fig. 2.9 for the main scenarios. It is obvious that the rate of H_2S/SO_2 reduction is the highest for the CP case which has the highest initial value and the lowest initial fO_2 (see Table 2.2). This is similar to the trend shown in Fig. 2.5 and addresses the fact that the lower the oxygen fugacity the faster the H_2S/SO_2 reduction. After depletion of hydrogen sulphide (when H_2S/SO_2 approaches 0), reaction 2.4 becomes a significant sink for SO_2 and continuously decreases it. Therefore, reduced scenarios can potentially inject more SO_2 into the atmosphere. In other words, the injected SO_2 into the atmosphere is not essentially generated directly from magma but it can be produced in the hot core as the result of H_2S oxidation (reaction 2.3).

As mentioned above, during mixing with ambient air (i.e., in presence of O_2), the transition results in depletion of reduced species in the system. Martin et al. [2006] proposed that the main sinks for oxygen in 1000°C magmatic gas are H_2S via the reaction 2.3 and H_2 via the reaction 2.6:

$$2H_2 + O_2 \rightleftharpoons 2H_2O \tag{2.6}$$

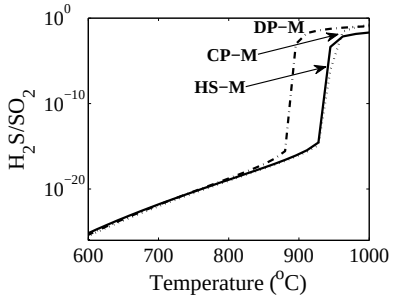

FIGURE 2.9: H_2S/SO_2 ratio as a function of temperature during cooling with air entrainment.

They showed that the location of the transition corresponds exactly to the complete removal of H_2 and H_2S [Martin et al., 2006]. In other words, the oxidation state of the system is controlled by the ratio of H_2 and H_2S content of it (i.e., two major sinks for the oxygen) to the amount of entrained oxygen from ambient air (i.e., the major source of the oxygen). Thus, this ratio can be treated as the ratio of the major sinks of the oxygen to its major source in the system and defined as:

$$X_{mix} = (n(H_2) + n(H_2S))/(0.21n(\text{air})) \tag{2.7}$$

where n corresponds to mole number of each species and the number 0.21 represents the 21% of the ambient air which is assumed to be oxygen. This ratio is calculated for different volcanic settings and shown in Fig. 2.10. This figure shows unambiguously that the critical value for $\log(X_{mix})$, after which the transition occurs, is between -2.50 and -3.00 for all types of volcanoes. Volcanic plume rises in the atmosphere as a result of air entrainment. Mixing of the magmatic gas with ambient air leads to addition of O_2 into the system as well as cooling which, according to the entropy effect, force reactions 2.3 and 2.6 toward the right side which means consumption of H_2 and H_2S. Therefore, during mixing of volcanic gas with air, X_{mix} decreases continuously until reaching the critical value which means depletion of reduced species in the system and transition into the oxidized state.

2.3.4 Model evaluation against observed volcanic clouds

In order to evaluate the findings of this research, we compare the results to observations. Here, we consider the data of the volcanic cloud form the Hekla 2000 eruption which has been reported by Rose et al. [2006] and Hunton et al. [2005] (Table 2.3). Various studies have been conducted on this eruption [e.g., Höskuldsson et al., 2007, Moune et al., 2006, 2007, 2009, Rose et al., 2003] resulting in a very good knowledge about its petrologic and volcanologic properties as well as atmospheric transport and dispersion. This eruption

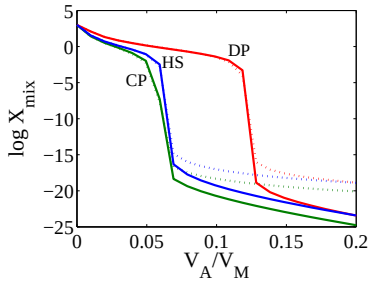

FIGURE 2.10: X_{mix} ratio as a function of V_A/V_M for different volcanoes; dash line: mixing at constant temperature (T=1000°C), solid line: mixing and cooling simultaneously (i.e., cooling with air entrainment).

is also unique regarding the direct sampling from the 33-34 hours old volcanic cloud [Rose et al., 2006]. If we assume that at temperatures less than 600°C and during the first few hours of the eruption the S speciation in the gas phase remains constant then the chemical composition in the output of the hot core (the box model in this study) could be compared to the few hours old volcanic cloud composition. It is notable that the condensation of H_2SO_4 can significantly affect its concentration in the gas phase even in a few hours old plume. Therefore, we omit this species in our evaluation study.

TABLE 2.3: Hekla plume observations on 28 February 2000 (33-34 hours after the eruption)

Study	Hunton et al. [2005]	Rose et al. [2006]
SO_2 (ppb)	895	1000-1200
H_2S (ppb)	0	0
H_2SO_4 (ppb)	0.31	0.205

Remote sensing studies propose that the Hekla 2000 eruption has injected approximately 1.6 Tg volcanic gas into the atmosphere [Hunton et al., 2005, Rose et al., 2003, 2006]. From this value 0.2 Tg is SO_2 [Rose et al., 2003] which corresponds to weight percentage of 12.5. In other words, to inject 0.2 Tg SO_2 into the atmosphere, the eruption plume of Hekla should contain 12.5 wt% SO_2 near the vent. The conversion of this value to mole fraction of SO_2 in the plume can be done using the molar weight of volcanic gas. As Hekla is located on a mid-ocean ridge but its geochemistry also suggests a hot spot signature [Schmincke, 2004] its magmatic gas composition can be compared to both DP and HS scenarios. Petrologic studies on the Hekla magma suggest an oxygen fugacity close to FMQ (Fayalite, Magnetite, and Quartz) at 1000°C [Baldridge et al., 1973, Moune et al., 2007] which corresponds to $\log fO_2$ of -10.50 to -11.00 [Lindsley, 1991]. Although in petrology this rage is known as reduced conditions, due to our definition of the oxidation states it happens to fall into the range of the main oxidation state scenarios (-10.89 for DP-M and -10.39 for HS-M). Therefore DP-M and HS-M scenarios are selected for the evaluation study. The gas composition in these scenarios has the

molar weight of approximately 24-28 g. According to the above calculations, 12.5 wt% of this value is SO_2 which corresponds to about 4.6-5.5 mole% of SO_2 in the volcanic cloud. These values are satisfactorily in the range of our predictions for DP-M and HS-M with 2.7% and 6.4%, respectively (Fig. 2.8). These scenarios also correspond to the value of 0 for H_2S concentration at 600°C which is also in agreement with the observations. If we assume that the hot spot setting is dominant at Hekla, HS-M scenario has an acceptable agreement with the observations. The overestimation of this scenario can be due to neglecting either scavenging of sulfur species by volcanic ash or the effect of other processes in the warm region of the volcanic plume (T<600°C). As it was snowing during the eruption [Höskuldsson et al., 2007], snow particles could have also washed gases out of the plume.

It is worth to mention that petrologic estimates suggest an injection of 0.6-3.8 Tg SO_2 into the atmosphere during Hekla 2000 eruption [Moune et al., 2007] which when compared to the remote sensing measurement of 0.2 Tg SO_2 release [Hunton et al., 2005, Rose et al., 2003, 2006] is surprising. This becomes less surprising when one considers the box model of this study and the effect of the hot core on S speciation. The initial SO_2 content of the HS-M scenario (19.16 mole% at 1000°C) reduces by the factor of 3 once it passes through the box model (6.4% at 600°C) as the result of the hot core oxidation processes (see Fig. 2.8). If we omit the hot core effect, then SO_2 injection, based on the initial SO_2 content of HS-M, is about 0.6 Tg which is close to the lower bound of the petrologic estimate. On the other hand, the above calculations show a good agreement between observed volcanic cloud and the predictions based on hot core box model. Therefore, the hot core effect on sulfur speciation can explain the differences between petrologic estimate of S degassing and remote sensing observations of SO_2 in the volcanic cloud.

2.4 Discussion and conclusion

The study of the high-T mixing of magmatic and atmospheric gases by considering a conceptual box model for the temperature range 600°C<T<1000°C confirms the hypothesis that the hot core of volcanic plumes can function as a hot oxidizing reactor for S species. Burgisser and Scaillet [2001] showed that the redox state that magma records at depth does not necessarily mirror that of its escaping gases. In addition, our results show that the redox state in volcanic clouds does not essentially reflect the magmatic gas composition at the vent. Therefore, volcanic emissions undergo significant compositional changes from the release point (i.e., magma) to the atmosphere (i.e., volcanic cloud). These changes are controlled by the effect of various processes such as cooling

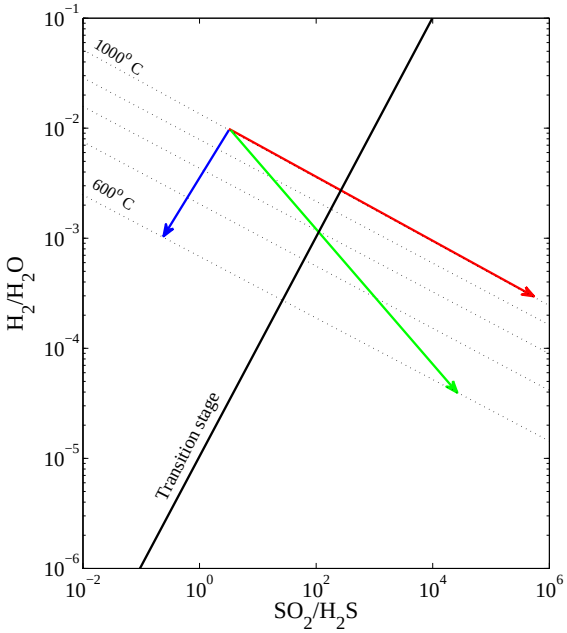

FIGURE 2.11: Equilibrium SO_2/H_2S and H_2/H_2O ratios in magmatic gases, calculated at 0.1 MPa pressure from relations (E3) and (E4) in a range of temperatures in this study (isotherms are shown) adopted from Aiuppa et al. [2011]; blue arrow: cooling without air entrainment; red arrow: mixing with ambient air at constant T; green arrow: mixing and cooling simultaneously.

and mixing with the ambient air. Cooling of the magmatic gas without air entrainment favors the reduced forms of S (e.g., H_2S) while mixing with air supplies molecular oxygen to the system making oxidized species dominant. During mixing with air as soon as two main reduced species reach a minimum value (H_2S and H_2 via reactions 2.3 and 2.3 respectively), the transition into a completely oxidized system occurs. Aiuppa et al. [2011] proposed the equations 2.8 and 2.9 for the thermodynamic equilibrium of reactions 2.3 and 2.3:

$$\log(SO_2/H_2S) = 27377/T - 3.986 + (1.5\log(fO_2)) - \log(fH_2O) \tag{2.8}$$

$$\log(H_2/H_2O) = -12707/T + 2.548 - 0.5\log(fO_2) \tag{2.9}$$

They finally obtained, using equations 2.8 and 2.9, the couples of equilibrium H_2/H_2O and SO_2/H_2S gas ratios, at each temperature (at 0.1 MPa pressure) (Fig. 2.11) [Aiuppa et al., 2011]. Schematic examples of the considered procedures in this study are shown in this figure. During cooling without adding air (blue arrow) by passing the isotherms the reduced species become favorable. The red and green arrows show the general pattern of the mixing at constant T and mixing with 25°C ambient air (i.e., simultaneous mixing and cooling), respectively. The results of this study show that when the relation between

SO_2/H_2S and H_2/H_2O (x and y axis, respectively in Fig. 2.11) reaches approximately 10^5, the transition to the complete oxidized system occurs. This is shown by the solid black line in Fig. 2.11 which has the slope of 10^5. The fate of the oxidation state of the system and its sensitivity to initial conditions (e.g., T and fO_2) can be explained using this figure. When the eruption begins the plume composition moves along the green arrow. The more the air entrainment rate, the less the slope of the line. In other words, in plinian and sub-plinian eruptions where air entrainment is the main cause of cooling and oxidation the green line tends closer to the red line and can pass the transition line quickly. On the other hand, in other eruptions where other causes may be important in cooling the green line inclines to be close to the blue line and even after reaching 600°C can remain on the left side of the transition line. Changing the initial temperature moves the starting point along the blue arrow. As shown in section 2.3.3, the transition happens very fast in CP volcanoes which depletes H_2S and reduces SO_2 concentration. But Fig. 2.11 demonstrates that the lower initial temperature (as in CPs) makes the injection of H_2S more likely. This effect can explain the detection of H_2S in volcanic clouds of some CP volcanoes [Clarisse et al., 2011].

With similar initial temperature, CP volcanoes inject S most predominantly in oxidized form and injection of H_2S from such volcanoes seems to be unlikely. For DP and HS volcanoes however, even though the oxidized species are dominant too, H_2S injection into the atmosphere could be expected. But it strongly depends on the oxidation state of the magma. Changing the initial fO_2 means moving of the start point along 1000°C isotherm. When the end of the green arrow (at 600°C) is very far from the transition line, not only H_2S is depleted but also SO_2 concentration is decreased. It is obvious that the lower the initial fO_2, the higher the final SO_2. Whilst the SO_2 content of the system decreases in the main and oxidized scenarios, it increases in the reduced scenarios. Consequently, the reduced magmas can potentially inject more SO_2 into the atmosphere even though they carry initially less SO_2 in the magmatic gas. In other words, the injected SO_2 into the atmosphere is not necessarily generated directly from magma but it can be produced in the hot core as the result of H_2S oxidation. In such conditions, the injection of small amounts of H_2S is also possible (especially in DP and HS). This may be an explanation for the known conflict between petrologic estimates and remote sensing observations regarding SO_2 emissions of large explosive eruptions. Conventional petrologic methods based on glass inclusions usually underestimate the SO_2 content of volcanic emissions [Gerlach et al., 1996]. However, depending on initial oxidation state, the hot core can function as a reactor for SO_2 formation and convert an initially SO_2-poor vapor (i.e., petrologic estimate) to a SO_2-rich plume (i.e., remote sensing observation). In the Hekla 2000 eruption the conflict is the other way round; i.e., petrologic methods overestimate the S injection. This can also be explained based

on the hot core effect as the hot core reduces the SO_2 in this case (see section 2.3.3). Oxidized magmas can inject sulfur into the atmosphere mainly in form of H_2SO_4 and SO_3 which are the products of SO_2 oxidation in the hot core of the plume. In these magmas, injection of H_2S into the atmosphere could be unlikely.

Several lines of evidence confirm the fact that the hot core of volcanic plume significantly controls the S speciation in volcanic emissions and makes oxidized species like SO_2 and H_2SO_4 more dominant in the system. Therefore the source parameters in volcanic cloud studies should be assigned considering the role of the hot core as an oxidizing reactor. This means that the implications of volcanic sulfur emissions in climate and atmospheric chemistry could be enhanced if one considers the effect of the hot core on S speciation in major explosive eruptions.

Chapter 3

High temperature volcanic controls on ash iron solubility

3.1 Introduction

Volcanic ash has been recently identified as a potential fertilizer for the surface ocean (see Duggen et al. [2010] for a detailed review). After the 1991 eruption of Mt. Pinatubo, Philippines, it was hypothesized that ash in contact with seawater releases iron and other nutrients in sufficient amounts to the surface ocean to stimulate marine primary productivity (MPP) and in turn, global atmospheric CO_2 drawdown [Sarmiento, 1993, Watson, 1997]. Frogner et al. [2001] found that the ash from the eruption of Hekla in 2000, Iceland, released significant amounts of dissolved iron, silicon, and manganese together with sulfate, chloride and fluoride upon exposure to seawater. Subsequent studies have confirmed that volcanic ash affects MPP through rapid iron release upon contact with seawater [Duggen et al., 2007]. The first direct evidence of a phytoplankton bloom following fertilization by volcanic ash deposition was reported by Langmann et al. [2010] in the wake of the 2008 eruption of Kasatochi volcano in the Aleutian islands.

Volcanic ash refers to tephra with a diameter <2 mm [Rose and Durant, 2009] and is typically composed of silicate glass and crystalline materials generated during an explosive eruption through magma fragmentation and to some extent, through erosion of the conduit wall rock [Heiken and Wohletz, 1992]. Iron in volcanic ash produced through magma fragmentation is essentially found in non-soluble forms, i.e., in silicate glass and in primary Fe-bearing silicates and Fe-oxide minerals [Heiken and Wohletz, 1992, Schmincke, 2004]. On the other hand, the source of iron in ash inferred to significantly alter the Fe budget in the surface ocean [Hamme et al., 2010] is suggested to consist of Fe-bearing soluble salts on the ash surface [Duggen et al., 2010]. The processes that

convert the insoluble iron in primary silicates and oxides into soluble iron compounds are so far poorly constrained. Ayris and Delmelle [2012b] emphasized that various volcanic and atmospheric processes can modulate ash Fe solubility. They suggested that both high and low temperature reactions within the eruption plume can significantly alter the ash surface composition, and hence iron mineralogy and speciation. These reactions are expected to modify the surface reactivity of the ash, thus potentially influencing further (photo)chemical reactions during transport of the ash in the atmosphere [Ayris and Delmelle, 2012b].

Within the hot core of the eruption plume, where temperatures above 600°C prevail, scavenging of volcanic acid volatiles (i.e., SO_2, HCl and HF) can occur through gas-ash interaction [Ayris et al., 2013, Óskarsson, 1980, Rose, 1977]. The reactions between these gases and the ash surface are thought to be partly responsible for the deposition of alkali and alkaline-earth sulfate and chloride salts on the ash surface [Delmelle et al., 2007]. In colder parts of the plume, the iron mobilization processes can be summarized in two principal ways: 1) formation and dissolution of soluble salt coatings on the surface of ash particles and 2) dissolution of glass shards in the ash in contact with a solute [Duggen et al., 2010]. Recent studies show admixture of air with the magmatic gases within the hot core of a volcanic eruption plume leads to a range of reactions and formation of unexpected chemical species [Hoshyaripour et al., 2012, Martin et al., 2009, Roberts et al., 2009]. At T>600°C, the reaction rates are sufficiently fast to ensure that the system is very close to thermodynamic equilibrium conditions [Symonds and Reed, 1993]. Thus, reactions within the hot core can be simulated using thermodynamic equilibrium models [Gerlach, 2004, Symonds and Reed, 1993]. This approach has been used in several studies aimed at describing the interaction between the hot magmatic gas and the wall rock (e.g., Africano et al. [2003], Symonds and Reed [1993] and the references therein) or atmospheric gases (e.g., Bobrowski et al. [2007], Gerlach [2004] and the references therein). Although the residence time of ash in the hot core of the eruption plume is short (from tens of seconds to few minutes) due to rapid cooling of the gas-ash mixture, the ash's high specific surface (surface per mass unit) and the high temperature (>600°C) most probably favors rapid attainment of thermodynamic equilibrium. Therefore, we consider that thermodynamic modeling of gas-ash reactions within the hot core of the eruption plume is a viable mean (i.e., first order approximation) to decipher new insights into the processes that control the mineralogy, and hence solubility, of iron in the surface of volcanic ash. This hypothesis is further evaluated in section 3.2.

Here we investigate gas-ash interaction in the hot core of the volcanic plume (T>600°C) in order to explore the effect of this part of the plume on Fe mineralogy and oxidation state on the ash's surface. First, our modeling concepts, assumptions and procedures are presented in section 3.2. Then, the gas-ash interactions in three typical volcanic

plume compositions (i.e., based on geochemical patterns of three tectonic settings) are simulated and the sensitivity analysis to initial conditions (e.g., oxidation state, ash composition etc.) is performed in section 3.3. Finally, the effects of the hot core on ash iron mobilization are discussed and conclusions are presented. We note that this study does not intend to reproduce any data or specific situation at one volcano but to explore the role of high temperature volcanic gas-ash interaction in Fe speciation and mineralogy in different tectonic settings in general.

3.2 Methodology

3.2.1 Modeling concepts

Considering the great diversity in the style of volcanic eruptions (i.e., from effusion of basaltic magma as lava flows and fire fountaining in Hawaiian eruptions to the generation of high altitude plumes during plinian eruptions), there are different mechanisms for high-T mixing of volcanic gas, ash and atmospheric gases. Mixing itself is controlled by temperature and eruption dynamics (i.e., turbulence and air entrainment). If the plume is able to entrain and heat enough air, it can reduce its density below that of the surrounding atmosphere and continues to rise. Otherwise, it would collapse as a low fountain and generate pyroclastic flows and surges [Sparks et al., 1997]. We focus on the mixing processes in the hot core of sub-plinian and plinian eruption plumes, which have high temperature (T>600°C) as well as high air entrainment rates due to high turbulence along the plume boundaries [Sparks et al., 1997]. For simplification, we assume that the effect of decompression on temperature is negligible and the main cause of the cooling is ambient air entrainment [Ogden et al., 2008].

To identify the potential role of the hot core on the oxidation state of iron and its speciation at the ash surface, a conceptual box model has been considered (Fig. 3.1) which covers the chemical processes in the temperature range 1000°C>T>600°C. Assuming thermodynamic equilibrium in this region of the plume, we use one of the most cited thermodynamic equilibrium models, GASWORKS [Symonds and Reed, 1993], to simulate the interaction among magmatic gases, ash and atmospheric gases. GASWORKS computes heterogeneous equilibria among gases, solids and liquids during the processes of cooling, gas-gas mixing, pressure changes and gas-rock reaction considering physical (e.g., temperature, pressure and heat capacity) and chemical (e.g., gas and solid phase composition) properties of each component in the system [Symonds et al., 1987]. More details of this program have been provided elsewhere (see Symonds and Reed [1993]) and thus, its description is not given here.

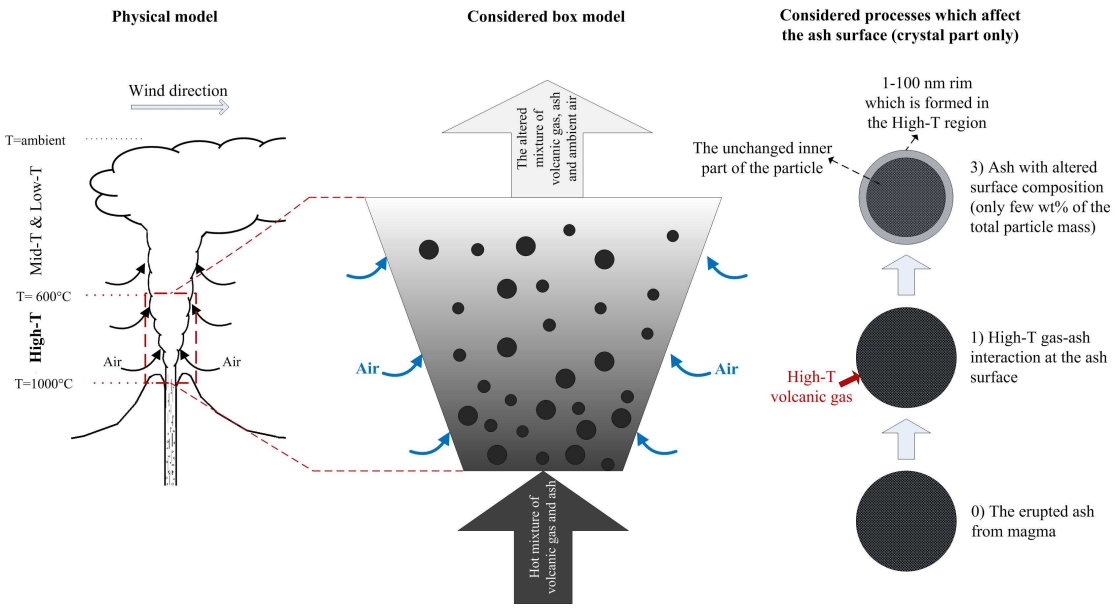

FIGURE 3.1: Sketch of the box model used for simulating gas-ash interaction within the volcanic plume hot core.

3.2.2 Thermodynamic equilibrium in high-T gas-ash interaction

The thermodynamic equilibrium assumption for reactions of volcanic gases at high-T (T>600°C) has been validated several times (see Symonds et al. [1994], especially pages 6-20, and the references therein) and widely used in previous studies (e.g., Gerlach [2004], Gerlach and Nordlie [1975], Martin et al. [2006, 2009], Roberts et al. [2009], Symonds and Reed [1993], Symonds et al. [1987]). Here, we evaluate the validity of this assumption for gas-ash interaction in high-T. Ideally, one would calculate the relaxation time (i.e., characteristic time to reach equilibrium) in order to verify the thermodynamic equilibrium assumption [Seinfeld and Pandis, 2006]. Unfortunately the data for those calculations for a high-T heterogeneous system containing minerals and magmatic gases are currently not available. Since the oxidation reactions are of special interest to this study, our first order attempt is therefore to attest that oxygen is available for oxidation in the different minerals as well as in glass. In other words, we verify if in a given amount of time, oxygen can diffuse into the mineral to a certain distance. Then we assume that once the oxygen is there, the oxidation reaction is much faster than the diffusion process [Cooper et al., 1996] and the mineral-oxygen interaction most probably favors rapid attainment of thermodynamic equilibrium.

It has been shown that the oxidation reaction of Fe^{2+}-bearing amorphous silicates is controlled by three diffusion mechanisms (sometimes acting in parallel): l) an inward flux of molecular oxygen (O_2) from the surface; 2) a inward flux of oxygen ions (O^{2-}) from the surface; and 3) an outward flux of network-modifying cations to the surface

(e.g., Ca^{2+} [Ayris et al., 2013]) [Moriizumi et al., 2009]. For the interaction of iron-carrying minerals with the volcanic and atmospheric gases, we assume that the limiting factor in iron oxidation in such minerals is (just as described for glass above) the inward diffusion of the oxygen into the solid phase [Cooper et al., 1996]. If we assume spherical solid particles, transport of oxygen in minerals is given by [Crank, 1975]:

$$\frac{\partial C}{\partial t} = D\left(\frac{\partial^2 C}{\partial r^2} + \frac{2}{r}\frac{\partial C}{\partial r}\right) \tag{3.1}$$

where C is the concentration of the diffusing component and D is the diffusion constant (here for simplicity it has been assumed that D is independent of C). This equation is subject to the following boundary conditions: at r=0, dC/dr=0 and at r=a, C is kept at C_0, respectively. a is the radius of the ash particle. The non-steady state solution to this equation is [Crank, 1975]:

$$\frac{C - C_1}{C_0 - C_1} = 1 + \frac{2a}{\pi}\sum_{1}^{\infty}\frac{(-1)^n}{n}\sin\frac{n\pi r}{a}\exp\left(-Dn^2\pi^2 t/a^2\right) \tag{3.2}$$

where C_1 is the initial concentration in the sphere. To evaluate the assumption of thermodynamic equilibrium in ash-gas interaction (i.e., mineral-oxygen), we make the following assumption: if the amount of diffused substance (i.e., oxygen which is the left side of the equation 3.2) reaches a "certain value", then the gas-ash interaction attains thermodynamic equilibrium. To get a sense of this "certain value" we examine the oxidation of fayalite (Fe_2SiO_4) to magnetite (Fe_3O_4) as an example:

$$3Fe_2SiO_4 + O_2 \rightarrow 2Fe_3O_4 + 3SiO_2 \tag{3.3}$$

In this reaction each 3 moles of fayalite (with molar weight of 204 g/mol) react with 1 mole of O_2 (with molar weight of 32 g/mol). Thus, each 612 g of fayalite needs only 32 g oxygen for oxidation to magnetite. This means if the weight ration of oxygen/fayalite reaches to 5%, the oxidation reaction can proceed. In a volcanic plume, ambient air entrainment is the major (and infinite) source of oxygen while the amount of fayalite available for reaction is limited to its concentration at the ash surface (among many other minerals and also glass). As an extreme case, one can assume that the number of moles of fayalite at the ash surface is the same as the number of moles of oxygen in the plume. Even under such extreme conditions, diffusion of 5% of the surrounding oxygen is enough to trigger the oxidation reaction. Therefore, we use 5% as the "certain value" needed for the oxidation reaction. This means only the solid mass affected by the diffusion of oxygen (i.e., ash rim thickness in which the oxygen concentration reached

to 5% of that in the surroundings) takes part in the oxidation. Therefore, by fixing the left side of equation 3.2 to 0.05, we can calculate the rim thickness (i.e., $a - r$) for given t, D and a. Here we use five diffusion coefficients (i.e., diffusion of ^{18}O in minerals at T>800°C proposed in experimental studies: 10^{-20} and 10^{-19} m^2/s for olivine as a major iron-carrying mineral [Brady, 1995], 10^{-17} m^2/s for typical minerals [Brady and Cherniak, 2010, Zhang, 2010], 10^{-16} m^2/s as an upper bound (i.e., diffusion in glass [Cooper et al., 1996]) and 10^{-18} m^2/s as the average. We also assume 10-50 seconds diffusion time, as this is about the length of time an ash particle spends in the hot core of an eruption column. The results of the calculations are shown in Fig. 3.2. It can be seen that the rim thickness for high diffusion coefficients (D=10^{-16} m^2/s) in very fine mineral particles (i.e., the black line) could reach >100 nm (i.e., more or less the whole mineral) while for small D (i.e., 10^{-20}, olivine) the rim thickness is almost independent of the size and is approximately 1 nm. It is also obvious that prolongation of the residence time (dashed-lines) increases the rim thikness. We conclude that the solid mass inherent to the ash rim with the thickness 1-100 nm in minerals and 10-300 nm in glass takes part in the thermodynamic equilibrium interactions with the surrounding gases.

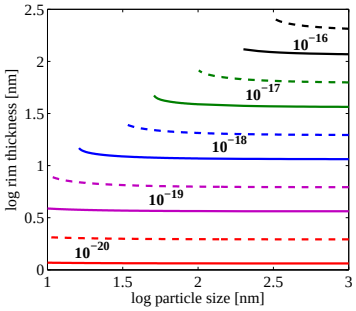

FIGURE 3.2: Ash rime thickness (in which the diffused oxygen concentration reaches 5% of that of the surrounding environment) as a function of particle size, a, for different diffusion coefficients, D, at t=10s (solid lines) and t=50s (dashed lines); values of D are shown on lines.

3.2.3 Gas and ash mixture

One of the most important inputs into the model is the composition of the gas-ash mixture leaving the vent (see Fig. 3.1). As the study of Olgun et al. [2011] has shown that ash from different volcanic settings release different amounts of Fe upon contact with seawater, we use high-T gas composition of three different types of volcanic settings (convergent plate (CP), divergent plate (DP) and hot spots (HS) (Table 3.1)) that are compiled in Chapter 2.

TABLE 3.1: Average high-T volcanic gas composition (concentrations are in mole%) extracted from Table 2.2

Volcano type	Convergent plate(CP)	Divergent plate(DP)	Hot spot(HS)
logfO_2	-10.94	-10.89	-10.39
T(°C)	1000	1000	1000
H_2O	91.05	75.78	75.94
CO_2	4.50	13.38	3.25
H_2	1.44	1.12	0.64
H_2S	0.29	0.85	0.39
SO_2	1.76	7.39	19.16
HCl	0.76	0.42	0.17
HF	0.06	0.42	0.18
CO	0.11	0.32	0.04

The solid mass associated to particle sizes <64 μm is considered in this study, which may represent a substantial contribution (>50%) to tephra deposits from explosive volcanic eruptions [Rose and Durant, 2009]. Particles in this size range not only have more specific surface area for interaction with the gas phase [Delmelle et al., 2005] but also can be lifted to high altitudes and can remain suspended in the atmosphere for several days before sedimentation [Sparks et al., 1997]. For simulation of the initial ash bulk composition, we use the method recommended by Symonds and Reed [1993]. In this procedure, magma of a given composition (for the whole rock composition used here see Table 3.2) is titrated into the gas phase step by step until a certain gas/rock ratio is reached. The program then determined the composition of minerals being in equilibrium with the given gas composition at a prescribed temperature, oxygen fugacity (fO_2) and pressure (P=1 atm). However, during the cooling and mixing with air discussed below fugacity and temperature will change. The equilibrium mineral assemblages are assumed to be randomly distributed in the ash. Therefore, their relative ratios are also representative for the composition one would find on the surface of ash samples. It is noteworthy that by this method, we only simulate the crystalline part of the volcanic ash produced during near surface magma degassing [Symonds and Reed, 1993] which will certainly contain glass too.

TABLE 3.2: The magma (whole rock) composition used in this study

Oxides	wt%	Oxides	wt%
SiO_2	54.5	Al_2O_3	14.3
FeO	8.1	CaO	6.5
Fe_2O_3	3.5	Na_2O	4.1
MgO	2.5	MnO	3.1
TiO_2	2.2	K_2O	1.2

Selection of the final gas/ash ratio (G/A) is crucial for the simulations. While high ratios (e.g., log(G/A)=6) reflect the very low ash concentrations (i.e., ash-poor plume), a low

ratio (e.g., log(G/A)=-2) corresponds to a very low gas concentration (i.e., magma), respectively. Thus, the selection of the final G/A ratio depends on the aim of the simulation [Symonds and Reed, 1993]. Since the scope of this study is the simulation of near vent processes, we can assume that about 1-10 wt% of the plume is gas and 90-99 wt% is ash. Therefore the appropriate G/A ratio is in the range of -2<log(G/A)<0. We should emphasis that only the surface layer of ash particles take part in the reactions (as discussed in section 3.2.2) while GASWORKS does not consider this physical limitation and assumes the whole solid phase is available for the reactions. To overcome this limitation, it is essential to consider only the surface of the ash as the available solid phase mass for the reactions. As demonstrated above, the gas-ash interaction in high-T region could penetrate up to 1-100 nm into the particle surface. Studies on volcanic ash surface area show that the ash's specific surface area is in the range 1.1-2.1 m^2/g [Delmelle et al., 2005, Mills and Rose, 2010]. Assuming the mixture of 1 mole pure magmatic gas with mean molar weight of approximately 25 g (see Chapter 2 for more details) and 3 wt% gas in the plume, the total amount of ash coexisting with 1 mole of volcanic gas is ∼830 g. Considering the mean specific surface area of 1.6 m^2/g, a density of 2500 kg/m^3 for the volcanic ash and the reaction surface thickness range of 1-100 nm, the mass contained in the ash rim is 4-350 g. This amount would be true in case the material is totally crystallized. In explosive volcanic eruptions, however, the crystal fraction is in the range of 20-60% [Blundy et al., 2006]. Therefore, in our standard calculations we assume that only 40% of the calculated mass is crystallized and interacts with the gas. This reduces the estimate the mass of solid phases available in our simulation to be 2-140 g which corresponds approximately to log(G/A)=-1.0-1.0. We select log(G/A)=-0.5 (corresponding to ∼80 g solid phase) as the final log(G/A) in this study for our standard calculations. The sensitivity of the results to the gas/ash ratio (i.e., changing log(G/A) in the range of 1.0 to -1.0), which reflects variations in the assumptions above (degree of crystallization, ash surface rim thickness, etc.), is discussed in detail in section 3.3.4.

After constraining the appropriate gas/ash ratio, the volcanic plume (i.e., 1000°C mixture of magmatic gases and ash) is mixed with the 25°C ambient air (78% N_2, 21% O_2, O.1% Ar) by increasing the air to magmatic gas ratio (V_A/V_M) at constant pressure (1 atm) thereby oxidizing the system while cooling it. Air is mixed incrementally with the magmatic material until a temperature of 600°C is reached which corresponds to V_A/V_M∼1.0. Inherent to this procedure are two different physical processes: cooling of the plume and mixing of the plume with air (i.e., oxidation). In order to understand the effect of each process we perform two simulations: cooling without air entrainment and cooling with air entrainment.

3.3 Results and discussion

3.3.1 Initial ash mineralogy and composition

During explosive volcanic eruptions, the fundamental process driving ash generation is the mechanical fragmentation of magma within the subsurface volcanic conduit [Dingwell, 1996]. The formation of various Fe-bearing crystalline phases, including aluminosilicates and oxides, contained in the glass matrix and/or as individual crystals in the ash material can be traced back to the source magma [Ayris and Delmelle, 2012b]. Following the procedure outlined above the minerals, which are in equilibrium with the gas phase, are determined for the different volcanic settings (see Table 3.1 and Fig. 3.3 upper diagrams). Iron in volcanic ash coexists mainly with Mg, Si and Ti (e.g., in form of fayalite/forstrite ($(Fe,Mg)_2SiO_4$), magnetite (Fe_3O_4), ulvöspinel (Fe_2TiO_4) and ilmenite ($FeTiO_3$)) [Ayris and Delmelle, 2012b]. Thus for simplicity we consider minerals containing Si, Fe, Ti and Mg oxides only and assume all other phases to be inert (see Fig. 3.3, bottom diagrams). This assumption facilitates the convergence of GASWORKS during calculation. We did carry out all calculations using the full mineral assemblage down to about 800°C and did not find any significant differences between the full calculations and the ones using the reduced mineral assemblage, which we take as an indication that the reduction of the phase is a valid step to do. The effects of the formation of feldspars, pyroxene, etc. and the limitation of this assumption are further considered and discussed in detail in section 3.3.5.

The results of the calculations are shown in Fig. 3.3. In all three settings fayalite (Fe_2SiO_4) and ilmenite ($FeTiO_3$) are the main Fe-carrying species. Due to the slightly higher oxygen fugacity (fO_2=-10.39), small amounts of magnetite (Fe_3O_4) and ulvöspinel (Fe_2TiO_4) precipitate in the hot spot (HS) setting. While in convergent plate (CP) and divergent plate (DP) cases the fO_2 is close to FMQ buffer (Fayalite-Magnetite-Quatrz) which is about -11.00 at 1000°C [Lindsley, 1991], the HS scenario is nearly 0.6 log units below FMQ allowing the formation of more oxidized minerals.

3.3.2 Cooling without air entrainment

As detailed above, the processes discussed hereafter are assumed to impact only the surface rim of the ash (i.e., 1-100 nm thick layer around the particle which is only few weight percent of the total ash). Thus the mineralogy of the inner part of the ash remains unchanged and the composition reported in the following only refers to the rim and does not represent the bulk composition of the entire ash particle. In order to understand the combined effect of cooling and oxidation on Fe speciation in the ash, the 1000°C

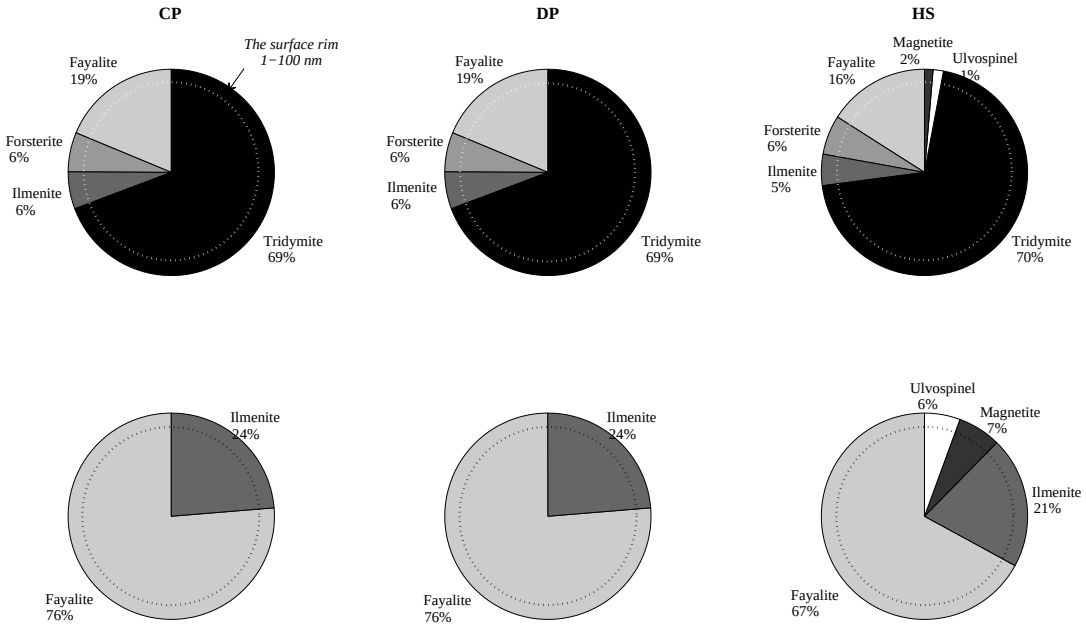

FIGURE 3.3: Mineral assemblages found in our starting material at 1000°C and 1bar (in wt%). The upper row of diagrams shows all minerals present, whereas the lower row of diagrams shows only those phases containing iron, which are considered in the figures and discussions from here on. We assume that these minerals are randomly distributed in the ash. However, cooling and mixing processes only affect those mineral phases exposed at the surface and in a small layer below the surface (the 1-100 nm rim discussed in the text shown with dotted line), which is only few wt% of total ash not the bulk composition.

mixture of magmatic gas and ash, which has been simulated in the previous section, is first cooled to 600°C without adding air into the system. Results are shown in Fig. 3.4 where magnetite (Fe_3O_4) is the main Fe species for all settings considered.

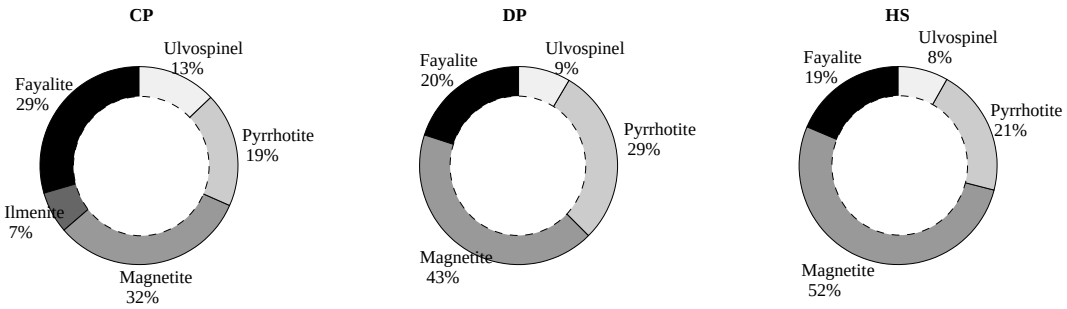

FIGURE 3.4: Fe speciation at the ash surface after cooling without air entrainment (T=600°C).

In the absence of atmospheric oxygen (O_2), magnetite is produced by oxidation of ferrous ions (Fe^{2+}) present in the crystal lattice of the iron-endmember fayalite by the protons (H^+) of water according to the following reaction:

$$3Fe_2SiO_4 + 2H_2O \rightarrow 2Fe_3O_4 + 3SiO_2 + 2H_2 \quad (3.4)$$

Ulvöspinel (Fe_2TiO_4) can substitute ilmenite ($FeTiO_3$):

$$2FeTiO_3 + Fe_2SiO_4 \rightarrow 2Fe_2TiO_4 + SiO_2 \tag{3.5}$$

And finally pyrrhotite ($Fe_{0.8}S$) forms according to the following reaction between magnetite and H_2 and H_2S [Kishima, 1989]:

$$0.8Fe_3O_4 + 0.2H_2 + 3H_2S \rightarrow 3Fe_{0.8}S + 3.2H_2O \tag{3.6}$$

It is obvious that this reaction also leads to scavenging of the H_2S by ash. About 75% of the erupted H_2S is scavenged by the ash surface in CP scenario during cooling while in DP and HS it is 32% and 11%, respectively.

3.3.3 Cooling with air entrainment

Mixing of hot magmatic gas with ambient air (T=25°C) in subplinian and plinian eruption plumes results in concurrent oxidation and cooling, which changes the gas phase and ash surface composition accordingly. The changes in iron speciation can be tracked considering the gas-ash interaction, which is shown in Fig. 3.5. At T>900°C magnetite forms due to fayalite oxidation according to the reaction 3.3. Then, at 750°C<T<900°C hematite (Fe_2O_3) precipitates and replaces magnetite:

$$2Fe_3O_4 + 0.5O_2 \rightarrow 3Fe_2O_3 \tag{3.7}$$

Finally, at 600°C <T<700°C sulfuric acid reacts with hematite and produce iron sulfate:

$$Fe_2O_3 + 3H_2SO_4 \rightarrow Fe_2(SO_4)_3 + 3H_2O \tag{3.8}$$

Vertical lines in the gas phase graphs in Fig. 3.5 show the transition stage, which corresponds to the depletion of reduced species (e.g., H_2S and H_2) and transition of the system to oxidized state. As discussed in section 2.3, during mixing with ambient air in the hot core, magmatic gas could become completely oxidized through a single-step transition which is in agreement with the patterns reported in other studies on gas-only mixtures (e.g., Bobrowski et al. [2007], Martin et al. [2006], Roberts et al. [2009]). However, as shown for the gas phase in Fig. 3.5, it is obvious that in presence of ash, the transition has two steps: The first step (i.e., dashed vertical lines) starts around 840-880°C in all scenarios whereby H_2S and H_2 rapidly decrease and H_2SO_4 increases. The

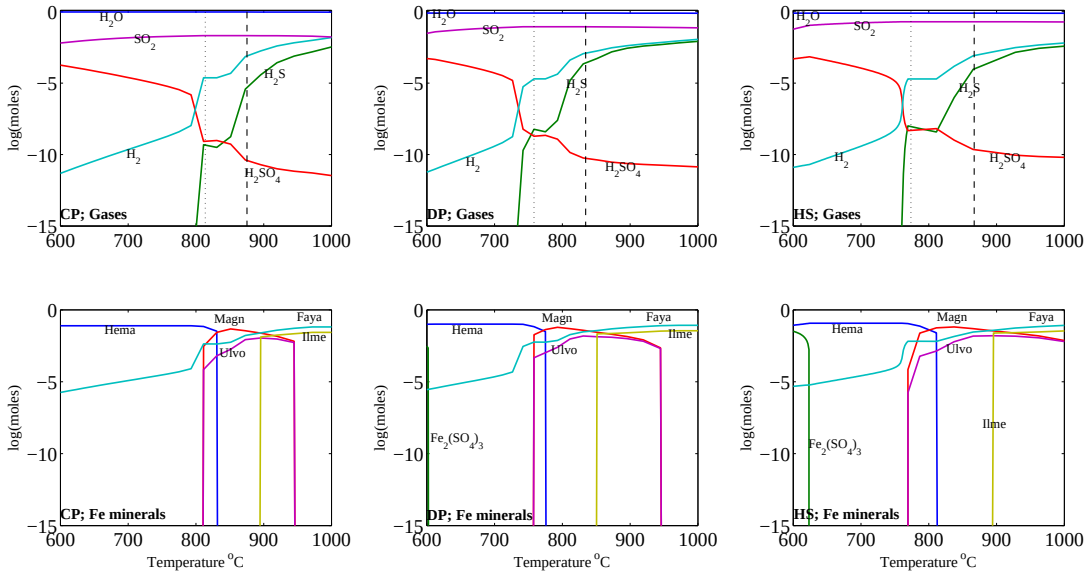

FIGURE 3.5: Gas-ash interaction during cooling with air entrainment for different tectonic settings; upper part: major gas species (vertical lines show the transition from reduced to oxidized state), lower part: Fe-carrying minerals at the ash surface.

concentrations become stable prior to the second step (i.e., dotted vertical line) after which the rapid changes in species concentrations take place and the system becomes completely oxidized.

The main cause for the differences between a single-step transition and double-step transition in this study is the presence of ash that acts as a sink for oxygen. In an ash-free case (e.g., Chapter 2, Martin et al. [2006], Roberts et al. [2009]) reduced gas species (e.g., H_2S and H_2) consume oxygen and transform to oxidized species (e.g., SO_2 and H_2SO_4) during the transition. However, in presence of ash, species at the ash surface can react with oxygen (e.g., reactions 3.3 and 3.7) in the system and affect the transition. Such reactions become more important as soon as the system passes the first transition step (dashed vertical line). Consumption of oxygen by the solid phase stabilizes the concentration of gas species until the depletion of reduced solid species, where the second transition step (dotted vertical line) happens. This process controls the iron oxidation state in the solid phase (e.g., precipitation of hematite that occurs as the result of reaction 3.7). More details about the transition are given in section 3.4.

The final ash surface composition (at T=600°C) is shown in Fig. 3.6. It is obvious that hematite (Fe_2O_3) is the main iron mineral at the ash surface in all scenarios but iron (III) sulfate ($Fe_2(SO_4)_3$) also forms in DP and HS volcanoes. This is due to the fact that DP and HS magmatic gases are more sulfur rich (see Table 3.1) resulting in higher sulfuric acid concentrations and proceeding of the reaction 3.8. However, reactions 3.3

and 3.7 result in complete oxidation of Fe^{2+} to Fe^{3+}, which is the less soluble oxidation state of iron. Presence of hematite as the main iron mineral might be surprising for some volcanologists; but it would be less surprising if one considers the fact that these results are the case for a thin surface rim which occupy only few weight percent of the total ash particle mass. In other words, hematite formation can be negligible in the bulk composition.

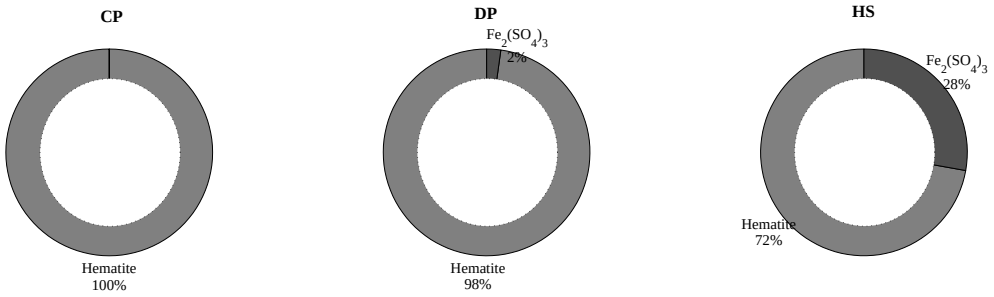

FIGURE 3.6: Ash surface composition (shown are only the iron carrying mineral phases) after cooling and mixing with ambient air.

It was reported that the gaseous C-O-H-S system [Gerlach and Nordlie, 1975] and also more complex C-O-S-H-F-Cl-Br-I-N-Ar systems [Martin et al., 2006] exhibit two clear compositional regimes, divided by a compositional discontinuity [Gerlach and Nordlie, 1975, Martin et al., 2006, Roberts et al., 2009] (a concept similar to the transition point discussed in Chapter 2). The compositional discontinuity in high temperature magmatic gases is related to the amount of oxygen required to remove reduced species from the gas [Martin et al., 2006, Roberts et al., 2009]. Based on this hypothesis, it is shown in Chapter 2 that the oxidation state of the magmatic gas during mixing with ambient air in the hot core is controlled by the ratio of its H_2 and H_2S content to the amount of entrained oxygen which is defined as:

$$X_{mix} = (n(H_2) + n(H_2S))/(0.21n(\text{Air}) \tag{3.9}$$

where n corresponds to mole number of each species and the coefficient 0.21 represents the entrained oxygen from ambient air. When X_{mix} reaches a critical value (log X_{mix}=-2.5∼-3.0), the system becomes completely oxidized (see section 2.3.3). However, as mentioned above, the transition mechanisms in ash-free cases are different from the transition in this study due to presence of ash. Fig. 3.7 shows the iron oxidation state versus X_{mix}. When the mixture of magmatic gas and ash is exposed to ambient air and undergoes cooling and oxidation, iron on the ash surface starts to oxidize according to reaction 3.3 resulting in a decrease in Fe^{2+}/Fe_{total}. This continues until log X_{mix}=-2.5∼-3.5 where the transition in the iron oxidation state happens for all studied volcanic

settings. Obviously iron is mostly in ferrous (Fe^{2+}) form before the transition and oxygen is mainly consumed by H_2 and H_2S. As soon as these two gases diminish in the system, there is more oxygen available for the reaction with iron that results in formation of ferric (Fe^{3+}) iron (the abundant iron species at 600°C).

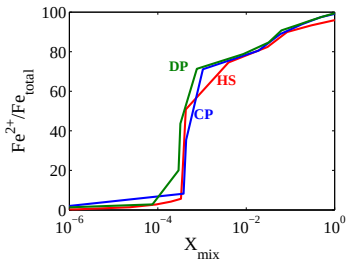

FIGURE 3.7: Iron oxidation state versus X_{mix} for different volcanoes.

3.3.4 Sensitivity study

3.3.4.1 Gas/ash ratio

As discussed in section 3.2.3 a gas/ash ratio is selected in this study in order to parameterize the amount of available solid phase at the ash surface for reaction with gas species in the thermodynamic equilibrium system. However, there are some uncertainties about this value mainly but not only due to the ash content of different explosive volcanic plumes, ash surface rim thickness and degree of crystallization. Therefore, it seems necessary to study the sensitivity of the model to different G/A ratios. Fig. 3.8 shows the iron carrying-minerals at the ash surface at 600°C with high (log(G/A)=-1.0) and low (log(G/A)=1) ash content (the mid ash content is log(G/A)=-0.8 presented in Fig. 3.4). Changes in G/A ratio do not affect the final Fe speciation in CP volcanoes. But for DP and HS settings the effects are obvious. Since the solid phases are nearly similar in all cases, the difference in relative amounts is related to the gas composition as discussed in section 3.3.3. It is obvious that with the higher ash content more hematite develops and less S scavenging occurs. This can be explained considering that Fe in the solid phase acts as a sink for oxygen parallel to H_2 and H_2S in the gas phase. With low ash content, more rapid oxidation of S species results in sulfuric acid formation and production of iron sulfate accordingly. At high ash contents, Fe provides a sink for the oxygen in the solid phase and inhibits the rapid oxidation of S species in the gas phase. This effect is more pronounced in the HS setting, with the highest S content, where ferrous sulfate ($FeSO_4$), a soluble iron compound, can precipitate:

$$Fe_2O_3 + SO_2 + SO_3 \rightarrow 2FeSO_4 \tag{3.10}$$

Higher ash content shifts the occurrence of the transition point to colder temperatures and thus, can control the oxidation state of the system. Therefore, in an ash and sulfur rich volcanic plume, formation of soluble iron in the hot core appears to be more likely. S scavenging is found to be more important in HS settings. While at low ash content about 66% of the erupted sulfur is scavenged by ash iron, at mid and high ash contents it is 48% and 23%, respectively. However, in CP and DP settings S scavenging by ash iron is negligible.

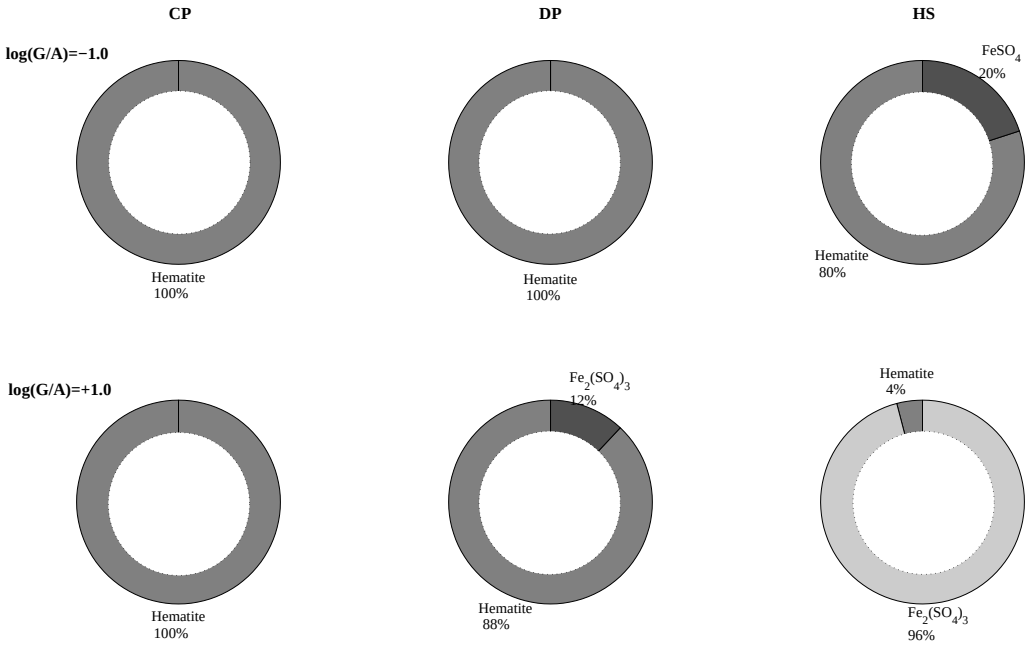

FIGURE 3.8: Iron carrying-minerals at the ash surface at 600°C as a function of the G/A ratio; the higher the G/A ratio, the lower the ash content of the plume.

If one considers a single ash particle, the gas concentration is highest on the ash surface and decreases rapidly below the ash surface. In other words, the first few nanometers of the ash surface rim can correspond to high G/A ratio while near the ash core the G/A ratio is very small. Therefore, the high and low G/A ratios do reflect different layers of the ash surface. Studies on fumarole wall rock alteration (i.e., a macro scale gas-solid interaction) show that the mineral incrustation assemblages are distributed in two main colored zones reflecting differences in the degree of alteration and also in the redox conditions prevailing during this alteration: (1) a black zone, located at the deepest levels, that contains mainly reduced species; (2) a red zone which is closer to the surface and reflects a higher oxidized environment than the previous zone [Africano and Bernard, 2000]. By analogy, the inner part of the ash surface rim (log(G/A)=-1.0 or black zone) can be less oxidized than the outer part of the ash surface (i.e., log(G/A)=1.0 or red zone), which is its oxidation front and can potentially contain more oxides. Therefore,

even in the assumed surface rim of the ash (i.e., 1-100 nm thickness) composition profile can vary.

3.3.4.2 Oxidation state

Chapter 2 demonstrated that the initial oxidation state of the magmatic gas plays a key role in the final sulfur speciation in the hot core of volcanic plumes. We reported that the transition stage in reduced magmas could be shifted to colder temperatures, which increase the possibility of presence of reduced S species in system. Due to the connection between the transition point in the gas and solid phase shown in section 3.3.3, we next constrain the effect of reduced conditions on Fe speciation in the hot core for different settings. The initial fO_2 of the magmatic gases are reduced by -1 (∼FMQ-1) and three reduced scenarios are defined: CP-R, DP-R and HS-R. Fig. 3.9 shows the gas-ash interaction in these scenarios. The transition is shifted to colder temperatures in CP-R (in comparison with Fig. 3.5) and even does not happen in DP-R and HS-R cases. In these scenarios reduced gas species (i.e., H_2 and H_2S) as well as ferrous iron (i.e., pyrrhotite, ulvöspinel, fayalite and magnetite) are present at 600°C. Therefore, under reduced conditions, not only injection of H_2S into the atmosphere is more likely (section sec:gas4) but also preservation of Fe^{2+} (i.e., the more soluble iron oxidation state) is more expected.

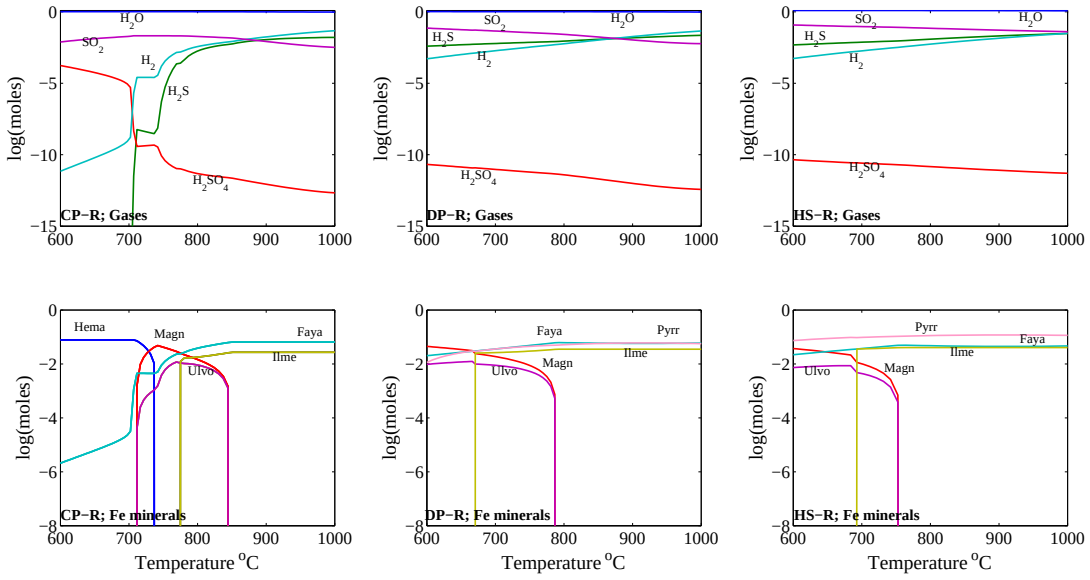

FIGURE 3.9: Gas-ash interaction during cooling with air entrainment for different tectonic settings under reduced conditions (∼FMQ-1); upper part: major gas species, lower part: Fe-carrying minerals at the ash surface.

Fig. 3.10 shows the initial and final iron carrying minerals at the ash surface under reduced conditions. It is obvious that changing the initial oxidation state does not affect Fe speciation in CP-R volcanoes and it is completely oxidized to Fe^{3+} in hematite. However, ash iron in DP-R and HS-R settings remains in its ferrous form. These results are comparable with studies on igneous rocks in different tectonic settings. The reported oxidizing conditions of igneous rocks are not far from those of the FMQ redox buffer [Lindsley, 1991]. Nonetheless, there are systematic differences that correlate with tectonic setting. Igneous rocks erupted in arc volcanoes typically record an oxygen fugacity 1 or more log units above those of the NiNiO (nickel-nickel oxide) buffer (i.e., oxidation of Fe^{2+} to Fe^{3+}). In contrast, in non-arc settings rocks typically record oxygen fugacities from about those of the FMQ buffer to a log unit or so more reducing than that buffer (i.e., some amount of iron remains in Fe^{2+}) [Lindsley, 1991]. The presence of iron sulphide (pyrrhotite, $Fe_{0.8}S$) is also consistent with the stability of this species under reducing conditions [Scaillet et al., 1998]. Fig. 3.11 shows the changes in ferrous to total iron ratio for different scenarios. Reduced conditions postpone the transition from ferrous to ferric iron. In CP, DP and HS scenarios iron is in ferric form even before 700°C. In CP-R case although the transition is shifted by about 100°C, iron is completely oxidized at 600°C too. But in DP-R and HS-R, 82% and 90% of the iron remains in ferrous, respectively.

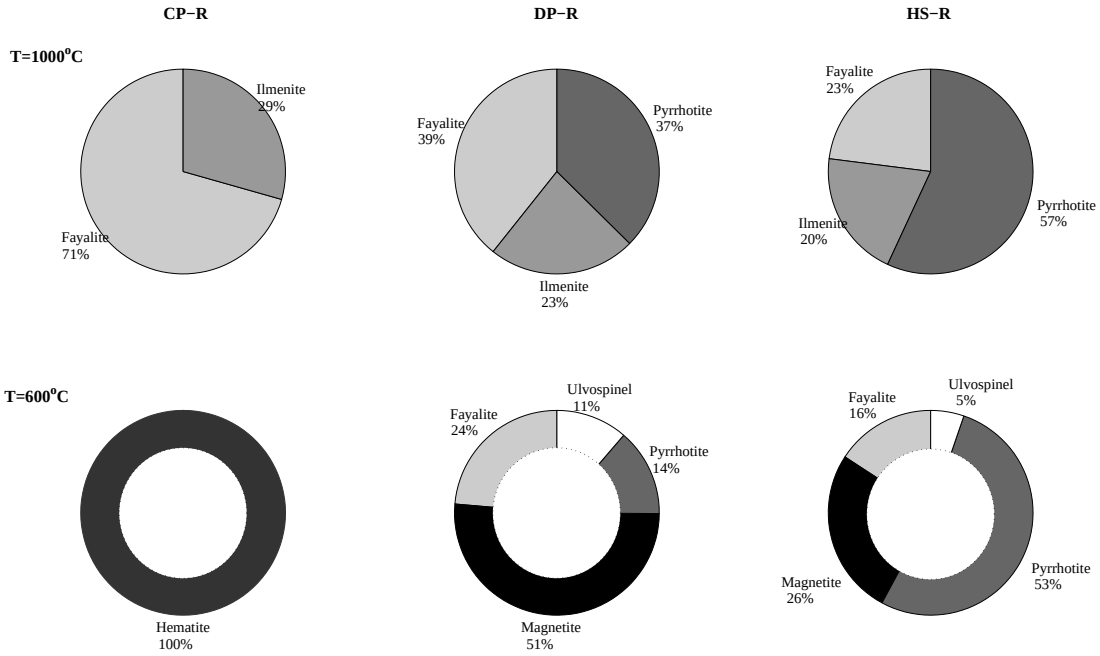

FIGURE 3.10: Initial (upper part) and final (lower part) iron carrying minerals under reduced (∼FMQ-1) conditions in different volcanic settings.

In general, H_2 and H_2S in the gas phase provide a sink for the entrained oxygen, which constrains the oxidation reactions in the solid phase. By depletion of these two species at the transition point, oxidation of Fe^{2+} to Fe^{3+} becomes more efficient whereby after this point, most of the iron is in ferric form. Under reduced conditions, the higher initial H_2 and H_2S content increases the sink for the oxygen and shifts the transition point in the solid phase to colder temperatures. Therefore, at the output of the box model (T=600°C) iron remains in ferrous form given the reduced initial conditions.

3.3.4.3 Rhyolitic magmas and arc volcanism

Highly viscous magmas (i.e rhyolitic) are expected to trigger most of the explosive eruptions, which is usually the case in CP setting [Schmincke, 2004]. So far we have studied basaltic composition (Table 3.2). For considering rhyolitic magma in arc volcanoes, first the magmatic gas is cooled to 850°C because such magmas usually have T<900°C [Schmincke, 2004]. Then a Si-rich composition (SiO_2 75%, FeO 2.5%, TiO_2 1.0%, MgO 1.0%) is titrated into the magmatic gas and this mixture is mixed with ambient air. We find that the initial ash surface composition contains fayalite (65%), magnetite (27%) and ulvöspinel (8%) as Fe-carrying minerals. However, in the final composition at 600°C hematite is the only Fe species at the ash surface as it is the case in the standard scenarios (CP in Fig.s 4 and 5).

3.3.5 Limitations

Magma contains several components bearing various elements like Si, Al, Ca, Mg, Mn, Na, Fe etc. The solid phases, which have been studied so far in this research, neglected some major species in order to reduce the complexity of the model as well as computational burdens. However, these species may play an important role during different processes. For instance, where alkali cations are not available, formation of discrete Fe^{3+} bearing phases like titanomagnetite, spinels and pyroxenes is more likely [Ayris and Delmelle, 2012b]. Therefore, existence of alkali metals in the solid phase can change the mineralogy of the ash iron. In addition, such metals can interact with the gas phase and affect the iron oxidation reactions. Thus, we will explore their impact on the Fe speciation on the ash surface.

As the number of input solid and gas compounds increases, GASWORKS become more sensitive to the initial compositions because it has to solve a much larger system of thermodynamic equations. The convergence is difficult to achieve specially in case of

simultaneous cooling and mixing [Symonds and Reed, 1993]. In our calculations we successfully achieved temperatures of 800°C for the full composition but for colder temperatures GASWORKS does not converge for complex compositions. In order to assess the differences between a calculation including the full composition and the results presented in sections 3.3.3 and 3.3.4, Fig. 3.12 shows the results of a complete ash composition calculation for a CP setting. Most of the Fe is contained in olivine (i.e., fayalite) but ilmenite (which we find in our simplified model) (see e.g., Fig. 3.5) does not precipitate when considering the full composition. This is due to the absence of alkali metals in the simplified scenario that allows formation of ilmenite. Some Fe-carrying pyroxene (e.g., hedenbergite ($CaFeSi_2O_6$), jadite ($Na(Al,Fe)Si_2O_6$) form too but their amount is negligible. During cooling without air entrainment (Fig. 3.12-b) fayalite is still the main iron species but small amount of spinels (i.e., magnetite and ulvöspinel) and pyrrhotite form too. This is also in good agreement with the results presented in section 3.3.2 for simplified solid phase composition (CP in Fig. 3.4). Finally, after mixing with ambient air (Fig. 3.12-b), hematite remains the major iron species. During mixing with ambient air and interaction with magmatic gases, hedenbergite and jadite decompose to separate Ca^{2+}, Na^{+} and Fe^{2+}-bearing phases (e.g., $CaSO_4$, Fe_3O_4). We note that these results are only valid for the ash surface rim. Inner parts of the particle remain unchanged and most likely carry iron similar to composition in Fig. 3.12-a. Alkali and alkali-earth metals can provide more reaction sites at the ash surface [Farges et al., 2009] and affect iron–gas interaction. For instance in the DP scenario Ca^{2+}-bearing phases scavenge sulfur (up to 30% of the erupted sulfur) and form Anhydrite ($CaSO_4$). In this case, S scavenging by other minerals is negligible.

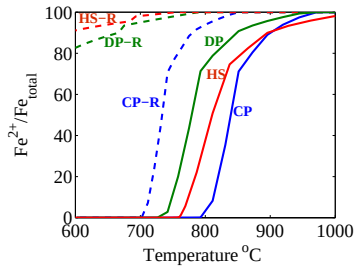

FIGURE 3.11: Changes in iron oxidation state as function of temperature for different tectonic settings and oxidation states under reduced conditions (FMQ-1).

Another limitation of this study is that GASWORKS assumes 100% crystallization (i.e., it does not produce any melt or glass). Thus, the glass–gas interaction cannot be simulated in this model. Ayris et al. [2013] found that $CaSO_4$ is a major cause of sulfur scavenging through experimental studies on high temperature volcanic glass but the mechanisms proposed is different from the one detailed above (e.g., their study focuses mainly on in-conduit processes while our approach deals with high-T in-plume

processes). Thus both the presence of surface defects (glass versus crystal) and network modifiers (alkali and alkali-earths) are proposed to be important for S to bond onto the ash surface [Farges et al., 2009]. Therefore, such processes overcome Fe-S reactions and restrain the formation of iron sulfide and sulfate. Moreover, in volcanic eruptions with low S content in the magmatic gas (CP and DP) formation of Fe sulfates could be unlikely while in sulfur-rich gas (HS), $Fe_2(SO_4)_3$ can precipitate on the ash in the hot core. Although S is considered as more prompt to be adsorbed on ash glass composition [Ayris et al., 2013, Farges et al., 2009], presence of alkali and alkali-earths cations (especially Ca) in the crystal part of the ash can play a significant role in S scavenging.

3.4 Discussion

The initial bulk composition of volcanic ash reflects the composition of the magma from which it derives. Magmas encompass a broad range of compositions, but in general, Fe content increases with decreasing Si content, from less than 2 wt.% in a typical rhyolite to 7-8 wt.% in a typical basalt composition [Maitre, 1976, Rogers and Hawkesworth, 2000]. The oxidation state of magma, which conventionally is expressed with reference to a known oxygen buffer, for example, fayalite-magnetite-quartz (FMQ), or nickel-nickel oxide (NNO), dictates the speciation of Fe within it. Maitre [1976] studied magmatic rocks and found that the mean ferrous iron to total iron ratios (wt.% Fe^{2+}/Fe_{total})) of the common igneous rocks ranged from 0.38 to 0.77, the basalt rocks being less oxidized than those high in silica. However, the oxidation ratio measured in freshly-deposited ash may not necessarily reflect that of the source magma due to oxidation processes occurring within the eruption plume [Horwell et al., 2003, Moriizumi et al., 2009]. In the current study, it is shown that high-T equilibrium can significantly change Fe mineralogy and speciation at the ash surface. Fig. 3.13 summarizes the effects of such processes on ash iron. In Fig. 3.13-a, solid black lines show the common buffers which are calculated according to the following equations [Giggenbach, 1987, Lindsley, 1991]:

$$\text{QIF(Quartz-Ilmenite-Fayalite): } logfO_2 = -29520.8/T + 7.492 \tag{3.11}$$

$$\text{FMQ(Fayalite-Magnetite-Quartz): } logfO_2 = -25096.3/T + 8.735 \tag{3.12}$$

$$\text{MH(Magnetite-Hematite): } logfO_2 = -25700.6/T + 14.558 \tag{3.13}$$

$$\text{Fe2-Fe3}(Fe^{2+}\text{-}Fe^{3+}):\ logfO_2 = -25414/T + 10736 \tag{3.14}$$

where T is the temperature in K. It can bee seen that the initial ash oxidation states in all scenarios are not far from FMQ which is consistent with studies on igneous rocks (e.g., Lindsley [1991]).

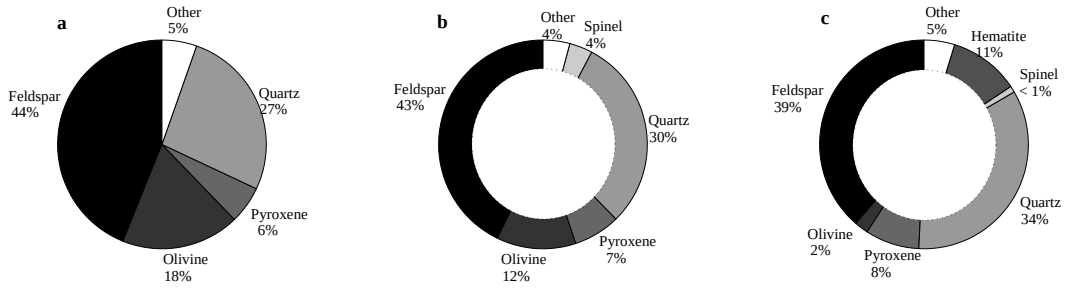

FIGURE 3.12: Ash surface composition with complete rock; a) initial composition at 1000°C, b) after cooling down to 800°C without air entrainment, c) after simultaneous cooling and mixing down to T=800°C. Precipitated mineral groups are Feldspar: albite ($NaAlSi_3O_8$), anhortite ($CaAl_2Si_2O_8$), sanidine ($(K,Na)(Si,Al)_4O_8$); Olivine: Fayalite (Fe_2SiO_4), Forsterite (Mg_2SiO_4), Tephroite (Mn_2SiO_4); Pyroxene: (diopside ($CaMgSi_2O_6$), hedenbergite ($CaFeSi_2O_6$), jadite ($Na(Al,Fe)Si_2O_6$), Spinel: magnetite (Fe_3O_4), ulvöspinel (Fe_2TiO_4, ilmenite ($FeTiO_3$), Other: pyrrhotite (Fe_xS_{1-x}), anhydrite ($CaSO_4$).

Mixing of the 1000°C magmatic ash-gas mixture with 25°C ambient air (simultaneous cooling and oxidation) affects the ash surface compositions differently regarding the tectonic setting and initial oxidation state. In CP, DP, HS and CP-R scenarios the system moves roughly parallel to FMQ during cooling and mixing until the first impulsive increase near Fe2-Fe3 (i.e., first transition), which leads the systems to the MH buffer. Then during a small temperature interval (∼50°C) they follow the MH buffer until the second impulsive increase in fO_2 occurs (i.e., second transition). While in these scenarios the system passes the MH line, which means significant decrease in Fe^{2+}/Fe_{total}, in DP-R and HS-R scenarios the system remains between FMQ and MH preserving high Fe^{2+}/Fe_{total} at 600°C. It also slightly passes the Fe2-Fe3, which explains formation of Magnetite in these scenarios (see Fig. 3.9).

Giggenbach [1987] classified the geochemical redox systems based on Fe2-Fe3 (equation 3.14), which is a non-specific buffer simply involving Fe^{2+} and Fe^{3+}: before reaching this line, the system is under reducing conditions and after that, it becomes oxidized. However, this buffer not only barely fits the first transition point, but also does not control the oxidation state alone and is followed by another transition. Although in all scenarios there is a span of about 100°C between the transitions, their occurrence is

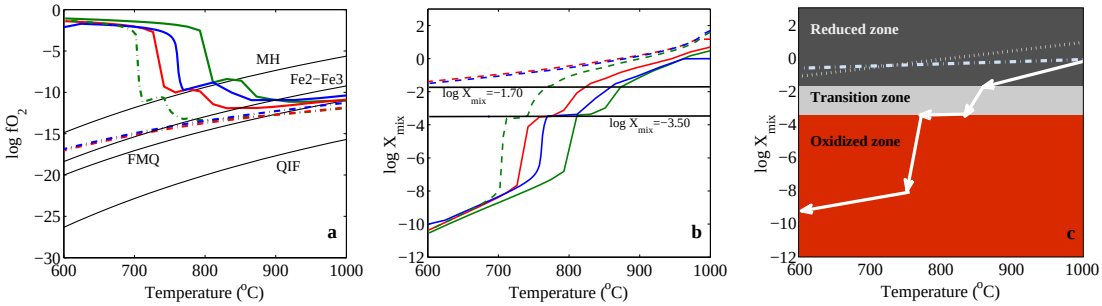

FIGURE 3.13: Changes in the iron oxidation state at the ash surface as a function of temperature during the mixing of the plume with ambient air; Colored lines show: green: CP, blue: DP, red: HS. Dashed lines represent reduced scenarios. a) fO_2 of the system and common mineral buffers in solid black lines; b) X_{mix} of the system and controlling X_{mix} values in dashed black lines; c) The schematic changes in oxidation state of the iron as a function of temperature and X_{mix}. Solid line: mixing of plume with ambient air; doted line: mixing of plume with ambient air under reduced conditions; dash-doted line: cooling of the system without air entrainment.

constrained neither by log(fO_2) nor temperature. In Chapter 2 it is reported that X_{mix} ratio controls the transition stage of sulfur species in the gas phase. This parameter is depicted versus temperature in Fig. 3.13-b for all scenarios during mixing of the magmatic ash-gas mixture with 25°C ambient air. In this figure two transition stages are clear and unambiguously correlated to log X_{mix}. The first transition point (at log X_{mix}=-1.70) controls the gas phase oxidation and the second one (at log X_{mix}=-3.50) controls the solid phase. Therefore, X_{mix} ratio as a temperature-independent parameter can be used to estimate the system's oxidation state. It can be seen that log X_{mix}=-1.70 and log X_{mix}=-3.50 correspond approximately to Fe2-Fe3 and MH buffers in Fig. 3.13-a, respectively. The schematic trend of the changes in the system is shown in Fig. 3.13-c. In this figure three zones (reduced, transition and oxidized zones) are shown separated by transition lines. During air entrainment, the plume cools and oxidizes simultaneously and moves along the solid line. Therefore, the oxidation state of the gas phase as well as the ash surface changes. However, it can remain in the reduced zone under reduced initial conditions (dotted line) as well as cooling without air entrainment (dash-dotted line) and maintain the iron in ferrous form down to lower temperatures. This explains the sensitivity of the model to initial conditions. In case of colder initial temperatures (e.g., rhyolitic magma discussed above) the starting point of the solid line moves along the dash-dotted line, which obviously shifts the whole solid line and the transition point toward the left (i.e., colder temperatures). On the other hand, reducing initial conditions means shifting the start point of the solid line up and then following the dotted line. However, as shown above, the final ash surface composition is much more sensitive to initial oxidation conditions rather than the temperature. Reduced scenarios seem more favorable for keeping the iron in the ferrous form in the hot core of volcanic plume.

Although some studies have been conducted on ash Fe release in water [Duggen et al., 2007, Frogner et al., 2001, Jones and Gislason, 2008, Olgun et al., 2011], iron mineralogy and speciation at the ash surface are lacking. Duggen et al. [2010] report that the experimentally-measured Fe release from ash produced by subduction zone and hot spot volcanism is in the ranges 100-400 and 35-107 nmol Fe/g ash, respectively. They concluded that subduction zone volcanism could be more favorable for bio-available iron production. Nevertheless, they excluded the ash from the 2000 eruption of Hekla, Iceland, which exhibited the highest Fe release in deionised water [Frogner et al., 2001, Jones and Gislason, 2008]. The strong acidity and elevated fluoride concentration in the eruption plume of Hekla is assumed to have promoted deposition of readily soluble Fe-bearing phases [Ayris and Delmelle, 2012b]. However, these effects are not unique to this eruption. Ayris and Delmelle [2012b] suggested that the origin of the soluble Fe in Hekla ash relates to efficient in-plume scavenging of H_2S by the ash's Fe-oxide constituents. But studies on the effect of the hot core on S speciation in volcanic plumes showed that H_2S could be depleted very fast via high-T oxidation reaction. Absence of H_2S in a few hours old volcanic cloud of Hekla, which is studied using aircraft measurements, confirms this hypothesis [Rose et al., 2006]. Therefore, additional processes may have contributed to the formation of soluble Fe. As Hekla is located on a mid-ocean ridge but its geochemistry also suggests a hot spot signature [Schmincke, 2004] its magmatic gas composition can be compared to both DP and HS scenarios. In addition, petrological estimates suggest $\log(fO_2)$=-10.50 (close to DP and HS scenarios) to -11.00 (closer to DP-R and HS-R) for the basaltic Hekla magma prior to eruption [Moune et al., 2007]. The different behavior of the Hekla ash can be considered in agreement with our results for DP-R and HS-R scenarios in which >80% of the ash iron remains in the ferrous form (i.e., more soluble oxidation state). Further in-plume and in-cloud processes (e.g., leaching by acid and water condensates) can then produce soluble iron oxides. On the other hand, in DP and HS scenarios iron is completely oxidized to hematite. In this case, mid and low temperature in-plume and cloud processes could be expected to play the main role in Fe mobilization in Hekla ash and hot core effect is negligible. However, such processes are beyond the scope of this work and more studies are needed in order to understand their effect on ash iron mobilization.

3.5 Conclusion

The hot core of the volcanic plume does not produce bio-available iron but significantly controls the Fe mineralogy and oxidation state, which is center to studying further in-plume and in-cloud processes. While these results may represent an extreme case, they nevertheless suggest that reduced initial magmatic conditions, high ash content

and lower initial temperatures in divergent plate and hot spot volcanism appear to be more favorable for soluble iron formation because they maintain iron in a more soluble oxidation state (i.e., ferrous or Fe^{2+}). However, convergent plate volcanoes (subduction zones), which are thought to be more relevant to plinian and sub-plinian eruptions as well as ocean fertilization [Duggen et al., 2007], produce iron mainly in ferric form (i.e., Fe^{3+} in Hematite).

Mineral dust studies show that iron is mainly in form of hematite in such particles which can be mobilized during atmospheric transport due to interaction with natural and anthropogenic gases and aerosols [Johnson et al., 2010, Meskhidze et al., 2003]. By analogy, hematite from CP volcanoes can finally transform to soluble iron salts. Nevertheless, chemical and physical conditions in volcanic ash clouds are quite different from dust clouds. Therefore, studying mid and low-T conditions in volcanic plume and in-cloud processes are very important in order to understand the causes of ash iron mobilization. Besides, experimental characterization of the volcanic ash surface (e.g., mineralogy, surface area, porosity etc.) is a key to determine favorable source and atmospheric conditions for bio-available iron production.

Chapter 4

Ash iron mobilization in volcanic eruption plumes

4.1 Introduction

In 2010, sockeye salmon mysteriously reached record numbers in British Columbia's Fraser River after dismally low numbers during recent decade [Jones, 2010, Larkin, 2010]. It is suggested that iron in the ash from the volcanic eruption of Kasatochi in 2008, which stimulated a phytoplankton bloom, could have indirectly provided a feast for the salmon [Parsons and Whitney, 2012] through an enhanced marine primary productivity (MPP) [Lindenthal et al., 2013] and phytoplankton bloom [Olgun et al., 2013]. This phytoplankton bloom was indeed the first direct evidence of a fertilization effect of volcanic ash on the surface ocean [Hamme et al., 2010, Langmann et al., 2010]. However, it is not yet fully understood how the insoluble iron in the mineral and glass components of the volcanic ash could be transformed into soluble iron species to become bio-available at the surface ocean.

Volcanic ash refers to tephra with a diameter <2 mm [Rose and Durant, 2009] and is typically composed of silicate glass and crystalline materials generated during an explosive eruption through magma fragmentation and erosion of the conduit wall rock [Heiken and Wohletz, 1992]. Various volcanic and atmospheric processes are proposed which can modulate ash iron solubility (see Duggen et al. [2010] or Ayris and Delmelle [2012b]). It is suggested that both high and low temperature reactions within the eruption plume could significantly alter the ash surface composition, and hence iron mineralogy and speciation (see Chapter 3 and also Ayris and Delmelle [2012b]). These reactions are expected to modify the surface reactivity of the ash, thus potentially influencing further (photo)chemical reactions during transport of the ash in the atmosphere [Ayris and

Delmelle, 2012b]. However, there is lack of theoretical work as well as data with respect to the role of the hot, warm and cold regions of the volcanic plumes in bio-available iron production [Ayris and Delmelle, 2012b].

During its journey from the magma fragmentation level to the high altitudes and finally to the surface ocean, ash passes through various environmental conditions and undergoes numerous physicochemical processes [Ayris and Delmelle, 2012b]. Here we partition the environmental conditions in three zones: in-conduit, in-plume and in-cloud (Table 4.1). In-conduit processes refer to high-T post-fragmentation subterranean gas-ash interactions recently studied by Ayris et al. [2013]. Their results imply that large explosive eruptions with deep magma fragmentation depth are likely to be affected by significant gas-tephra interaction at temperatures above 600°C. They suggest that high temperature SO_2 scavenging by glass-rich tephra proceeds by a Ca^{2+} diffusion-driven mechanism Ayris et al. [2013]. As shown in Table 4.1, in-plume processes encompass a wide range of temperatures and the distance from the vent to the neutral buoyancy level (NBL) during which the magmatic gases are mixed with the ambient air. Chapter 3 constrained the high-T in-plume processes to T>600°C (see Fig. 4.1, zone 1) which control iron mineralogy and oxidation state at the ash surface assuming thermodynamic equilibrium. We concluded that such an oxidation effect is more pronounced in large explosive eruptions with shallow magma fragmentation depth and emphasized that mid and low in-plume (zones 3 and 4 in Fig. 4.1) as well as the in-cloud processes (zones 4 and 5 in Fig. 4.1) can play a significant role in ash iron mobilization. These zones are bounded with the temperature ranges and also formation of liquid sulfuric acid and water. They condense when the temperature of the mixture reaches their dew point. Regarding the atmospheric pressure at high altitudes and species concentrations in volcanic plumes, T∼150°C and ∼50°C seem valid estimates for dew points of sulfuric acid and water, respectively, which are also the lower boundaries of mid and low-T in-plume zones (see section 4.3 for more details). Sulfuric acid condenses first followed almost immediately by water condensation at about 50°C and thus, dissociates to H^+ and HSO_4^-. After this point, we can assume that the processes are similar to conventional in-cloud processes considered in atmospheric sciences [Seinfeld and Pandis, 2006]. However, since the freezing has a significant impact on the system, we consider two subsections for the in-cloud zone: warm (i.e., without ice/before freezing) and cold (i.e., with ice/after freezing). In the warm in-cloud zone, the aqueous phase scavenges volatiles (e.g., HCl and SO_2) from the surrounding atmosphere and also dissolves the ash solid constituents. These processes release cations (e.g., Na^+, Fe^{2+}, Al^{3+}) and anions (e.g., Cl^-, SO_4^{2-}, F^-) into the liquid phase, which can further react with each other in an aquatic regime generating soluble salts [Stumm and Morgan, 1996]. When the temperature of the system reaches the freezing point (cold in-cloud zone), ice forms at the ash surface and interacts with

the surrounding atmosphere [Textor et al., 2004] and also the ash's solid constituents. The freezing/melting and also dissolution/precipitation cycles during in-cloud zones can significantly contribute to the ash iron mobilization [Duggen et al., 2010]. It is noteworthy that the boundaries of the zones mentioned above could slightly change according to atmospheric conditions and eruption dynamics and also have some overlap with each other. However, they are viable first order approximations to better identify the role of different environmental conditions on gas-ash/aerosol interactions.

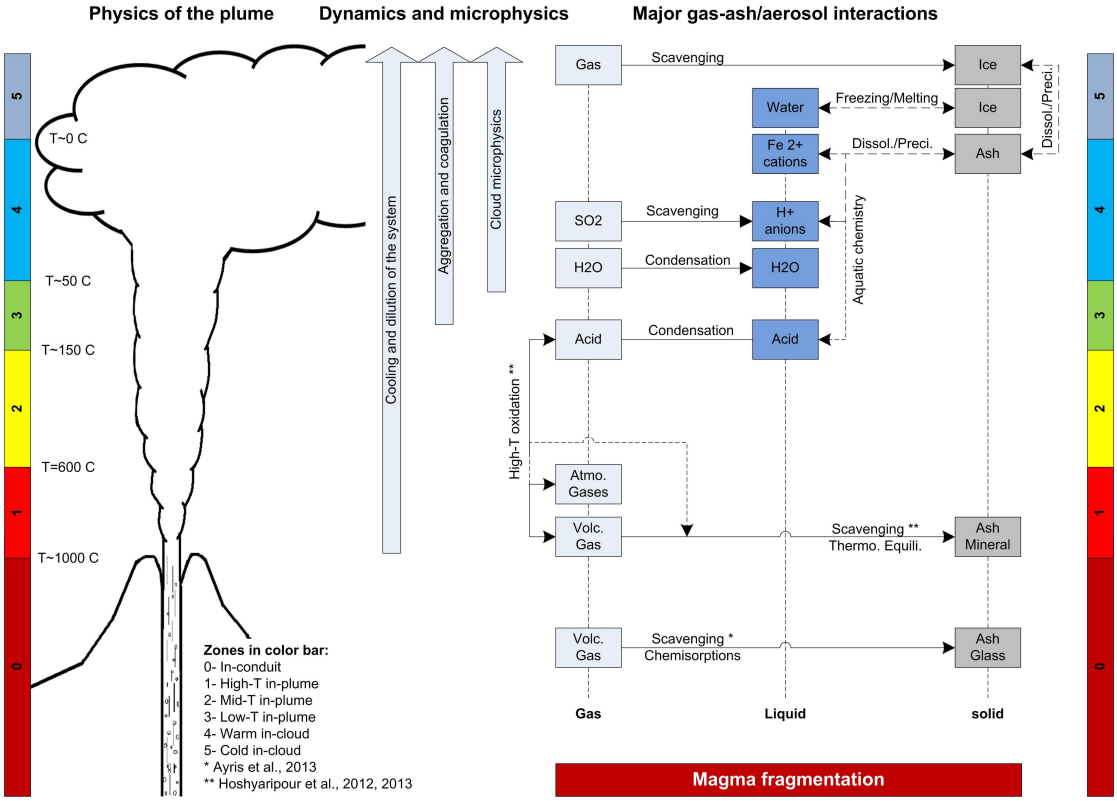

FIGURE 4.1: The interaction between ash surface, liquid film and the surrounding gases. During high-T zones (zones 0 and 1 in the color bar) direct gas-ash interaction significantly controls the iron speciation at the ash surface. At lower temperatures however (zones 2, 3, 4 and 5, such interactions are negligible. The formation of liquid phase at the ash surface and its interactions with the surrounding gases (i.e., scavenging) and with the ash constituents (i.e., dissolution) mainly control the ash iron mobilization in zones 3 and 4. Zone 5 is beyond of the scope of this research.

Studying mid and low-T conditions in volcanic plume and in-cloud processes is necessary in order to understand the causes of ash iron mobilization. This study investigates the mid and low-T in-plume and also warm in-cloud processes, which can affect iron mobilization. We consider a box model in which the lower boundary is the material leaving the hot core into mid-T zone (i.e., T=600°C) and the upper boundary is the output of warm in-cloud zone (i.e., T∼0°C). The condensation of sulfuric acid and water are simulated together with gas scavenging and ash dissolution. The main research question is how much iron II and iron III are dissolved in the aqueous phase when

T=0°C is reached. Therefore, aqueous chemistry of ions and all the processes involving ice (i.e., cold in-cloud zone) are beyond the scope of this study. In the following sections we first present the modeling concept and tools. Then results of the modeling study and its sensitivity to different parameters are discussed. Finally the conclusions are given.

TABLE 4.1: Different zones of the plume that affect the fine ash during a plinian and sub-plinian volcanic eruption

Zone	Location	Subzones	Time scale[a]	Length scale	Temperature
Conduit	Fragmentation level to vent	-	6-275 s	Few meters to few km	T>600°C
Plume	Vent to NBL	high-T[b] mid-T low-T	150-250 s	Few km to tens of km	>ambient
Cloud	After NBL	warm[c] cold	hours to days	>Hundreds of km	∼ambient

[a] Time scales are estimated based on Ayris et al. [2013], Mastin [2007] and Rose and Durant [2009] for conduit, plume and cloud zones, respectively.

[b] high-T: T>600°C, mid-T: 150°C<T<600°C and low-T: 50°C<T<150°C

[c] warm zone: T>freezing point (∼0°C), cold zone: T<freezing point

4.2 Methodology

4.2.1 Properties of ash

Particle sizes <1 mm are considered in this study, which corresponds to the definition of fine ash [Rose and Durant, 2009]. Fine ash is thought to represent a substantial contribution (50-97 wt%) to tephra deposits from plinian and sub-plinian volcanic eruptions [Rose and Durant, 2009]. Particles in this size range not only have more specific surface area (relative to coarser particles) for interaction with the gas/aqueous phases [Delmelle et al., 2005] but also can be lifted to high altitudes and remain suspended in the atmosphere for several days before sedimentation [Sparks et al., 1997]. Among others, Rose and Durant [2009] investigated the ash content of volcanic eruption plumes and suggested a typical polymodal size distribution for ash subdivided into 27 bins (Fig. 4.2a). For this binned representation of fine volcanic ash, the total number of bins between 0.01 μm to 1000 μm (see Fig. 4.2a) is denoted by *nclass*. Each bin is considered to be monodisperse with a radius R_p^i which is given by [Pirjola et al., 1999]:

$$\log_{10}(R_p^i) = \log_{10}(r_{min}) + \frac{\log_{10}(r_{max}) - \log_{10}(r_{min})}{nclass}(i-1) \tag{4.1}$$

Here we use $nclass$=27 (see also Fig. 4.2a) which is also recommended by [Pirjola et al., 1999]. Using R_p^i and an ash density of 2300 kg m^{-3} [Rose and Durant, 2009], we calculate the mass of a single particle in each bin. Assuming that near the vent approximately 3 wt% of the plume is gas and about 97 wt% is ash [see Mastin, 2007], we proposed in Chapter 3 that for each mole of volcanic gas (with an average weight of 25 g), the erupted material contains approximately 830 g ash, which at T=1000°C and P=1 bar corresponds to in-plume ash concentration of 0.005 g cm^{-3} near the vent. Finally, using wt% of each size bin (Fig. 4.2a), the mass of a single particle and the ash concentration calculated above, we compute the number of particles in each bin per cm^3, which is shown in Fig. 4.2b. According to this plot, we estimate the total number concentration near the vent to be approximately 10^{12} particles per cm^3 having a total surface area of ash 45 cm^2 cm^{-3}.

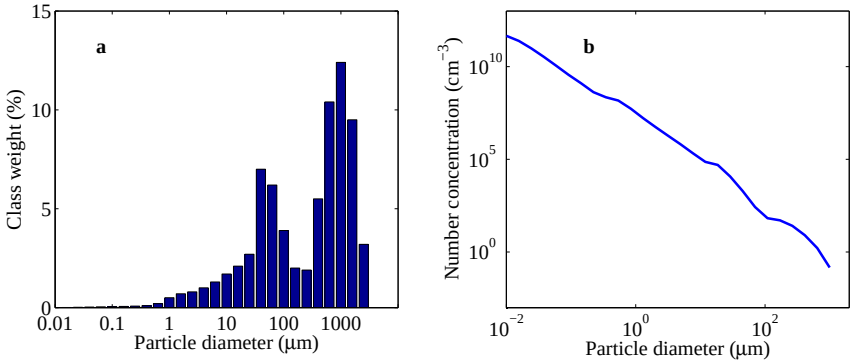

FIGURE 4.2: a) Typical distal ash-fall particle size analysis from Rose and Durant [2009] b) particle number concentration calculated using the same data

According to previous studies, the specific surface area of fine volcanic ash is in the range 0.2-2.1 m^2 g^{-1} [Delmelle et al., 2005, Mills and Rose, 2010]. Based on the estimates above, we find 0.9 m^2 g^{-1} as the specific surface area of fine ash in this study, which is well in the range mentioned above. Considering the dilution and expansion due to air entrainment, it is suggested that the plume radius of an explosive eruption at neutral buoyancy level can be 500-600 times bigger than its radius near the vent [Mastin, 2007]. If we assume a control volume with radius r and a constant height, the expansion of this control volume from vent to the neutral buoyancy level is $V_1/V_0 = (r_1/r_0)^2$=2-4×10^5 where V_0, V_1 and r_0, r_1 are the volume and radius at the vent and neutral buoyancy level, respectively. Therefore, the in-plume ash concentration mentioned above could be diluted by an order of 10^5 near neutral buoyancy level (∼10^7 particles cm^{-3} and ∼5×10^4

μg m^{-3}) and even further in volcanic clouds. Rose and Durant [2009] estimated the bulk density of ash in the cloud of Crater Peak, Alaska, to be 1.3×10^4 μg m^{-3}, which is half an order of magnitude less than our estimate for ash concentrations near the neutral buoyancy level. However, if one considers further in-cloud dilution effects, these values are in good agreement. It is noteworthy that these ash concentrations are quit high in comparison with typical atmospheric aerosol concentrations (e.g., PM10 concentration in a polluted urban atmosphere is 100-300 μg m^{-3} [Seinfeld and Pandis, 2006]).

While physical properties of ash (size distribution, surface area etc) usually reflect the fragmentation and eruption mechanism [Dingwell et al., 2012], its bulk mineralogy is controlled by cooling and crystallization of the magma. However, the surface of the ash acts as the oxidation front in exposure to volcanic gases and ambient air and does not necessarily reflect the bulk mineralogy (see Chapter 3). According to section 3.3 and also the analytical studies of Bayhurst et al. [1991], we assume that ash is composed of silicate glass (60%) and minerals (40%) [Blundy et al., 2006] with species mentioned in Table 4.2. We note that these are the major Fe carrying species considered in this study.

4.2.2 Mass balance equations

Concentrations of gas- and particulate-phase species in the plume are determined by solving a system of coupled mass balance equations. In its most general form, this equation is [Meskhidze et al., 2005]:

$$\frac{d}{dt}C_i = P_i - D_i - \alpha_{dep}[C_i] - \alpha_{dill}[C_i] \tag{4.2}$$

where C_i is the concentration of species i within the plume (in units of mole m^{-3}), P_i and D_i are production and destruction rates for species i (in units of mole m^{-3} s^{-1}), α_{dill} is a rate constant for dilution of the plume due to mixing with ambient air, α_{dep} is the rate constant for loss of species contained within ash and aerosols due to fallout and deposition (wet and dry) and n is the number of species considered (see Table 4.2). In this study we focus on calculation of P_i and D_i terms via kinetic and thermodynamic reactions in the atmospheric gas and aqueous phase. The term α_{dill} is calculated based on the expansion of the plume due to temperature and pressure changes following the universal gas law. As explained above, since we focus on in-plume and warm in-cloud processes (see Table 4.1), we can safely neglect the term α_{dep} for the fine ash. At each step, a system of n ordinary differential equations (ODE) is solved using the ode15s solver in MATLAB [Shampine and Reichelt, 1997]. All considered gas-phase reactions

and their rate parameters are listed in Table 4.3 [Jacobson, 2005, Sander et al., 2011, Seinfeld and Pandis, 2006].

TABLE 4.2: The major species considered in this study

Phase	Species
Gas	H_2, H_2O, H_2O_2, SO_2, H_2S, SO_3, H_2SO_4, CO, CO_2, O_3, HF, HCl, HClO, OH, O, H, Cl, ClO, SO, HS, HSO_3, NO, NO_2, NO_3, HNO_3, NH_3, N_2, O_2
Liquid	H_2O, H_2O_2, OH, H_2SO_4, SO_2, NO_2, NO_3, HNO_3, NH_3, H^+, OH^-, SO_4^{2-}, SO_3^{2-}, HSO_4^-, HSO_3^-, Cl^-, F^-, NH_4^+, Fe^{2+}, Fe^{3+}, Al^{3+}
Solid	fayalite: Fe_2SiO_4, magnetite: Fe_3O_4, hematite: Fe_2O_3, glass

TABLE 4.3: Gas-phase reactions and rate coefficients

No.	Reaction	Rate coefficient	Reference*
R1	$SO_2+0.5O_2 \rightarrow SO_3$	$1.3\times10^{-33}(600/T)^{3.6}$	1, 2
R2	$SO_3+O_3 \rightarrow SO_3+O_2$	$3.0\times10^{-12}e^{-7100/T}$	1
R3	$SO_2+OH \rightarrow HSO_3$	$4.0\times10^{-31}(300/T)^{3.3}$	1, 2
R4	$HSO_3+O_2 \rightarrow SO_3+H_2O$	$1.3\times10^{-12}e^{-330/T}$	1, 2
R5	$SO_3+H_2O \rightarrow H_2SO_4$	6.0×10^{-15}	3, 2
R6	$H_2S+OH \rightarrow HS+H_2O$	$6.3\times10^{-12}e^{-80/T}$	1, 2
R7	$HS+O_2 \rightarrow SO+OH$	4.0×10^{-19}	3
R8	$SO+O_2 \rightarrow SO_2+O$	$2.1\times10^{-13}e^{-2280/T}$	1, 2
R9	$HCl+OH \rightarrow Cl+H_2O$	$2.4\times10^{-12}e^{-330/T}$	1, 2
R10	$HClO+O \rightarrow ClO+OH$	$1.0\times10^{-11}e^{-1300/T}$	1, 2
R11	$NO+O_3 \rightarrow NO_2+O_2$	$1.8\times10^{-12}e^{-1370/T}$	1, 3
R12	$OH+O \rightarrow H+O_2$	$2.3\times10^{-11}e^{110/T}$	1, 2
R13	$OH+O_3 \rightarrow HO_2+O_2$	$1.9\times10^{-12}e^{-1000/T}$	2, 3
R14	$OH+H_2 \rightarrow H_2O+H$	$7.7\times10^{-12}e^{-2100/T}$	1, 2
R15	$OH+OH \rightarrow H_2O+O$	$4.2\times10^{-12}e^{-240/T}$	1, 3

* 1: [Sander et al., 2011], 2: [Jacobson, 2005], 3: [Seinfeld and Pandis, 2006].

4.2.3 Sulfuric acid condensation

At mid temperatures (150°C<T<600°C) in the eruption plume, heterogeneous reactions involving the gas phase and the ash material take place. In the gas phase, some of the SO_2 oxidizes to sulfite (SO_3), which upon cooling readily reacts with water vapor to

form vapor-phase sulfuric acid (H_2SO_4) (see Chapter 2). As cooling continues, the temperature eventually drops below the dew point of the complex gas mixture, allowing condensation of the H_2SO_4 onto the ash surfaces [Ayris et al., 2013]. Sulfuric acid has the highest dew point of all constituents and therefore, always condenses first [Verhoff and Banchero, 1974]. We calculate the dew point of sulfuric acid T_{dew} in Kelvin from [Jeong and Levy, 2012]:

$$\frac{1}{T_{dew}} = 2.27 \times 10^{-5} - 2.94 \times 10^{-7} \cdot \ln(P_{H_2O}) - 8.58 \times 10^{-6} \cdot \ln(P_{H_2SO_4}) + 6.2 \times 10^{-6} \cdot \{\ln(P_{H_2O}) \cdot \ln(P_{H_2SO_4})\} \quad (4.3)$$

where, P_{H_2O} and $P_{H_2SO_4}$ are partial pressures of water vapor and sulfuric acid, respectively, in mmHg. When the temperature of the plume drops below sulfuric acid condenses onto the ash particles. This process is expected to lead to high concentrations of dissolved H_2SO_4 in the condensate associated with the ash, and thus to strongly acidic pH values of the liquid film on the ash surface [Ayris and Delmelle, 2012b]. In this study the Fuchs-Sutugin interpolation formula is used to describe the condensation rate of H_2SO_4 molecules to the ash particles [Fuchs and Sutugin, 1970]. The single particle condensation coefficient is given by:

$$K_{FS} = \alpha K_{kin} \left[1 + \frac{3\alpha}{4\mathrm{Kn}} \times \left(1 - 0.623 \frac{\mathrm{Kn}}{1 + \mathrm{Kn}} \right) \right]^{-1} \quad (4.4)$$

where
α = the accommodation coefficient of H_2SO_4 ($\sim$1 in this study [Clement et al., 1996]),
K_{kin} = the kinetic condensation coefficient = $\pi R_p^2 c_b$,
c_b = the average thermal velocity of H_2SO_4 gas molecules = $[8kT/\pi M]^{1/2}$,
Kn = is the particle Knudsen number= l/R_p,
l = the mean free path of H_2SO_4 molecules = $3D_b/c_b$,
D_b = the H_2SO_4 diffusion coefficient = 0.08 cm^2 s^{-1},
T = the absolute temperature in Kelvin,
k = the Boltzmann's constant,
M = the mass of H_2SO_4 molecule and
R_p = the particle radius.

With respect to the previous section, we calculate the condensation rate onto a polydisperse ash distribution. In that case, the condensation coefficient X_c is defined as:

$$X_c = \int_0^\infty K_{FS}(R_p) n(R_p) dR_p \tag{4.5}$$

where $n(R_p)dR_p$ is the concentration of particles with radius between R_p and $R_p + dR_p$ according to Rose and Durant [2009]. The condensation rate onto a polydisperse distribution is finally given by:

$$CS = \int_0^\infty K_{FS}(R_p) n(R_p) \times [N_g - N_g^e(R_p)] dR_p \tag{4.6}$$

where N_g is the H_2SO_4 vapor pressure in the gas phase and $N_g^e(R_p)$ is the equilibrium vapor pressure over a particle with radius R_p. In a volcanic eruption plume $N_g^e(R_p)$ is negligible in comparison to N_g. Hence equation 4.6 simplifies to:

$$CS = X_c N_g \tag{4.7}$$

4.2.4 Water condensation

The mass-flux of water condensing onto a single, spherical particle with radius R_p is given by [Jacobson, 2005]:

$$K_{FW} = \frac{4\pi D_v \left(p_v - p_{v,s}\right)}{\frac{D_v L_e p_{v,s}}{k_a T}\left(\frac{L_e}{R_v T} - 1\right) + R_v T} \tag{4.8}$$

where
D_v = the molecular diffusion coefficient of water vapor in air = 0.234 cm^2 s^{-1},
p_v = the vapor pressure of water vapor in plume in hPa,
$p_{v,s}$ = the saturation vapor pressure at the particle surface = $6.112 exp(17.67 T_c/(T_c + 243.5))$,
T_c = the temperature in degree Celsius,
L_e = the latent heat of water evaporation = 2260 J g^{-1},
R_v = the gas constant for water vapor = 461.40 J kg^{-1}K^{-1},
k_a = the thermal conductivity of moist air $\approx k_d[1 - (1.17 - 1.02\frac{k_v}{k_d})\frac{n_v}{n_v + n_d}]$,
k_d, k_v = the thermal conductivities of dry air and water vapor, respectively and
n_d, n_v = the number of moles of dry air and water vapor, respectively.

Finally, the condensation rate of water onto a polydisperse aerosol distribution is calculated by:

$$CW = \int_0^\infty K_{FW}(R_p) n(R_p) dR_p \tag{4.9}$$

4.2.5 Thermodynamic equilibrium

Once the concentrations of the major species listed in Table 4.2 have been determined at a given time step using the equations described above, these species must be speciated into their various possible chemical forms. This is accomplished in the model by invoking thermodynamic equilibrium between the gas and liquid phase. We use the mass flux iteration method (MFI) to solve for thermodynamic equilibrium [Jacobson, 2005]. MFI solves each equilibrium equation iteratively and iterates over all equations while conserving mass and charge (for more details, see Jacobson [2005]). Gas dissolution (i.e., scavenging) and molecular dissociation are simulated using MFI method in this study. The thermodynamic equilibrium reactions considered in this study and the parameters for calculating their equilibrium coefficient (K_{eq}) are shown in Table 4.4. K_{eq} for each reaction at temperature T is calculated by [Jacobson, 2005]:

$$K_{eq}(T) = A \exp\left\{ B\left(\frac{T_0}{T} - 1\right) + C\left(1 - \frac{T_0}{T} + \ln\frac{T_0}{T}\right)\right\} \tag{4.10}$$

where T_0=298.15 K.

TABLE 4.4: Equilibrium reactions and rate coefficients [Jacobson, 2005]

No.	Reaction	A	B	C
E1	$SO_2(g) \rightleftharpoons SO_2(aq)$	1.22	10.55	0
E2	$H_2O_2(g) \rightleftharpoons H_2O_2(aq)$	7.45×10^{4}	22.21	0
E3	$NO_2(g) \rightleftharpoons NO_2(aq)$	1.00×10^{-2}	8.38	0
E4	$NO_3(g) \rightleftharpoons NO_3(aq)$	2.10×10^{5}	29.19	0
E5	$OH(g) \rightleftharpoons OH(aq)$	2.50×10^{1}	17.12	0
E6	$HNO_3(g) \rightleftharpoons HNO_3(aq)$	2.10×10^{5}	0	0
E7	$NH_3(g) \rightleftharpoons NH_3(aq)$	5.76×10^{1}	13.79	-5.39
E8	$SO_2(aq) + H_2O \rightleftharpoons H^+ + HSO_3^-$	1.71×10^{-2}	7.04	0
E9	$HSO_3^- \rightleftharpoons H^+ + SO_3^{2-}$	5.99×10^{-8}	3.74	0
E10	$HCl(g) \rightleftharpoons H^+ + Cl^-$	$1.97\times10^{+6}$	30.19	19.91
E11	$HF(g) \rightleftharpoons H^+ + F^-$	3.94	25.04	16.34
E12	$NH_3(aq) + H_2O \rightleftharpoons NH_4^+ + OH^-$	1.85×10^{-5}	-1.5	0
E13	$H_2SO_4 \rightleftharpoons H^+ + HSO_4^-$	$1.00\times10^{+3}$	0	0
E14	$HSO_4^- \rightleftharpoons H^+ + SO_4^{2-}$	1.02×10^{-2}	8.85	25.14

4.2.6 Ash dissolution

The liquid film or droplets at the ash surface not only scavenge volatiles out of the gas but also dissolve the ash surface. This dissolution process results in formation of Fe^{2+} and Fe^{3+} in the aqueous phase (together with other ions) which is central to further iron mobilization processes. Here, we assume d_i as the dissolution rate of mineral species i which will be calculated based on a simplified temperature independent formulation proposed by Palandri and Kharaka [2004]:

$$\log d_i = \log k_i - n_i \cdot \mathrm{pH} \tag{4.11}$$

where d_i is in mole m^{-2} s^{-1}, $\log k_i$ is the log rate constant computed at 25°C and pH=0, n is the reaction order with respect to H^+. Table 4.5 shows the rate parameters used in this study for different ash constituents. These parameters are accurate to a first order approximation over the range of acidic pH [Palandri and Kharaka, 2004]. We note that the dissolution rates used here are temperature independent which is a valid assumption if one considers the short residence time of particles at a certain temperature (i.e., few seconds).

TABLE 4.5: Ash dissolution reactions and rate parameters

Species	Reaction	*logk*	*n*	Reference*
Fayalite	$Fe_2SiO_4+4H^+ \rightarrow 2Fe^{2+}+3H_2O$	-5.80	1.0	1,2
Magnetite	$Fe_3O_4+8H^+ \rightarrow 2Fe^{2+}+Fe^{3+}+4H_2O$	-8.59	0.279	1,2
Hematite	$Fe_2O_3+6H^+ \rightarrow 2Fe^{3+}+3H_2O$	-9.39	0.421	1,2
Glass	$SiAl_{0.36}O_2(OH)_{1.08}+1.08H^+ \rightarrow SiO_2+0.36Al^{3+}+1.08H_2O$	-12.30	-	3

* 1: [Palandri and Kharaka, 2004], 2: [Bandstra et al., 2007], 3: [Oelkers and Gislason, 2001].

4.2.7 Initial conditions

It is known that convergent plate volcanism is more likely to generate plinian and sub-plinian eruptions [Schmincke, 2004] in which huge amounts of fine ash could be transported thousands of kilometers and reach the ocean [Duggen et al., 2010]. Therefore, we consider the 600°C magmatic gas composition of convergent plate volcanoes as the reference scenario for this study (Table 4.6). This composition reflects the magmatic gas and air mixture leaving the hot core of the plume (T>600°C), and is taken as input into

our modeling study. Ash in the reference scenario consists only of magnetite (Fe_3O_4) as the iron-carrying mineral. Magnetite contains iron in both oxidation states (ferric and ferrous) and is considered as an iron-carrying mineral with intermediate oxidation state (see Chapter 3). It is also reported in analytical studies on volcanic ash [Bayhurst et al., 1991]. To evaluate the effect of this simplification for ash composition, other minerals and glass are considered too in a detailed sensitivity study in section 4.4.2 .

TABLE 4.6: Major gas species leaving the hot core of the volcanic plume (T>600°C) from Chapter 3, which is the plume composition in the reference scenario (convergent plate setting). This composition represents the hot magmatic gas which is diluted by the ambient air (i.e., O_2 and N_2). Trace species (concentrations<0.01 mol%) are not shown in this table.

Gas species	mol%	Gas species	mol%
H_2O	57.70	H_2SO_4	0.01
CO_2	2.80	HCl	0.45
H_2	0.01	HF	0.04
H_2S	0.01	CO	0.11
SO_2	0.40	O_2	5.10
SO_3	0.87	N_2	32.10

4.2.8 Plume dynamics

Considering the great diversity in style of volcanic eruptions (i.e., from effusion of basaltic magma as lava flows and fire fountaining in Hawaiian eruptions to the generation of high altitude plumes during plinian eruptions), there are different mechanisms for high-T mixing of volcanic gas, ash, and atmospheric gases. Mixing itself is controlled by temperature and eruption dynamics (i.e., turbulence and air entrainment). If the plume is able to entrain and heat enough air, it can reduce its density below that of the surrounding atmosphere and continues to rise. Otherwise, it would collapse as a low fountain and generate pyroclastic flows and surges [Sparks et al., 1997]. Here we focus on the mixing processes in sub-plinian and plinian eruption plumes in which air entrainment reduces the density and also the temperature of the plume. As a first order approximation, the travel time from the vent to neutral buoyancy level is 150-250 seconds during which the plume temperature is lowered by ∼1000°C [Mastin, 2007]. Thus, we can assume an average cooling rate of 4-7°C per seconds in the convective region of the plume. We also use 40-80 m/s as the plume's ascent velocity in this region [Mastin, 2007]. The standard atmosphere is considered according to the United States Committee on Extension to the Standard Atmosphere [1976] having a sea level temperature of 0°C, a thermal lapse rate in the troposphere of 6.5°C/km, a troposphere thickness of 11 km, a 9-km-thick tropopause, and no atmospheric humidity. Since the processes that involve ice (T<0°C) and also the stratospheric processes (H>10-15 km [Seinfeld and Pandis, 2006]) are out

of the scope of this study, we set 0°C plume temperature and/or 11 km as the upper boundary of our box model. In the reference scenario, we use a plume cooling rate of 5°C/s, an ascent velocity of 50 m/s and an ascent time of 200 s [Mastin, 2007] leading to 0°C at 11 km altitude (assuming a vent altitude of 1 km). The results discussed below are not sensitive to these particular parameter values, over a wide range of variation.

4.3 Results and discussion

4.3.1 Mid and low-T in-plume processes: water and sulfuric acid condensation

Fig. 4.3 shows the vertical profile of water and sulfuric acid in both vapor and liquid phases as well as the temperature profile of the eruption plume and the surrounding atmosphere (all concentrations given in this paper are in mol cm^{-3} of plume). Zones that are defined in Fig. 4.1 and Table 4.1 are indicated in the temperature profile (Fig. 4.3). H_2SO_4 has the highest dew point in the mixture [Verhoff and Banchero, 1974] and condenses at ∼150°C (boundary between mid and low-T zones). This suggests that at least in our model the 338°C as the sulfuric acid dew point proposed by Óskarsson [1980] is too high for volcanic plumes.

The concentration of the liquid sulfuric acid increases and reaches a plateau near 50°C (boundary between in-plume and in-cloud zones). At this point water vapor starts condensing (H_2O(g) and H_2O(aq) in Fig. 4.3) which is followed by rapid depletion of H_2SO_4 due to its dissociation in contact with liquid water. At T<50°C gaseous sulfuric acid continues to condense (H_2SO_4(g) in Fig. 4.3) and dissociate rapidly into H^+ and HSO_4^-, thus no liquid H_2SO_4 forms (H_2SO_4 (aq) in Fig. 4.3). More than 80% of the mass (all fractions given in this research are mass fractions if not otherwise noted) of the sulfuric acid condenses in low-T in-plume and warm in-cloud zones.

At the neutral buoyancy level the temperature of the plume is close to that of the surrounding atmosphere [Mastin, 2007]. Hence, as shown in the temperature profile in Fig. 4.3, the end of our calculations (boundary between warm and cold in-cloud zones) is not far from neutral buoyancy level because atmospheric and plume temperature are converging at the top boundary. We note that the eruption dynamics and gas composition can vary the boundaries of mid and low-T in-plume zones (i.e., ∼150°C for H_2SO_4 condensation and ∼50°C for H_2O condensation). But the values presented here are valid first order approximations for the conceptual model used in this study. It is also noteworthy that the altitudes at which the plume reaches these boundaries are significantly variable in different eruptions. While the elevation of neutral buoyancy

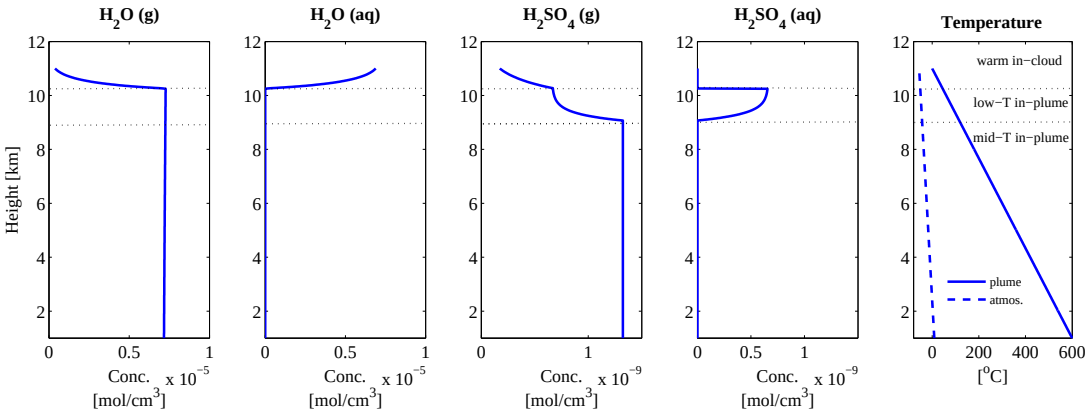

FIGURE 4.3: Vertical profiles of the water and sulfuric acid concentrations (gas and liquid phases) as well as the temperature in the eruption plume from output of the hot core (T=600°C) up to ∼NBL (T∼0°C). Please note the significant differences in concentrations between H_2O and H_2SO_4 (four orders of magnitude).

level in some eruptions is close to the tropopause (e.g., Hekla 2000 [Höskuldsson et al., 2007]), some eruptions may reach the upper stratosphere (e.g., Pinatubo 1991 [Minnis et al., 1993]).

In contrast to high-T in-plume zone (Chapter 3), the impact of the mid and low-T zones (i.e., direct gas-ash interaction) on ash surface composition is negligible. Homogeneous reactions in the gas phase (Table 4.3) are also insignificant in these zones due the rather low temperatures and short residence time. Condensation of sulfuric acid and water in theses zones are the main controlling factors of ash iron mobilization.

4.3.2 Warm in-cloud zone

4.3.2.1 Scavenging of gases and dissociation

Volcanic particles (tephra and also the liquid phase) scavenge gas species in volcanic eruption plume [Óskarsson, 1980, Rose, 1977]. When water droplets form in the plume (the warm in-cloud zone), they dissolve the surrounding gases [Textor et al., 2004]. Since the solubility of HCl is about four orders of magnitude higher than that of SO_2, it is likely to be completely scavenged by water drops thereby increasing the acidity of the aqueous phase and consequently decreasing SO_2 scavenging [Tabazadeh and Turco, 1993] which is also observed in our calculations (Fig. 4.4, right panel). While more than 98% of the HCl is removed from the gas phase, only less than 5% of the SO_2 is scavenged by the liquid water. Therefore, a high fraction of SO_2 can reach the stratosphere, while

a much lower fraction of HCl remains in the gas phase [Tabazadeh and Turco, 1993, Textor et al., 2004].

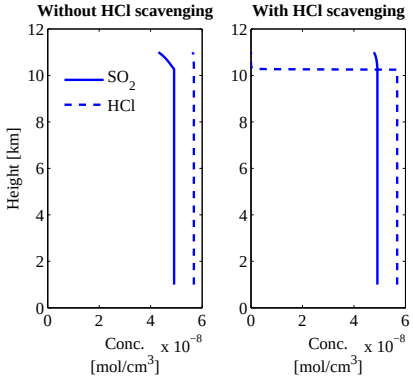

FIGURE 4.4: SO_2 and HCl vertical profile; left panel: with very low HCl scavenging (e.g., very low halide concentration in sulfur rich plumes); right panel: with high HCl scavenging (e.g., halides rich plumes).

In general, the solubility of acid gases decreases with increasing acidity of the aqueous phase [Atkins, 1986]. Since HCl dissolves more efficiently, it increases the acidity of the aqueous phase and hinders the SO_2 scavenging. If we neglect HCl scavenging in the parameterization (Fig. 4.4, left panel) about 15% of the SO_2 is removed from the gas phase in the warm in-cloud zone. Therefore, the concentration of HCl in the eruption plume controls the SO_2 scavenging efficiency: the higher the HCl concentration, the lower the SO_2 scavenging in the warm in-cloud zone. As noted before, dissolution of the major gas species in the aqueous phase is usually followed by their rapid dissociation (E8 to E14 in Table 4.4). Fig. 4.5 shows the major products of the dissociation processes. Formation of all theses anions is concurrent with H^+ release in the aqueous phase, which increases the acidity of the solution. Since Cl^- has the highest concentration (2 to 9 order of magnitudes greater than other anions), HCl dissolution and dissociation mainly control the pH of the liquid phase. The final pH in the reference scenario is 0.32 (extremely acidic), which significantly affects the ash dissolution. HSO_4^- (dissociation of sulfuric acid) and HSO_3^- (dissociation of SO_2) are the more abundant species following Cl^-. These species can further take part in aquatic reactions with the ions dissolved from the ash surface and produce salts like NaCl, $CaSO_4$, and $FeSO_4$ etc. During evaporation of the water these salts can precipitate at the ash surface. However, these processes are beyond the scope of this study.

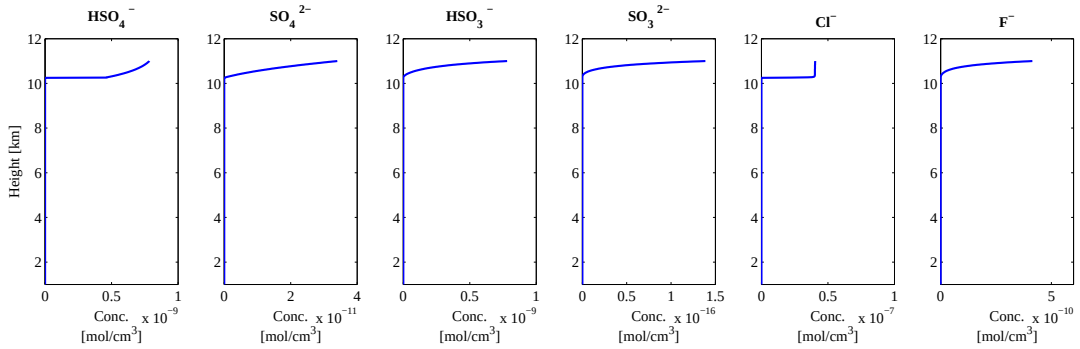

FIGURE 4.5: Vertical profiles of the major anions in the aqueous phase. HSO_4^- and SO_4^{2-} mainly form due to sulfuric acid dissociation while HSO_3^- and SO_3^{2-} are the products of SO_2 scavenging and dissociation. Cl^- and F^- are produced due to HCl and HF dissociation, respectively (See Table 4.4 for the dissolution and dissociation reactions).

4.3.2.2 Ash dissolution

The condensation, dissolution and dissociation processes in the plume generate an acidic coating which dissolves the minerals and other solids (e.g., glass) at the ash surface. Fig. 4.6 shows the dissolved iron (ferric and ferrous) from magnetite in the reference scenario. The acidic liquid phase (pH<0.5) dissolves the magnetite in the ash with dissolution rate of 6.44×10^{-12} mol $cm^{-2}s^{-1}$. Only 0.15% of the total magnetite is dissolved which releases Fe^{2+} and Fe^{3+} in the aqueous phase. The dissolved iron could react with the ions mentioned in the previous section and remain on the ash as soluble salts, such as $FeCl_2$, after the water had evaporated. Although the amount of the dissolved iron is very small, one has to take into account that huge amounts of ash are erupted during major eruptions. For instance, the eruption of Kasatochi volcano in 2008 injected 4.5-6×10^{11} kg of ash into the atmosphere [Langmann et al., 2010]. Assuming a typical Fe content in the ash 2-8 wt% [Ayris and Delmelle, 2012b] and mass of the ash particle surface as approximately 10% of the total mass, the surface rim of the ash from the Kasatochi eruption carries approximately 1-4×10^9 kg iron. Dissolution of 0.15% of total iron at the ash surface means release of 1.5-6×10^5 kg or 0.3-1×10^{17} nmol iron in the aqueous phase which is in the range proposed by Langmann et al. [2010] as the required iron for ocean fertilization after Kasatochi eruption (0.9-1.2×10^{17} nmol). Although the fate of the dissolved iron depends on the further in-cloud processes, the calculations above indicate that even a very small wt% of ash means a huge amount of mass with potentially significant impacts.

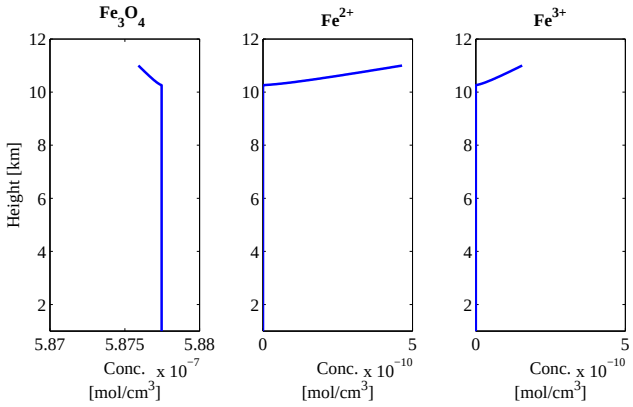

FIGURE 4.6: Vertical profile of magnetite, Fe^{2+} and Fe^{3+} concentrations. The acidic liquid phase dissolves the magnetite at the ash surface and produces Fe^{2+} and Fe^{3+} in the aqueous phase (See Table 4.5 for the dissolution reactions).

4.4 Sensitivity analysis

4.4.1 Tectonic setting

It is suggested that the ash from different volcanic settings release different amounts of Fe upon contact with seawater [Olgun et al., 2011]. Magmatic gas chemistry is also correlated to the tectonic settings [Gerlach, 2004]. Therefore, we use gas composition of three different types of volcanic settings (convergent plate (CP), divergent plate (DP) and hot spots (HS) (Table 4.7)) that were compiled in Chapter 2. The CP composition is indeed the reference scenario discussed above. The ash is assumed to be composed of magnetite in all these runs. The results are shown in Table 4.8. Since the amount of dissolved iron is of interest in this research, Table 4.8 shows the key parameters relevant to iron dissolution. In all tectonic settings, HCl is readily scavenged by the aqueous phase which consequently controls the SO_2 scavenging, pH of the liquid and finally the ash dissolution rate. Under CP setting the lowest pH and the highest dissolved iron and dissolution rate is attained. However, this pattern is correlated to neither sulfuric acid condensation nor SO_2 scavenging.

Fig. 4.7 shows the changes in pH versus HCl concentration in the gas phase and also the dissolution rate. It is obvious that the HCl scavenging controls the pH of the system and consequently the dissolution rate. Therefore, the volcanic gases that are HCl rich seem more favorable for mobilizing the iron. In Chapter 3 we hypothesized that DP and HS settings maintain the ash iron in a more soluble oxidation state (i.e., ferrous or Fe^{2+}). On the other hand, volcanic gas from CP volcanoes contains higher proportion of Cl [Symonds et al., 1994], which can result in lower pH and higher dissolution

TABLE 4.7: Average volcanic gas composition of convergent plate (CP), divergent plate (DP) and hot spot (HS) settings at T=600°C from Chapter 3

Gas species	CP	DP	HS
H_2O	57.70	50.00	53.50
CO_2	2.80	8.50	2.2
H_2	0.01	0.01	0.01
H_2S	0.01	0.01	0.01
SO_2	0.40	1.90	3.96
SO_3	0.87	3.00	2.85
H_2SO_4	0.01	0.03	0.03
HCl	0.45	0.26	0.11
HF	0.04	0.26	0.12
CO	0.11	0.20	0.22
O_2	5.10	2.40	4.10
N_2	32.10	33.40	33.70

rate. Therefore, both iron mineralogy at the ash surface and the HCl content of the eruption play significant roles in iron mobilization. Duggen et al. [2010] report that the experimentally-measured Fe release from ash produced by subduction zone and hot spot volcanism is in the ranges 100-400 and 35-107 nmol Fe g^{-1} ash, respectively. They concluded that subduction zone (CP) volcanism could be more favorable for bio-available iron production which is in agreement with our findings presented above. This is further discussed in more detail in section 4.5.

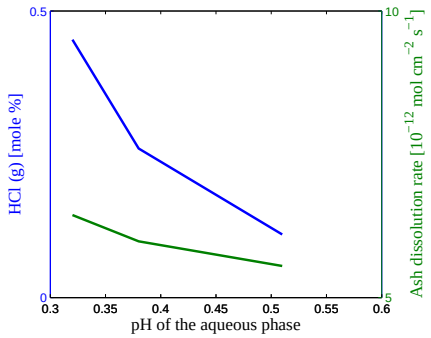

FIGURE 4.7: Correlation between pH, HCl content of magmatic gas (blue line) and the ash dissolution rate (green line). Lowest pH corresponds to the highest HCl content (CP setting) and the highest ash dissolution rate.

4.4.2 Ash composition

One important aspect of this study is that ash contains different minerals (and not only magnetite as assumed above) as well as considerable amounts of glass. In this section, the effect of ash mineralogy and composition on iron mobilization is discussed. Other iron carrying phases, being precipitated under more reduced or oxidized conditions include

TABLE 4.8: Sensitivity of the key iron mobilization parameters to the tectonic setting of the volcano

Parameter	CP	DP	HS
pH of the aqueous phase	0.32	0.38	0.51
Scavenged SO_2 %	2.86	2.59	3.60
H_2SO_4 %	87.32	85.60	86.40
Fe^{2+} dissolved %	0.11	0.08	0.07
Total dissolved iron %	0.15	0.11	0.10
Dissolution rate mol $cm^{-2}s^{-1}$	6.44×10^{-12}	5.98×10^{-12}	5.55×10^{-12}

olivin (here fayalite will be the iron carrying phase), and hematite (see for example Chapter 3). In addition the glass, which is a major component of volcanic ash, will contain iron in an amount equivalent to the original magma prior to eruption. Since the iron content of fayalite, hematite and magnetite is much higher than in glass, we can safely neglect the iron release from the glass due to its dissolution. Thus, glass acts only as a sink for H^+ and can represent the effect on other ash constituents on H^+ consumption. Table 4.9 shows the results of the control run in which magnetite is replaced by four different ash compositions:

A) 100% glass,

B) 70% glass+30% hematite,

C) 70% glass+30% fayalite,

D) 70% glass+10% hematite+10% fayalite+10% magnetite.

In the scenarios that include pure glass and glass+hematite (compositions A and B), the pH and the amount of scavenged SO_2 are not significantly different from that of the reference scenario (CP in Table 4.7). The dissolution rates of the glass and hematite are 7 and 1 order of magnitude smaller than that of magnetite (the reference scenario), respectively. For the compositions including fayalite at the ash surface (compositions C and D), significant changes in pH and SO_2 scavenging are observed. Since the fayalite dissolution rate is 2 orders of magnitudes greater than that of magnetite (i.e., reference scenario), 33% and 25% of the total iron is dissolved in the aqueous phase in the warm in-cloud zone for compositions C and D. Such a significant dissolution consumes H^+ more rapidly (see Table 4.5), reduces the acidity and consequently enhances the SO_2 scavenging. Accordingly, dissociation of the SO_2 can increase the acidity again and intensify the ash dissolution. Chapter 3 showed that under reduced magmatic conditions ($\log fO_2 < -11$), crystallization of fayalite and partly magnetite are favored. According to the results of this study, fayalite has the highest dissolution rate among other Fe-carrying minerals considered in this study. It also releases iron in the Fe^{2+} form, which has more potential for producing soluble salts [Duggen et al., 2010]. Therefore, reduced initial conditions in magma could be particularly favorable for soluble iron formation during in-cloud processes.

TABLE 4.9: The effect of ash composition on key iron mobilization parameters. Gas composition in these runs is according to the reference scenarion in Table 4.6

Ash composition	A	B	C	D
pH of the aqueous phase	0.31	0.32	1.35	1.36
Scavenged SO_2 %	2.81	2.81	19.30	19.60
Fe^{2+} dissolved %	-	0	33	25.12
Total dissolved iron %	-	0.03	33	25.21
Dissolution rate mol $cm^{-2}s^{-1}$	2.2×10^{-19}	6.0×10^{-13}	2.2×10^{-10}	2.1×10^{-10}

4.5 Conclusion

A conceptual model for volcanic eruption plumes is developed in order to identify the processes and conditions that modulate ash iron solubility. The model is composed of 5 temperature dependant zones: in-conduit, high-T, mid-T and low-T in-plume and finally, warm and cold in-cloud (see Table 4.1 and Fig. 4.1). Based on the results of Chapter 3, a numerical model is developed to solve the kinetic and thermodynamic interaction of gas-ash/aerosol in mid-T and low-T in-plume and warm in-cloud zones. Cold in-cloud processes that involve ice and the stratosphere are beyond the scope of this study. Results show that >80% of H_2SO_4 condenses in the low-T in-plume zone (50°C <T<150°C) followed by water condensation in the warm in-cloud zone (0°C <T<50°C) resulting in dissociation of sulfuric acid to H^+ and HSO_4^-. Water drops also scavenge the acid gas species (HCl, HF and SO_2), which is followed by their dissociation and release of H^+ and anions (Cl^-, F^-, HSO_3^- etc) into the aqueous phase. Since the concentrations of theses gases are usually few orders of magnitudes higher than that of sulfuric acid, their dissolution and dissociation mainly controls the pH of the liquid phase. HCl is usually readily removed from the gas phase because of its higher solubility (in comparison with the other gases). This increases the acidity of the liquid phase (pH<0.5) and slows down HF and also SO_2 scavenging. Therefore, in the eruption plumes with high halides (HCl and HF) content (i.e., convergent plate volcanoes), dissolution and dissociation of HCl (and partly HF) mainly controls the pH of the aqueous phase at the ash surface in the warm in-cloud zone. For these volcanoes SO_2 scavenging seems to be more important in colder zones and in contact with ice [Textor et al., 2004]. On the other hand, during sulfur rich eruptions (divergent plate and hot spot volcanoes) SO_2 scavenging in the warm in-cloud zone is more likely and could be the main agent in controlling the pH. Here about 15% of the SO_2 is scavenged by water drops which results in pH∼1.2.

The acidic coating formed at the ash surface starts to dissolve the ash's solid constituents (minerals and glass) with an average dissolution rate of 6×10^{-8} mol m^{-2} s^{-1}, which is in the range reported in experimental studies [Bagnato et al., 2013]. This process consumes H^+ and produces cations (Fe^{2+} or Fe^{3+}), which can also react with the anions in the

liquid phase and generate soluble iron salts. These salts can precipitate at the ash surface after water has evaporated. This is supported by the fact that the surface of the ash particles are coated by a thin layer of salts in the form of Fe sulfates and Fe halides in the eruption plume [Delmelle et al., 2007, Naughton et al., 1974]. Although <1% of the total iron is dissolved in the reference scenario, first order approximations show that even this small percent means a huge amount of mass which could be enough for explaining the iron fertilization by the ash from Kasatochi eruption in 2008.

The dissolution efficiency depends not only on pH and temperature but also on the mineral composition [Blesa et al., 1994]. Chapter 3 constrained the potential iron-carrying minerals in the volcanic ash based on tectonic settings and magma oxidation state. By studying the effects of high-T in-plume zone on ash iron speciation, we suggested three oxidation states for the iron at the ash surface: reduced, transition and oxidized states that could be characterized by fayalite, magnetite and hematite, respectively. We used these data to investigate the sensitivity of the results to the ash composition. Reduced compositions (i.e., fayalite and partly magnetite) seem more favorable for iron mobilization because they not only produce iron in ferrous form (which is more soluble) but also have higher dissolution rates (few orders of magnitude). This can explain the exceptional Fe release from the erupted ash from the Hekla 2000 eruption in deionised water [Frogner et al., 2001, Jones and Gislason, 2008]. Petrological estimates suggest reduced conditions for the basaltic Hekla magma prior to eruption [Moune et al., 2007]. The observed mineral phases in the Hekla ash include olivine, clinopyroxene and spinel [Höskuldsson et al., 2007], which is close to the C and D scenarios in Table 4.9. In section 3.4, we attributed the different behavior of the Hekla ash to the fact that under reduced conditions >80% of the ash iron remains in the ferrous form at the output of the high-T in-plume zone (i.e., fayalite and magnetite). The strong acidity and elevated halide concentration in the eruption plume of Hekla is also assumed to have promoted deposition of readily soluble Fe-bearing phases [Ayris and Delmelle, 2012b]. According to the results presented above, although total dissolved iron in the warm in-cloud zone is usually in the range of 0.1 to 4%, having reduced iron species and high halide content concurrently in the eruption plume can result in mobilization of >20% of the total iron. The erupted ash from Hekla in 2000 is estimated as 0.189 km^3 DRE (dense rock equivalent) [Höskuldsson et al., 2007] which, assuming a density of 2400 kg/m^3 for basaltic ash, is approximately equal to 4.5×10^{11} kg. Assuming a total iron content of 11% [Jones and Gislason, 2008] and surface mass of the ash 5-10% (here defined as the mass that can be affected by surface processes, i.e., a layer of 200 nm thickness), there is approximately 2-5$\times10^9$ kg iron at the Hekla ash surface. Thus dissolution of 20% of the iron in the warm in-cloud zone is equivalent to 0.4-1$\times10^9$ kg or 0.7-1.8$\times10^{10}$ moles of iron in the aqueous phase, which means Fe release of 10-60 μmol g^{-1} of ash. Jones and Gislason

[2008] reported that the ash from Hekla eruption in 2000 releases 10.8 μmol g^{-1}, which is in good agreement with our estimate above. Although further in-cloud processes can change the iron speciation and fate, these calculations hint a correlation among high iron release from the Hekla ash, the reduced magmatic conditions, the halide contents and scavenging.

Duggen et al. [2010] and later, Olgun et al. [2011] suggested a correlation between tectonic setting and ash iron fertilization and considered subduction zone (convergent plat) volcanism as the more favorable setting for soluble iron production. However, in their comparisons, they neglected the exceptional behavior of the ash from the Hekla eruption in 2000. The distribution of their samples seems also statistically biased to CP volcanism as they analyzed 40 samples form CP volcanoes and only 4 samples form HS setting. Regarding the results presented above, the fact that the eruption plumes from CP volcanoes contain more HCl and potentially higher dissolution rates, may suggest CP settings are more favorable for iron mobilization. On the other hand, magma oxidation state could play a significant role by controlling the ash mineral assemblage (reduced species of iron have higher dissolution rates under acidic conditions [Palandri and Kharaka, 2004]). Non-arc settings (DP and HS) typically record reduced conditions in comparison to CP settings [Lindsley, 1991]. Thus, DP and HS settings could be favorable for iron fertilization too with respect to their initial magma oxidation state. The Hekla eruption in 2000 had both reduced magmatic conditions (as usual for DP and HS) and high halides content (as usual for CP) which leads to an exceptional iron release behavior. Therefore, our results suggest that attributing the fertilization potential of volcanic ash to the tectonic setting seems to be not always the case. Rather, high halide contents and reduced conditions in magma seem to play the major role in iron mobilization.

Under acidic pH conditions, the dissolution of iron oxides could be greatly enhanced in the ice phase compared to that in water [Jeong et al., 2012]. As dissolution consumes H^+, it reduces the acidity and can accelerate the SO_2 scavenging by ice [Textor et al., 2004]. Therefore, sulfur scavenging by volcanic ash and aerosols seems to be insignificant during mid and low-T in-plume as well as the warm in-cloud processes. Instead, high-T (both in-conduit [Ayris et al., 2013] and in-plume (Chapter 3)) and cold in-cloud [Textor et al., 2004] zones appear to be more relevant for sulfur scavenging. Aqueous chemistry and stratospheric processes could also significantly affect the fate of the dissolved iron. Therefore, further modeling and experimental study is necessary to appreciate the fate of the dissolved iron during cloud processes.

Chapter 5

Conclusion

In this thesis I explored the iron mobilization in volcanic ash due to the gas-ash/aerosol interactions in eruption plumes. Based on physical and thermodynamic properties of each zone in plinian and sub-plinian volcanic plumes, a conceptual box model was developed which divides the plume into 3 temperature dependent zones: high, mid and low temperatures. Each zone is explored by developing and solving a system of kinetic and/or thermodynamic equilibrium reactions. The key questions raised in the introduction of this thesis can now be answered.

5.1 How does the high temperature zone control the gas and ash compositions?

The hot core of the volcanic plume (T>600°C) functions as an oxidizing reactor for both sulfur and iron species in the gas and solid phase, respectively. Processes inside the hot core usually decrease the H_2S content of the system but can either increase or decrease SO_2 depending on the initial oxidation state. Therefore, the SO_2 injected into the atmosphere is not necessarily generated directly from the magma but it can be produced in the hot core. Moreover, the volcanic cloud composition is not the mirror of the source conditions and could be weakly correlated to the high temperature gas emissions from volcanoes (see Hoshyaripour et al. [2012] or Chapter 2 of this thesis for more details). This is in agreement with the studies on the high-T magmatic gas systems [Gerlach and Nordlie, 1975, Martin et al., 2006] which reported two clear compositional regimes (i.e., reduced and oxidized regimes), divided by a compositional discontinuity [Roberts et al., 2009]. The compositional discontinuity (which is called transition point in this study) is related to the amount of oxygen required to remove reduced species from the gas [Martin et al., 2006, Roberts et al., 2009] discussed in Chapter 2.

The effect of the hot core on the ash composition is however limited to the surface rim (i.e., the ash's oxidation front with the thickness of <100 nm). Since Fe release from ash exposed to seawater is an interfacial process [Ayris and Delmelle, 2012b], the Fe mineralogy and speciation at the ash surface is of special interest to this study. It is suggested that high-T gas-ash interaction could result in precipitation of soluble Fe species on the ash surface (e.g., Duggen et al. [2010]). This statement differs in emphasis from the results presented in Chapter 3 of this thesis which showed that the hot core does not produce soluble iron species directly. However, it significantly controls the mineralogy and oxidation state of the iron on the ash surface which is a key parameter for further physicochemical processes in the colder zones. Studies on oxidation of iron-carrying minerals at high temperatures confirm this hypothesis. Lepp [1957], for instance, reported that at T>550°C, bulk oxidation of magnetite produces hematite; at lower temperatures (200-375°C) however, the reaction is limited to the surface. Among different source conditions, high ash content lower initial temperatures and reduced magmas at divergent plate and hot spot volcanoes keep most of the iron (>80%) in the reduced form (e.g., iron rich olivin (fayalite) and magnetite) which is indeed the more soluble oxidation state (see Chapter 3 of this thesis for more details).

In general, chapters 2 and 3 of this thesis suggest that in simulating and interpreting the ash-gas/aerosol interactions in volcanic plumes it is necessary to consider the source parameters (e.g., magma oxidation state, temperature, ash content etc) and also the impacts of the hot core on gas and ash composition.

5.2 What are the key parameters/processes which control iron mobilization in the plume?

Some studies have suggested that adsorption of volcanic salt aerosols is the main process responsible for the presence of soluble compounds on ash [Smith et al., 1983, Taylor and Stoiber, 1973]. On the other hand, some investigators have argued that the sulfuric acid condensation onto ash can induce dissolution reactions, thereby providing the source of the soluble cations on ash surface [Delmelle et al., 2007, Rose, 1977]. Based on the results presented in this thesis (Chapter 4), I infer that acid-mediated dissolution of ash during in-plume and in-cloud gas-ash/aerosol interaction mainly determines the amount and composition of soluble iron deposited on the ash surface. However, I found the role of halides more dominant than sulphuric acid (see section 4.5 for more details). This hypothesis is in agreement with experimental studies on volcanic ash [Bagnato et al., 2013, Delmelle et al., 2007], which emphasize the decisive control of ash dissolution and heterogeneous chemistry for cation composition of soluble materials on ash surface.

Delmelle et al. [2007], for instance, attributed the presence of sulphate and halide salts on the ash mainly to dissolution of the ash's silicate glass and minerals by acids followed by precipitation at the ash–liquid interface. I propose that three major parameters dominantly control the ash dissolution efficiency in context of producing soluble iron in volcanic plumes:

A. X_{mix} ratio: It is the ratio of the H_2 and H_2S content of the magmatic gas to the amount of entrained oxygen in the high temperature zone. This parameter is known to play a significant role in magmatic gas composition by creating two clear compositional regimes (i.e., reduced and oxidized regimes) [Gerlach and Nordlie, 1975, Martin et al., 2006, Roberts et al., 2009, von Glasow et al., 2009]. A similar role in controlling the iron oxidation state at the ash surface is reported for X_{mix} in section 3.4 of this thesis. Results indicate that the ash iron mineralogy in the hot core is likely to be independent of temperature and oxygen fugacity and is closely correlated to X_{mix}. If $\log X_{mix}$ reaches -3.5 in the hot core, most of the iron will be oxidized to Fe^{3+} which is the less soluble form. Otherwise, it would remain mainly in the form of Fe^{2+} in fayalite and magnetite at the ash surface.

B. Iron oxidation state at the ash surface: It is well known that dissolution efficiency decreases with increasing oxidation [Martin, 2005, Palandri and Kharaka, 2004]. This fact have a decisive control of ash dissolution efficiency in mid and low-T zones of the plume (Chapter 4) where the reduced iron species (e.g., fayalite) have higher dissolution rates in comparison with oxidized species (e.g., hematite). Therefore, under similar physical and chemical conditions in the eruption plume, ash composed of reduced species releases a few orders of magnitude more iron into the aqueous phase. According to the results of Chapter 3 and also the studies on volcanic rocks (e.g., Lindsley [1991] and the references therein), the ash erupted from divergent plate and hot spot volcanoes potentially contains more reduced species than that of convergent plate volcanism. Hence, I conclude that, in the context of ash composition, the reduced conditions in divergent plate and hot spot volcanoes seem to be more favorable for soluble iron production.

C. Halides contents of the magmatic gas: In the low-T zone the liquid water at the ash surface scavenges the surrounding gases (see Chapter 4). Halides (HCl and HF) are more soluble than SO_2 and thus, dissolved more rapidly in the aqueous phase and control its pH [Tabazadeh and Turco, 1993, Textor et al., 2004]. Their concentrations in the gas phase are also few orders of magnitude higher than that of sulfuric acid (see section 4.3). Thus, HCl and HF are the dominant species controlling the pH and accordingly, the dissolution efficiency. This statement differs from the hypothesis which emphasizes the role of sulfuric acid condensation in ash dissolution [Hinkley and Smith, 1982, Rose, 1977]. The higher the halides concentrations, the lower the pH of the aqueous phase

and the higher the ash dissolution rate. Therefore, higher halides concentrations in the gas phase (i.e., convergent plate volcanoes [Symonds et al., 1994]) seem quite favorable for iron mobilization.

I used the data and observations form Hekla eruption in 2000 to evaluate the results presented in this research. Various studies on this eruption (e.g., Höskuldsson et al. [2007], Moune et al. [2006, 2007, 2009], Rose et al. [2003]) tightly constrained its petrologic and volcanologic properties as well as atmospheric transport and dispersion. This eruption is unique regarding the direct sampling from the 33-34 hours old volcanic cloud [Rose et al., 2006] and also the exceptionally high Fe release from its ash in contact with water [Frogner et al., 2001, Jones and Gislason, 2008]. The parameters mentioned above could satisfactorily explain the observations of this eruption. The calculations using $\log X_{mix}$ explains not only the absence of H_2S in 33-34 hours old volcanic cloud [Rose et al., 2006] (section 2.3.4) but also the presence of reduced olivine, clinopyroxene and spinel [Höskuldsson et al., 2007, Moune et al., 2007] on the ash surface (section 3.4). I infer that the elevated HF concentrations in Hekla eruption plume [Moune et al., 2006] (parameter C above) concurrent to the presence of reduced iron species at the ash surface [Höskuldsson et al., 2007] (parameter B above) has resulted in a very high ash dissolution rate and accordingly, precipitation of soluble Fe species at the ash surface (see section 4.3 for more details).

5.3 How much iron would be finally dissolved in the aqueous phase?

The amount of the dissolved iron in the aqueous phase varies between 0.1 to 35 wt.% of the total iron at the ash surface or (assuming 10% of the total mass as the surface rim) 0.01 to 3.5 wt.% of the total iron in the bulk composition (see section 4.3). According to the controlling parameters detailed above and also in Chapter 4, the lower end of the estimate most likely occurs at low halide concentrations and oxidized iron carrying minerals (e.g., hematite) at the ash surface, while the upper end is correlated to high halide concentrations and reduced iron minerals (e.g., fayalite). However, even the lower end could result in a significant amount of bio-available iron if one takes into account that a few megatons of ash are usually erupted during major eruptions. The calculations for the eruption of Kasatochi volcano in 2008 confirm this hypothesis. The upper end of the estimate and the processes involved in it could explain the extraordinary behavior of the ash from Hekla eruption in 2000 (see section 4.3 for more details).

In Fig. 5.1, I qualitatively summarize the impact of halide concentrations in the gas phase and iron oxidation state at the ash surface on the amount of Fe dissolved in the aqueous

phase. The dissolved iron could react with the ions in the aqueous phase and generate soluble iron salts during cloud processes, which are beyond the scope of the research of my thesis. It was shown in previous studies that the ash dissolution efficiency reduces with increasing distance from the vent (i.e., it is most efficient during in-plume and first few minutes of in-cloud zones) [Delmelle et al., 2007, Moune et al., 2006]. Therefore, I surmise that the results presented in this thesis could reflect the dominant mode of ash dissolution in the eruption plume and accordingly, mirror the final ratio of the soluble iron to total iron in the ash (see section 4.5). Olgun et al. [2011] constrained the iron release from volcanic ash in contact with see water to 0.003 to 0.2% of the total iron (Dissolved Fe/Total Fe)×100. By taking into account the possible aging effect (which substantially decreases the iron release), uncertainties in the measurements and also the fact that the ash from Hekla eruption in 2000 is excluded [Olgun et al., 2011], this range fits well in the theoretical range proposed above (0.01 to 3.5%).

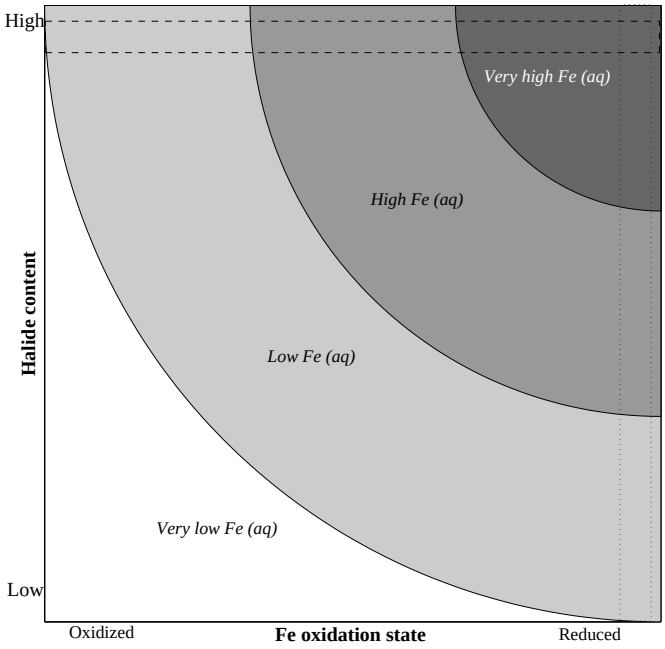

FIGURE 5.1: Amount of the dissolved Fe in the aqueous phase as a function of the iron oxidation state at the ash surface and halide concentration in the gas phase. High halide concentration and reduced conditions are more favorable for soluble iron production. The horizontal dotted rectangle shows the typical halide content of convergent plate volcanoes while the vertical dashed line rectangle shows typical ash oxidation state in divergent plate and hot spot volcanoes. When these two boxes cross, an exceptional iron release from the ash could be expected like the ash from Hekla eruption in 2000.

5.4 Which tectonic setting is more favorable for bio-available iron production?

The results of my research indicate that bio-available iron production is not correlated to the tectonic setting. Instead, halide contents of the plume and ash Fe oxidation state are the key parameters that control the iron mobilization. As discussed above, while the former parameter is more likely in arc volcanoes (convergent plates), the later is more the case in non-arc volcanoes (divergent plate and hot spot). Therefore, linking the iron release behavior of the ash to the tectonic setting of the volcano [Duggen et al., 2010, Olgun et al., 2011] seems an inconsistent hypothesis.

5.5 Outlook

All reactions and processes mentioned in this research are a strong function of environmental conditions like temperature, pressure and humidity, which are known to vary significantly as a function of height in volcanic eruption columns. In addition, many of these reactions are in a state of disequilibrium, so the time that a volume of volcanic gas and ash spends at a certain temperature/pressure interval will be another critical parameter controlling the whole system. There are also further processes (e.g., microphysics) and materials (e.g., volcanic glass) in the plume that can affect the ash–gas/aerosol interactions. In this research I tried to investigate the role of some of these parameters by using simplified schemes (e.g., for plume dynamics) and/or conducting sensitivity studies (e.g., for volcanic glass). However, this could be further improved by extending my models along the following lines:

1. 1D, 2D and 3D eruption plume models could be used to solve the plume dynamics instead of the simplified rising and cooling rates used in this study. Such models are capable of handling different eruption parameters and atmospheric conditions that are key variables for the in-plume processes.

2. The plume microphysics (e.g., aggregation) is discounted in this research because it is more important in cloud zones. Parameterization of microphysics in the chemical and thermodynamic equations could provide an added value to the whole system. This can especially control the particle size distribution which plays a significant role in ash-gas/aerosol (e.g., ash dissolution is a function of specific surface area and thus, the size distribution.)

3. Volcanic ash contains different minerals (and not only Fe carrying minerals as assumed in this study) as well as a considerable amount of glass. Studying the impact of such

solid material (e.g., feldspars) on the gas-ash/aerosol interaction and iron mobilization could further improve the generality of the simulation. These additional minerals as well as the glass could act as sinks for hot gases in the high-T zone (via direct gas-ash interaction) or for H^+ in the cloud zone (via ash dissolution).

4. A dry atmosphere is assumed in this study. However, moisture in the surrounding atmosphere can have a significant impact on the partial pressure of water vapor and water condensation. Future studies should explore the impact of wet atmospheric conditions (i.e., eruptions in tropical regions).

5. There is a significant lack of direct evidence and samples from in-plume ash iron mobilization processes. In order to validate the modeling results, experimental studies on ash surface mineralogy, topology and composition are necessary. A series of analysis on natural and synthetic ash samples could be helpful to constrain the in-plume processes experimentally.

6. Aqueous chemistry could alter the fate of the dissolved material on the ash surface. Cations (e.g., Fe^{2+}, Na^+) and anions (e.g., SO_4^{2-}, Cl^-) produced due to ash and volatile dissolution, respectively, can react with each other and generate soluble salts (e.g., $FeSO_4$, NaCl) which are observed in ash leachate analysis (e.g., Bagnato et al. [2013], Olgun et al. [2011] and the references therein). Therefore, incorporating the aqueous chemistry in the model presented in this study, could determine the final fate and speciation of the iron in volcanic ash.

7. Finally, formation of ice in the eruption plume can have a significant impact on both ash and gas. The dissolution of iron oxides could be greatly enhanced in the ice phase compared to that in water [Jeong et al., 2012]. Moreover, the scavenging of volatiles by super-cooled water and ice could be also significant [Textor et al., 2004]. Thus, simulating the ice formation and its interaction with the ash and gas could add some more lines to our knowledge about ash iron mobilization in volcanic cloud.

Bibliography

F. Africano and A. Bernard. Acid alteration in the fumarolic environment of Usu volcano, Hokkaido, Japan. *J. Volcanol. Geotherm. Res.*, 97:475–495, 2000.

F. Africano, A. Bernardand, and M. Korahinsky. High temperature volcanic gas geochemistry (major and minor elements) at Kudryavy volcano, Iturup island, Kuril arc, Russia. *Vulcnica*, 01:87–94, 2003.

A. Aiuppa, S. Inguaggiato, A. J. S. McGonigle, M. O'Dwyer, C. Oppenheimer, M. J. Padgett, D. Rouwet, and M. Valenza. H_2S fluxes from Mt. Etna, Stromboli, and Vulcano (Italy) and implications for the sulfur budget at volcanoes. *Geochim. Cosmochim. Ac.*, 69:1861–1871, 2005.

A. Aiuppa, E. Bagnato, M. L. I. Witt, T. A. Mather, F. Parello, D. M. Pyle, and R. S. Martin. Real-time simultaneous detection of volcanic Hg and SO_2 at La Fossa crater, Vulcano (Aeolian Islands, Sicily). *Geophys. Res. Lett.*, 34:L21307, 2007a.

A. Aiuppa, A. Franco, R. Von Glasow, A. G. Allen, W. D. Alessandro, T. A. Mather, D. M. Pyle, and M. Valenza. The tropospheric processing of acidic gases and hydrogen sulphide in volcanic gas plumes as inferred from field and model investigations. *Atmos. Chem. Phys.*, 7:1441–1450, 2007b.

A. Aiuppa, H. Shinohara, G. Tamburello, G. Giudice, M. Liuzzo, and R. Moretti. Hydrogen in the gas plume of an open-vent volcano, Mount Etna, Italy. *J. Geophys. Res.*, 112:B10204, 2011.

P. W. Atkins. *Physical Chemistry*. Oxford Univ. Press, New York, 1986.

P. M. Ayris. *High temperature SO_2 chemisorption on model systems. Implications for in-plume processes*. PhD thesis, University of York, 2010.

P. M. Ayris and P. Delmelle. The immediate environmental effects of tephra emission. *Bull. Volcanol.*, 74(9):1905–1936, 2012a. ISSN 0258-8900. doi: 10.1007/s00445-012-0654-5.

P. M. Ayris and P. Delmelle. Volcanic and atmospheric controls on ash iron solubility: A review. *Phys. Chem. Earth, Parts A/B/C*, 45-46:103–112, 2012b.

P. M. Ayris, A. F. Lee, K. Wilson, U. Kueppers, D. B. Dingwell, and P. Delmelle. SO_2 sequestration in large volcanic eruptions: High-temperature scavenging by tephra. *Geochim. Cosmochim. Ac.*, 110:58–69, 2013.

E. Bagnato, A. Aiuppa, A. Bertagnini, C. Bonadonna, R. Cioni, M. Pistolesi, M. Pedone, and A. Hoskuldsson. Scavenging of sulphur, halogens and trace metals by volcanic ash: The 2010 Eyjafjallajökull eruption. *Geochim. Cosmochim. Ac.*, 103(0):138–160, 2013. ISSN 0016-7037. doi: 10.1016/j.gca.2012.10.048.

W. S. Baldridge, T. R. McGetchin, and F. A. Frey. Magmatic evolution of Hekla, Iceland. *Contrib. Mineral. Petrol.*, 42:245–258, 1973.

J. Z. Bandstra, H. L. Buss, R. K. Campen, L. J. Liermann, J. Moore, E. M. Hausrath, A. K. Navarre-Sitchler, J. H. Jang, and S. L. Brantley. *Kinetics of Water Rock Interactions*, chapter Appendix: Compilation of Mineral Dissolution Rates, pages 731–733. Springer, 2007.

C. Banzon-Bautista. *Fire and Mud: Eruptions and Lahars of Mt Pinatubo, Philippines*, chapter The Mount Pinatubo disaster and the people of Central Luzon, pages 151–161. University ofWashington Press / Philippine Institute of Volcanology and Seismology, Seattle / Quezon City, 1996.

T. S. Bates, B. K Lamb, A. Guenther, J. Dignon, and R. E. Stoiber. Sulfur emissions to the atmosphere from natural sources. *J. Atmos. Chem.*, 14:315–337, 1992.

P. J. Baxter. *Encyclopaedia of Volcanoes*, chapter Impacts of eruptions on human health, pages 1035–1043. Academic Press, New York, 1999.

G. K. Bayhurst, K.H. Wohletz, and A.S. Mason. *Volcanic ash and aviation safety: Proceedings of the First International Symposium on Volcanic Ash and Aviation Safety*, chapter A method for characterizing volcanic ash, page 16 p. USGS, 1991.

S. Bekki. Oxidation of volcanic SO_2: A sink for stratospheric OH and H_2O. *Geophys. Res. Lett.*, 22:913–916, 1995.

M. A. Blesa, P. J. Morando, and A. E. Regazzoni. *Chemical Dissolution of Metal Oxides*. CRC Press, 1994.

J. Blundy, K. Cashman, and M. Humphreys. Magma heating by decompression-driven crystallization beneath andesite volcanoes. *Nature*, 443:76–80, 2006.

N. Bobrowski, R. von Glasow, A. Aiuppa, S. Inguaggiato, I. Louban, O. W. Ibrahim, and U. Platt. Reactive halogen chemistry in volcanic plumes. *J. Geohys. Res., D*, 112 (D6):D06311, 2007. ISSN 2156-2202. doi: 10.1029/2006JD007206.

J. B. Brady. *Mineral Physics and Crystallography: A Handbook of Physical Constants.*, chapter Diffusion data for silicate minerals, glasses, and liquids, pages 269–290. Ahrens TH (ed) AGU Reference Shelf 2, American Geophysical Union, Washington, DC, 1995.

J. B. Brady and D. J. Cherniak. Diffusion in Minerals: An Overview of Published Experimental Diffusion Data. *Rev. Mineral. Geochem.*, 72:899–920, 2010.

A. Burgisser and B. Scaillet. Redox evolution of a degassing magma rising to the surface. *Nature*, 445:194–197, 2001.

S. N. Carey. *Volcanoes and the Environment*, chapter Understanding the physical behavior of volcanoes, pages 1–54. Cambridge University Press, 2005.

M. R. Carroll and J. R. Holloway. *Volatiles in Magmas*, chapter Solubilities of sulfur, noble gases, nitrogen, chlorine, and fluorine in magmas, pages 231–271. Mineralogical Society of America, Washington DC, 1994.

T. J. Casadevall. *Volcanic Ash and Aviation Safety: Proceedings of the First International Symposium on Volcanic Ash and Aviation Safety.* USGS, 1991.

L. Clarisse, P. F. Coheur, S. Chefdeville, J. L. Lacour, D. Hurtmans, and C. Clerbaux. Infrared satellite observations of hydrogen sulfide in the volcanic plume of the August 2008 Kasatochi eruption. *Geophys. Res. Lett.*, 38:L10804, 2011.

F. C. Clement, M. Kulmala, and T. Vesala. Theoretical consideration on sticking probabilities. *J. Aerosol. Sci.*, 27:869–882, 1996.

R. F. Cooper, J. B. Fanselow, and D. B. Poker. The mechanism of oxidation of a basaltic glass: chemical diffusion of networkmodifying cations. *Geochim. Cosmochim. Ac.*, 60: 3253–3265, 1996.

J. Crank. *The Mathematics of Diffusion.* Oxford University Press, 1975.

P. Delmelle. *Volcanic Degassing*, chapter Environmental impacts of tropospheric volcanic gas plumes, pages 381–399. Geological Society Special Publication, 2003.

P. Delmelle, F. Villieras, and M. Pelletier. Surface area, porosity and water adsorption properties of fine volcanic ash particles. *Bull. Volcanol.*, 67:160–169, 2005.

P. Delmelle, M. Lambert, Y. Dufrene, P. Gerin, and N. Óskarsson. Gas/aerosolash interaction in volcanic plumes: New insights from surface analyses of fine ash particles. *Earth. Planet. Sci. Lett.*, 259:159–170, 2007.

D. B. Dingwell. Volcanic dilemma: flow or blow? *Science*, 273:1054–1055, 1996.

D. B. Dingwell, Y. Lavallee, and U. Kueppers. Volcanic ash: A primary agent in the Earth system. *Phys. Chem. Earth, Parts A/B/C*, 45-46(0):2–4, 2012. ISSN 1474-7065. doi: 10.1016/j.pce.2011.07.007.

S. Duggen, P. Croot, U. Schacht, and L. Hofmann. Subduction zone volcanic ash can fertilize the surface ocean and stimulate phytoplankton growth: Evidence from biogeochemical experiments and satellite data. *Geophys. Res. Lett.*, 34:L01612, 2007.

S. Duggen, N. Olgun, P. Croot, L. Hofmann, H. Dietze, and C. Teschner. The role of airborne volcanic ash for the surface ocean biogeochemical iron cycle: A review. *Biogeosciences*, 7:827–844, 2010.

F. Farges, H. Keppler, A. M. Flank, and P. Lagarde. Sulfur K-edge XANES study of S sorbed onto volcanic ashes. *Phys. Conf. Ser.*, 190:012177, 2009.

P. Frogner, S. R. Gislason, and N. Òskarsson. Fertilizing potential of volcanic ash in ocean surface water. *Geology*, 29:487–490, 2001.

N. A. Fuchs and A. G. Sutugin. *Highly Dispersed Aerosols*. Ann Arbor Science Publ., Ann Arbor, Michigan, 1970.

J. C. Gaillard. Alternative paradigms of volcanic risk perception: The case of Mt. Pinatubo in the Philippines. *J. Volcanol. Geotherm. Res.*, 172(34):315–328, 2008. ISSN 0377-0273. doi: 10.1016/j.jvolgeores.2007.12.036.

T. M. Gerlach. Volcanic sources of tropospheric ozone-depleting trace gases. *Geochem. Geophys. Geosys.*, 5:Q09007, 2004.

T. M. Gerlach and B. E. Nordlie. The C-O-H-S gaseous system, part II: Temperature, atomic composition, and molecular equilibria in volcanic gases. *Am. J. Sci.*, 275: 377–394, 1975.

T. M. Gerlach, H. R. Westrich, and R. B. Symonds. *Fire and Mud: Eruptions and Lahars of Mount Pinatubo, Philippines*, chapter Pre-eruption Vapor in Magma of the Climactic Mount Pinatubo Eruption: Source of the Giant Stratospheric Sulfur Dioxide Cloud, pages 415–433. Univ. of Wash. Press, Seattle, 1996.

A. Getahun, M. H. Reed, and R. Symonds. Mount St. Augustine volcano fumarole wall rock alteration: mineralogy, zoning, composition and numerical models of its formation process. *J. Volcanol. Geotherm. Res.*, 71:73–107, 1996.

W. F. Giggenbach. Geothermal gas equilibria. *Geochim. Cosmochim. Ac.*, 44:2021–2032, 1980.

W. F. Giggenbach. Redox processes governing the chemistry of fumarolic gas discharges from White Island, New Zealand. *Appl. Geochem.*, 2:143–161, 1987.

W. F. Giggenbach. *Monitoring and Mitigation of Volcanic Hazards*, chapter Chemical composition of volcanic gases, pages 221–256. Springer Verlag, 1996.

M. M. Halmer, H. U. Schmincke, and H. F. Graf. The annual volcanic gas input into the atmosphere, in particular into the stratosphere: A global data set for the past 100 years. *J. Volcanol. Geotherm. Res.*, 115:511–528, 2002.

R. C. Hamme, P. W. Webley, W. R. Crawford, F. A. Whitney, M. D. DeGrandpre, S. R. Emerson, C. C. Eriksen, K. E. Giesbrecht, J. F. R. Gower, M. T. Kavanaugh, M. A. Panea, C. L. Sabine, S. D. Batten, L. A. Coogan, D. S. Grundle, and D. Lockwood. Volcanic ash fuels anomalous plankton bloom in subarctic northeast Pacific. *Geophys. Res. Lett.*, 37(19):L19604, 2010. ISSN 1944-8007. doi: 10.1029/2010GL044629.

G. Heiken and K. Wohletz. *Volcanic ash.* University of California Press, London, 1992.

T. K. Hinkley and K. S. Smith. Leachate chemistry of ash from the May 18, 1980 eruption of Mount. St. Helens. *U.S. Geol. Surv. Prof. Pap.*, 1397-B:27–64, 1982.

C. J. Horwell, I. Fenoglio, K. Vala Ragnarsdottir, R. S. J. Sparks, and B. Fubini. Surface reactivity of volcanic ash from the eruption of Soufrire Hills volcano, Montserrat, West Indies with implications for health hazards. *Environ. Res.*, 93(2):202–215, 2003. ISSN 0013-9351. doi: 10.1016/S0013-9351(03)00044-6.

G. Hoshyaripour, M. Hort, and B. Langmann. How does the hot core of a volcanic plume control the sulfur speciation in volcanic emission? *Geochem. Geophys. Geosys.*, 13: 100–115, 2012.

A. Höskuldsson, N. Óskarsson, R. Pedersen, K. Grönvold, K. Vogfjörò, and R. Ólafsdóttir. The millennium eruption of Hekla in February 2000. *Bull. Volcanol.*, 70:169–182, 2007.

D. E. Hunton, A. A. Viggianoa, T. M. Millera, J. O. Ballenthina, J. M. Reevesb, J. C. Wilsonb, Shan-Hu Leeb, B. E. Andersonc, W. H. Bruned, H. Harderd, J. B. Simpasd, and N. Óskarsson. In-situ aircraft observations of the 2000 Mt. Hekla volcanic cloud: Composition and chemical evolution in the Arctic lower stratosphere. *J. Volcanol. Geotherm. Res.*, 145:23–34, 2005.

M. Z. Jacobson. *Fundamentals of Atmospheric Modeling.* Cambridge University Press, 2005.

D. Jeong, K. Kim, and W. Choi. Accelerated dissolution of iron oxides in ice. *Atmos. Chem. Phys.*, 12:11125–11133, 2012.

K. Jeong and E. K. Levy. Theoretical prediction of sulfuric acid condensation rates in boiler flue gas. *Int. J. Heat. Mass. Tran.*, 55(2526):8010–8019, 2012. ISSN 0017-9310. doi: 10.1016/j.ijheatmasstransfer.2012.08.037.

M. S. Johnson, N. Meskhidze, F. Solmon, S. Gass, P. Y. Chuang, D. M. Gaiero, R. M. Yantosca, S. Wu, Y. Wang, and C. Carouge. Modeling dust and soluble iron deposition to the South Atlantic Ocean. *J. Geohys. Res., D*, 115(D15):D15202, 2010. ISSN 2156-2202. doi: 10.1029/2009JD013311.

M. T. Jones and S. R. Gislason. Rapid releases of metal salts and nutrients following the deposition of volcanic ash into aqueous environments. *Geochim. Cosmochim. Ac.*, 72(15):3661–3680, 2008. ISSN 0016-7037.

N. Jones. Sparks fly over theory that volcano caused salmon boom. *Nature News*, October 2010, 2010.

N. Kishima. A thermodynamic study on the pyrite-pyrrhotite-magnetite-water system at 300-500°C with relevance to the fugacity /concentration quotient of aqueous H_2S. *Geochim. Cosmochim. Ac.*, 53:2143–2155, 1989.

B. Langmann, K. Zaksek, M. Hort, and S. Duggen. Volcanic ash as fertiliser for the surface ocean. *Atmos. Chem. Phys.*, 10:3891–3899, 2010.

K. Larkin. Canada sees shock salmon glut. *Nature News*, September 2010, 2010.

H. Lepp. Stages in the oxidation of magnetite. *Am. Mineral.*, 42:679–681, 1957.

A. Lindenthal, B. Langmann B., J. Paetsch, I. Lorkowski, and M. Hort. The ocean response to volcanic iron fertilisation after the eruption of Kasatochi volcano: a regional scale biogeochemical ocean model study. *Biogeosciences.*, 10(7):37153729, 2013.

D. H. Lindsley. *Oxide minerals: petrologic and magnetic significance.* Mineralogical Society of America Reviews in Mineralogy, 1991.

R. W. Le Maitre. The chemical variability of some common igneous rocks. *J. Petrology.*, 17:589–637, 1976.

J. Marti and G.G.J. Ernst. *Volcanoes and the Environment.* Cambridge University Press; 1 edition, 2005.

J. H. Martin and S. E. Fitzwater. Iron deficiency limits phytoplankton growth in the north-east Pacific subarctic. *Nature*, 331:341–343, 1988.

R. S. Martin, T. A. Mather, and D. M. Pyle. High-temperature mixtures of magmatic and atmospheric gases. *Geochem. Geophys. Geosys.*, 7:Q04006, 2006.

R. S. Martin, T. J. Roberts andT. A. Mather, and D. M. Pyle. The implications of H_2S and H_2 kinetic stability in high-T mixtures of magmatic and atmospheric gases for the production of oxidized trace species (e.g., BrO and NOx). *Chem. Geol.*, 263: 143–150, 2009.

S. T. Martin. *Environmental Catalysis*, chapter Precipitation and Dissolution of Iron and Manganese Oxides, pages 61–156. CRC Press, 2005.

L. G. Mastin. A user-friendly one-dimensional model for wet volcanic plumes. *Geochem. Geophys. Geosys.*, 8(3):Q03014, 2007. ISSN 1525-2027. doi: 10.1029/2006GC001455.

T. A. Mather. Volcanism and the atmosphere: the potential role of the atmosphere in unlocking the reactivity of volcanic emissions. *Phil. Trans. R. Soc. A*, 336:4581–4595, 2008.

N. Meskhidze, W. L. Chameides, A. Nenes, and G. Chen. Iron mobilization in mineral dust: can anthropogenic SO_2 emissions affect ocean productivity? *Geophys. Res. Lett.*, 30, 2003. doi: doi:10.1029/2003GL018035.

N. Meskhidze, W. L. Chameides, and A. Nenes. Dust and pollution: A recipe for enhanced ocean fertilization? *J. Geohys. Res., D*, 110(D3):D03301, 2005. ISSN 2156-2202. doi: 10.1029/2004JD005082.

O.P. Mills and W.I. Rose. Shape and surface area measurements using scanning electron microscope stereo-pair images of volcanic ash particles. *Geosphere*, 6:805–811, 2010.

P. Minnis, E. F. Harrison, L. L. Stowe, G. G. Gibson, F. M. Denn, D. R. Doelling, and W. L. Smith Jr. Radiative Climate Forcing by the Mount Pinatubo Eruption. *Science*, 259:1411–1415, 1993.

G. Montegrossi, F. Tassi, O. Vaselli, A. Buccianti, and K. Garofano. Sulfur species in volcanic gases. *Anal. Chem.*, 73:3709–3715, 2001.

M. Moriizumi, S. Nakashima, S. Okumura, and Y. Yamanoi. Color-change processes of a plinian pumice and experimental constraints of color-change kinetics in air of an obsidian. *Bull. Volcanol.*, 71:1–13, 2009.

S. Moune, P. J. Gauthier, S. R. Gislason, and O. Sigmarsson. Trace element degassing and enrichment in the eruptive plume of the 2000 eruption of Hekla volcano, Iceland. *Geochim. Cosmochim. Ac.*, 70:461–479, 2006.

S. Moune, O. Sigmarsson, T. Thordarson, and P. J. Gauthier. Recent volatile evolution in the magmatic system of Hekla volcano, Iceland. *Earth. Planet. Sci. Lett.*, 255: 373–389, 2007.

S. Moune, F. Holtz, and R. B. Botcharnikov. Sulphur solubility in andesitic to basaltic melts: implications for Hekla volcano. *Contrib. Mineral. Petrol.*, 157:691–707, 2009.

J. J. Naughton, V. A. Lewis, D. Hammond, and D. Nishimoto. The chemistry of sublimates collected directly from lava fountains at Kilauea volcano, Hawaii. *Geochim. Cosmochim. Ac.*, 38:1670–1690, 1974.

M. O'Dwyer, M. J. Padgett, A. J. S. McGonigle, C. Oppenheimer, and S. Inguaggiato. Real-time measurement of volcanic H_2S and SO_2 concentrations by UV spectroscopy. *Geophys. Res. Lett.*, 30:1652, 2003.

E. H. Oelkers and S. R. Gislason. The mechanism, rates and consequences of basaltic glass dissolution: I. An experimental study of the dissolution rates of basaltic glass as a function of aqueous Al, Si, and oxalic acid concentration at 25 C and pH=3 and 11. *Geochim. Cosmochim. Ac.*, 65:3671–3681, 2001.

D. E. Ogden, K. H. Wohletz, G. A. Glatzmaier, and E. E. Brodsky. Numerical simulations of volcanic jets: Importance of vent overpressure. *J. Geophys. Res.*, 113:B02204, 2008.

H. Olgun, S. Duggen, B. Langmann, M. Hort, C.F. Waythomas, L.J. Hoffmann, and P. Croot. Can volcanic ash fall-out trigger a salmon boom? *Mar. Ecol. Prog. Ser.*, (In Press / Accepted), 2013.

N. Olgun, S. Duggen, P. L. Croot, P. Delmelle, H. Dietze, U. Schacht, N. Oskarsson, C. Siebe, A. Auer, and D. Garbe-Schonberg. Surface ocean iron fertilization: The role of airborne volcanic ash from subduction zone and hot spot volcanoes and related iron fluxes into the Pacific Ocean. *Global. Biogeochem. Cy.*, 25:GB4001, 2011.

N. Óskarsson. The interaction between volcanic gases and tephra: Fluorine adhering to tephra of the 1970 Hekla eruption. *J. Volcanol. Geotherm. Res.*, 8:251–266, 1980.

Oxford-Economics. The Economic Impacts of Air Travel Restrictions Due to Volcanic Ash Report for Airbus. Technical report, Oxford, 2010.

J. L. Palandri and Y. K. Kharaka. *A Compilation of Rate Parameters of Water-Mineral Interaction Kinetics for Application to Geochemical Modeling.* USGS, 2004.

T. R. Parsons and F. A. Whitney. Did volcanic ash from Mt. Kasatoshi in 2008 contribute to a phenomenal increase in Fraser River sockeye salmon (Oncorhynchus nerka) in 2010? *Fish. Oceanogr.*, 21(5):374–377, 2012. ISSN 1365-2419. doi: 10.1111/j.1365-2419.2012.00630.x.

D. W. Peterson. *Geophysics Study Committee (National Research Council) Active Tectonics*, chapter Volcanoes: tectonic setting and impact on society, pages 231–246. National Academy Press, 1986.

Pinatubo Volcano Observatory Team. Lessons from a major eruption: Mt Pinatubo Philippines. *Eos, Trans. Amer. Geophys. Union*, 72(49):552–553, 1991.

L. Pirjola, M. Kulmala, M. Wilck, A. Bischoff, F. Stratmann, and E. Otto. Formation of sulphuric acid aerosols and cloud condensation nuclei: an expression for significant nucleation and model comparison. *J. Aerosol. Sci.*, 30(8):1079 –1094, 1999. ISSN 0021-8502. doi: 10.1016/S0021-8502(98)00776-9.

T. J. Roberts, C. F. Braban, R. S. Martin, C. Oppenheimer, J. W. Adams, R. A. Cox, R. L. Jones, and P. T. Griffiths. Modelling reactive halogen formation and ozone depletion in volcanic plumes. *Chem. Geol.*, 263(14):151–163, 2009. ISSN 0009-2541. doi: 10.1016/j.chemgeo.2008.11.012.

A. Robock. Volcanic eruptions and climate. *Rev. Geophys.*, 38:191–219, 2000.

N. Rogers and C. Hawkesworth. *Encyclopedia of Volcanoes*, chapter Composition of magmas. Academic Press, London, 2000.

W. I. Rose. Scavenging of volcanic aerosol by ash: Atmospheric and volcanologic implications. *Geology*, 5:621–624, 1977.

W. I. Rose and A. J. Durant. Total grain size distribution of explosive volcanic eruptions. *J. Volcanol. Geotherm. Res.*, 186:32–39, 2009.

W. I. Rose, Y. Gu, I. M. Watson, T. Yu, G. J. S. Bluth, A. J. Prata, A. J. Krueger, N. Krotkov, S. Carn, M. D. Fromm, D. E. Hunton, G. G. J. Ernst, A. A. Viggiano, T. M. Miller, J. O. Ballenthin, J. M. Reeves, J. C. Wilson, B. E. Anderson, and D. E. Flittner. *Volcanism and Earth's Atmosphere*, chapter The February–March 2000 Eruption of Hekla, Iceland from a Satellite Perspective, pages 107–132. Geophys. Monogr. Ser., 2003.

W. I. Rose, G. A. Millard, T. A. Mather, D. E. Hunton, B. Anderson, C. Oppenheimer, B. F. Thornton, T. M. Gerlach, A. A. Viggiano, Y. Kondo, T. M. Miller, and J. O. Ballenthin. Atmospheric chemistry of a 33–34 hour old volcanic cloud from Hekla Volcano (Iceland): insights from direct sampling and the application of chemical box modeling. *J. Geophys. Res.*, 111:D20, 2006.

S. P. Sander, J. Abbatt, J. R. Barker, J. B. Burkholder, R. R. Friedl, D. M. Goldenand R. E. Huie, C. E. Kolb, M. J. Kurylo, G.K. Moortgat, V. L. Orkin, and P. H. Wine.

Chemical kinetics and photochemical data for use in atmospheric studies, Evaluation No. 17. Jet Propulsion Laboratory, Pasadena, 2011.

J. L. Sarmiento. Atmospheric CO_2 stalled. *Nature*, 365:697–698, 1993.

B. Scaillet, B. Clemente, B.W. Evans, and M. Pichavant. Redox control of sulfur degassing in silicic magmas. *J. Geophys. Res.*, 103:23937–23949, 1998.

H. U. Schmincke. *Volcanism*. Springer-Verlag, Berlin Heidelberg, 2004.

J. H. Seinfeld and S. N. Pandis. *Atmospheric Chemistry and Physics: From Air Pollution to Climate Change*. John Wiley and Sons, New York, 2006.

S. Self. The effects and consequences of very large explosive volcanic eruptions. *Phil. Trans. R. Soc. A*, 364:2073–2097, 2006.

L. F. Shampine and M. W. Reichelt. The MATLAB ODE Suite. *SIAM J. Sci. Comput.*, 18:1–22, 1997.

D. B. Smith, R. A. Zielinski, H. E. Taylor, and M. B. Sawyer. Leaching characteristics of ash from the May 18, 1980, eruption of Mount St. Helens volcano, Washington. *Bull. Volcanol.*, 46:103–123, 1983.

R. S. J. Sparks, M. I. Bursik, S. N. Carey, J. S. Gilbert, L. S. Glaze, H. Siggurdsson, and A. W. Woods. *Volcanic Plumes*. John Wiley and Sons, New York, 1997.

S. M. Straub and H. U. Schmincke. Evaluating the tephra into Pacific Ocean sediments: distribution in time and space. *Geol. Rundsch.*, 87:471–476, 1998.

W. Stumm and J.J. Morgan. *Aquatic chemistry: chemical equilibria and rates in natural waters*. A Wiley-Interscience publication, 1996.

R. B. Symonds and M. H. Reed. Calculation of multicomponent chemical equilibria in gas-solid-liquid systems; calculation methods, thermochemical data, and applications to studies of high-temperature volcanic gases with examples from Mount St. Helens. *Am. J. Sci.*, 293:758–864, 1993.

R. B. Symonds, W. I. Rose, M. H. Reed, F. E. Lichte, and D. L. Finnegan. Volatilization, transport and sublimation of metallic and non-metallic elements in high temperature gases at Merapi Volcano, Indonesia. *Geochim. Cosmochim. Ac.*, 51:2083–2101, 1987.

R. B. Symonds, W. I. Rose, G. J. S. Bluth, and T. M. Gerlach. *Volatiles in Magma*, chapter Volcanic gas studies: methods, results and applications, pages 1–66. Reviews in Mineralogy, vol. 30. American Mineralogical Society, 1994.

A. Tabazadeh and R. P. Turco. Stratospheric chlorine injection by volcanic eruptions: HCl scavenging and implications for ozone. *Science*, 260:1082–1086, 1993.

P. S. Taylor and R. E. Stoiber. Soluble Material on Ash from Active Central American Volcanoes. *Geol. Soc. Am. Bull.*, 84:1031–1042, 1973.

C. Textor, H. F. Graf, C. Timmreck, and A. Robock. *Emissions of Atmospheric Trace Compounds*, chapter Emissions from volcanoes, pages 269–303. Springer Verlag, 2004.

R. I. Tilling. *Volcanoes and the Environment*, chapter Volcano hazards, pages 56–89. Cambridge University Press, 2005.

K. Toda, S. Ohira, T. Tanaka, and T. Nishimura. Field instrument for simultaneous large dynamic range measurement of atmospheric hydrogen sulfide, methanethiol and sulfur dioxide. *Environ. Sci. Technol.*, 38:1529–1536, 2004.

United States Committee on Extension to the Standard Atmosphere. *U.S. Standard Atmosphere*. Natl. Oceanic and Atmos. Admin., Washington, D. C., 1976.

F. H. Verhoff and J. T. Banchero. Predicting dew points of gases. *Chem. Eng. Prog.*, 78:71–72, 1974.

R. von Glasow, N. Bobrowski, and C. Kern. The effects of volcanic eruptions on atmospheric chemistry. *Chem. Geol.*, 263:131–142, 2009.

P. J. Wallace. Volcanic SO_2 emissions and the abundance and distribution of exsolved gas in magma bodies. *J. Volcanol. Geotherm. Res.*, 108:85–106, 2001.

A. J. Watson. Volcanic Fe, CO_2, ocean productivity and climate. *Nature*, 358:587–588, 1997.

X. Zhang. Diffusion in Minerals and Melts: Theoretical Background. *Rev. Mineral. Geochem.*, 72:5–59, 2010.

Erklärung:

Hiermit erkläre ich, Gholamali Hoshyaripour, dass ich die Dissertation mit dem Titel:

„Modulation of Ash Iron Solubility in Volcanic Eruption Plumes“

selbstständig verfasst und keine anderen als die angegebenen Hilfsmittel genutzt habe. Alle wörtlich oder inhaltlich übernommenen Stellen habe ich als solche gekennzeichnet.

Hamburg, den 19.12.2013

Ort, Datum

Unterschrift